High resolution retinal imaging

HIGH-RESOLUTION RETINAL IMAGING

DISSERTATION

To obtain the degree of Doctor at Maastricht University, on the authority of the Rector Magnificus

PROF.DR.PAMILA HABIBOVIC

in accordance with the decision of the Board of Deans, to be defended in public on

THURSDAY MAY 19, 2022

at 10:00 hours

by

SUPRIYA DABIR GAUTAM

Born August 1st, 1979

in Bangalore, India

SUPERVISOR

Prof. Dr. C.A.B. Webers

CO-SUPERVISORS

Dr. T.T.J.M. Berendschot
Dr.J.S.A.G. Schouten, Canisius Wilhelmina Ziekenhuis, Nikmegen

ASSESSMENT COMMITTEE

Prof. D.E.J. Linden (Chair)
Prof. N.M. Jansonius (University of Groningen)
Prof. A.A. Kroon
Dr. F.D. Verbraak (University of Amsterdam)
Prof. J.E. Wildberger

Every great advance in science has issued from a new audacity of imagination.

–John Dewey

TABLE OF CONTENTS

1.	INTRODUCTION	1
2.	ADAPTIVE OPTICS IMAGING OF THE RETINA *Indian Journal of Ophthalmology 2014; 62:60–65*	17
3.	VARIATIONS IN THE CONE-PACKING DENSITY WITH ECCENTRICITY IN EMMETROPES *Eye (London) 2014; 28:1488–1493*	35
4.	AXIAL LENGTH AND CONE DENSITY AS ASSESSED WITH ADAPTIVE OPTICS IN MYOPIA *Indian Journal of Ophthalmology 2015; 63:423–426*	47
5.	STRUCTURAL AND FUNCTION CORRELATION OF CONE-PACKING UTILIZING ADAPTIVE OPTICS AND MICROPERIMETRY *BioMed Research International 2015; 968672*	61
6.	MELANOMA-ASSOCIATED RETINOPATHY: A NEW DIMENSION USING ADAPTIVE OPTICS *Oman Journal of Ophthalmology 2015; 8:125–127*	71
7.	SPECTRAL DOMAIN OPTICAL COHERENCE TOMOGRAPHY ANGIOGRAPHY FEATURES IN A PATIENT OF CENTRAL RETINAL ARTERIAL OCCLUSION BEFORE AND AFTER PARACENTESIS *Retina 2016; 36:e36–38*	81
8.	ASSESSMENT OF MICROVASCULAR CHANGES USING OPTICAL COHERENCE TOMOGRAPHY ANGIOGRAPHY AFTER PHACOEMULSIFICATION SURGERY IN AN INDIAN POPULATION *Journal of Clinical and Experimental Ophthalmology, 2021: 12: 1–6*	87
9.	EARLY VISUAL FUNCTIONAL OUTCOMES AND MORPHOLOGICAL RESPONSES TO ANTI-VASCULAR GROWTH FACTOR THERAPY IN DIABETIC MACULAR EDEMA USING OPTICAL COHERENCE TOMOGRAPHY ANGIOGRAPHY *Clinical Ophthalmology 2021; 15:331–339*	101
10.	NEED FOR MANUAL SEGMENTATION IN OPTICAL COHERENCE TOMOGRAPHY ANGIOGRAPHY OF NEOVASCULAR AGE-RELATED MACULAR DEGENERATION *Plos one 2020; 15:e0244828*	119
11.	ISOLATED RACEMOSE ANGIOMA *Ophthalmology 2020; 127:1370*	135
12.	GENERAL DISCUSSION	139

13. SUMMARY 151
14. IMPACT 157
15. ACKNOWLEDGEMENTS 163
16. CURRICULUM VITAE AND PUBLICATIONS 167

CHAPTER 1

INTRODUCTION

The human eye is an organ that reacts with light and allows light perception, color vision and depth perception. The eye is not shaped like a perfect sphere, rather, a fused two-piece unit, composed of an anterior (front) segment and a posterior (back) segment.

The anterior segment is made up of the cornea, iris and lens. The cornea is transparent and curved, and is linked to the larger posterior segment, composed of the vitreous, retina, choroid and the outer white shell, the sclera, as seen in Figure 1a.[1,2] The iris is a pigmented circular structure concentrically surrounding the centre of the eye, the pupil, which appears to be black. The size of the pupil, which controls the amount of light entering the eye, is adjusted by the iris dilator and sphincter muscles.

Light energy enters the eye through the cornea, through the pupil and then through the lens. The lens shape is changed for near focus (accommodation) and is controlled by the ciliary muscle. Photons of light falling on the light-sensitive cells of the retina (photoreceptor cones and rods) are converted into electrical signals that are transmitted to the brain by the optic nerve and interpreted as sight and vision.

The spaces of the eye are filled with aqueous humour anteriorly, between the cornea and lens, and vitreous humour, a jelly-like substance, behind the lens, filling the entire posterior cavity. The aqueous humour is a clear watery fluid and vitreous humour is a clear substance composed of water and proteins.[1,2]

Figure 1. (a) Anatomy of the eye and (b) fundus image

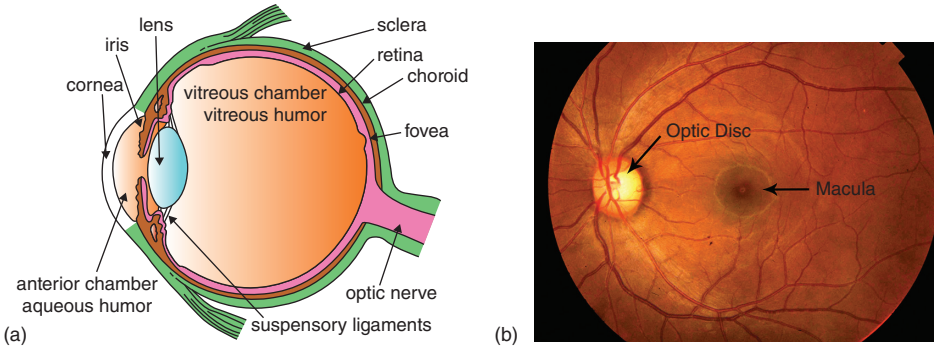

1.1. ANATOMY OF THE RETINA

The retina is the innermost layer of the eyeball, which is a thin, delicate and transparent membrane. It extends from the optic disc to the ora serrata and has a surface area of about 266 mm^2, as seen in Figure 1b.[3,4]

1.1.1. OPTIC DISC

The optic disc is a well-defined circular structure of about 1.5 mm diameter with a depression seen centrally, called the physiological cup and through the center of this cup, the central retinal vessels emerge. All the retinal layers terminate at the optic disc, except the nerve fibers, which pass through the lamina cribrosa to run into the optic nerve.

1.1.2. MACULA LUTEA

The macula lutea is a retinal area of about 5.5 mm in diameter, situated at the posterior pole of the eyeball, temporal to the optic disc and between the temporal vascular arcade. The centre of the macula is the fovea centralis. It is the central depressed area of the macula, which is about 1.5 mm in diameter. It consists of the foveola, umbo, clivus and the foveal avascular zone (FAZ). The FAZ is an area which is devoid of retinal vessels.

1.2. MICROSCOPIC STRUCTURE[3,4,5]

The retina consists of ten layers, as seen in Figure 2(a) in histology and Figure 2(b) on spectral domain optical coherence tomography (SD-OCT). These ten layers from sclera inward are:

1. Retinal pigment epithelium
2. Layers of rods and cones
3. External limiting membrane
4. Outer nuclear layer
5. Outer plexiform layer
6. Inner nuclear layer
7. Inner plexiform layer
8. Ganglion cell layer
9. Nerve fiber layer
10. Internal limiting membrane

Figure 2. Layers of the retina: (a) Histology (b) Spectral domain optical coherence tomography

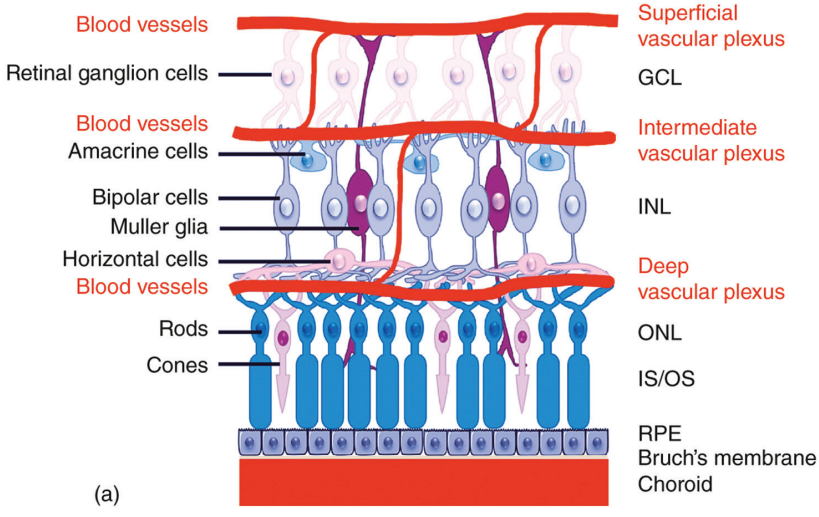

(a)

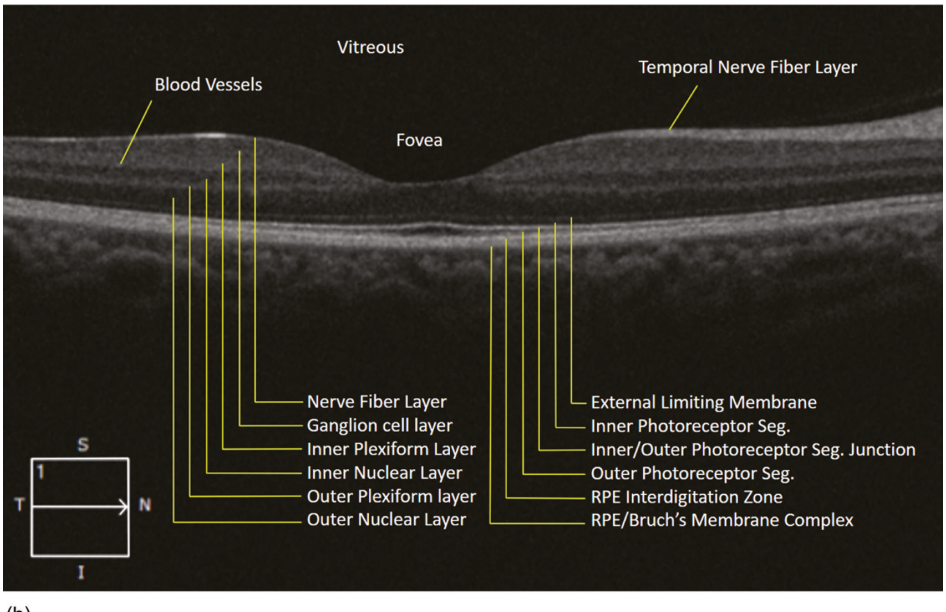

(b)

1.2.1. RETINAL PIGMENT EPITHELIUM

The retinal pigment epithelium (RPE) is the outermost layer of the retina. It consists of a single layer of hexagonal-shaped cells containing pigment. The RPE is firmly adherent to

the underlying Bruch's membrane, while loosely attached to the layer of rods and cones of the sensory retina. The subretinal space is a potential space between RPE and the sensory retina. The adjacent RPE cells are connected with each other by tight junctions, zonulae occludentes and zonulae adherents. This constitutes the outer blood-retinal barrier.

1.2.2. LAYER OF RODS AND CONES (NEUROEPITHELIUM)

The layer of rods and cones contains the outer segments of photoreceptor cells, that are arranged in a palisade manner. Rods form 90% of all photoreceptors, are 120 million in number and contain rhodopsin as the visual pigment. Highest density is below the optic disc, reduces towards the periphery and absent at the fovea. They are responsible for peripheral vision. Cones constitute 5% of photoreceptors, are 6.5 million in number and contain iodopsin as the visual pigment. Maximum number of cones are at the fovea and it falls rapidly, being only 6000 cones/mm^2, 3 mm away from fovea and 4000 cones/mm^2, 10 mm away.

1.2.3. EXTERNAL LIMITING MEMBRANE

The external limiting membrane is a fenestrated membrane that extends from the ora serrata to the edge of the optic disc. It is formed by the junctions (zonulae adherens) between the cell membrane of photoreceptors and Muller's cells.

1.2.4. OUTER NUCLEAR LAYER

The outer nuclear layer is formed by the nuclei of rods and cones. The bulk of this multi-layered outer nuclear layer is formed by the rod nuclei, except in the foveal region which is dominated by the cones.

1.2.5. OUTER PLEXIFORM LAYER

The outer plexiform layer contains the synapses between the rod spherules and cone pedicles with the dendrites of the bipolar cells and processes of the horizontal cells. It is thickest at the macula.

1.2.6. INNER NUCLEAR LAYER

The inner nuclear layer resembles the outer nuclear layer. It disappears at the fovea. This layer consists of the following bipolar cells, horizontal cells, amacrine cells, the soma of the Muller's cells and capillaries of the central retinal vessels.

1.2.7. INNER PLEXIFORM LAYER

The inner plexiform layer consists of synapses between the axons of bipolar cells, dendrites of ganglion cells and the processes of integrative amacrine cells. This layer is absent at the foveola.

1.2.8. GANGLION CELL LAYER

The ganglion cell layer contains the cell bodies and the nuclei of the ganglion cells, which form the second-order neurons of the visual pathway.

1.2.9. NERVE FIBRE LAYER

The nerve fibre layer (NFL) consists of the unmyelinated axons of the ganglion cells. These converge at the optic nerve head and pass through the lamina cribrosa. Posterior to the lamina, these fibers become ensheathed by myelin.

1.2.10. INTERNAL LIMITING MEMBRANE

The internal limiting membrane consists mainly of a periodic acid shiff positive true basement membrane. It forms the interface between retina and vitreous.

1.3. IMAGING OF THE RETINA: THE JOURNEY SO FAR

Unlike the imaging of everyday objects, imaging of the retina is limited by the size of the entrance pupil, and the outgoing rays being imaged are restricted by the size of the same exit pupil.[6,7] The invention of the direct ophthalmoscope gave a boost to the study of retinal diseases, with the knowledge of reversibility of rays and paraxial viewing. A further development was the indirect ophthalmoscope, which allowed rays to form real images using the same system that converged the light into the eye.

The ability to retrieve these outgoing rays and form an image was possible with the development of the fundus camera. Although limited initially by the film, its resolution and image characteristics were significantly enhanced with charge-coupled devices (CCD cameras) producing a digital image.[8]

Despite technological advancements, imaging of the retina was limited by the optical aberrations of the eye, also expressed as 'wave aberrations'. Wave front distortions of incoming light limit the cones' resolution capacity. Conversely, wave front distortions of light emerging from the eye limit the capacity of optical systems' lateral resolution.

Wave front aberrations may be low order (LOA, defocus or astigmatism) or high order (HOA-coma, trefoil and spherical aberration).[9] The LOA aberrations constitute about 90% of all aberrations of the human eye and have been addressed effectively in many optical imaging devices including the fundus camera. However, HOAs still pose a limit to the lateral resolution capability, as they are not stable. Recognition and correction have to be continuous to allow for excellent resolution.[9,10]

Optical coherence tomography (OCT) added a new dimension to retinal imaging with the ability to develop cross-sectional images of retinal tissue to a submicron axial resolution and millimetre penetration using a low-coherence interference technique combined with a broadband light source.[11] Time domain initially and later Fourier domain OCT techniques have further improved axial resolution of tissue cross-section.

1.3.1. HIGH-RESOLUTION IMAGING

Current retinal imaging techniques are still limited in their ability to detect abnormalities of the retinal photoreceptors cells and capillaries. Newer high-resolution imaging modalities that are able to detect retinal microstructures, similar to in-vivo histology, could detect changes at this micro-level. These can be used to detect early structural changes on cellular level.

(A) ADAPTIVE OPTICS

Adaptive optics (AO) retinal imaging can theoretically improve the lateral resolution to 2 µm and therefore provide information about the retinal microstructures that cannot be obtained with current retinal imaging techniques, as seen in Figure 3.[9,11,12]

Figure 3. The optics of the adaptive optics camera

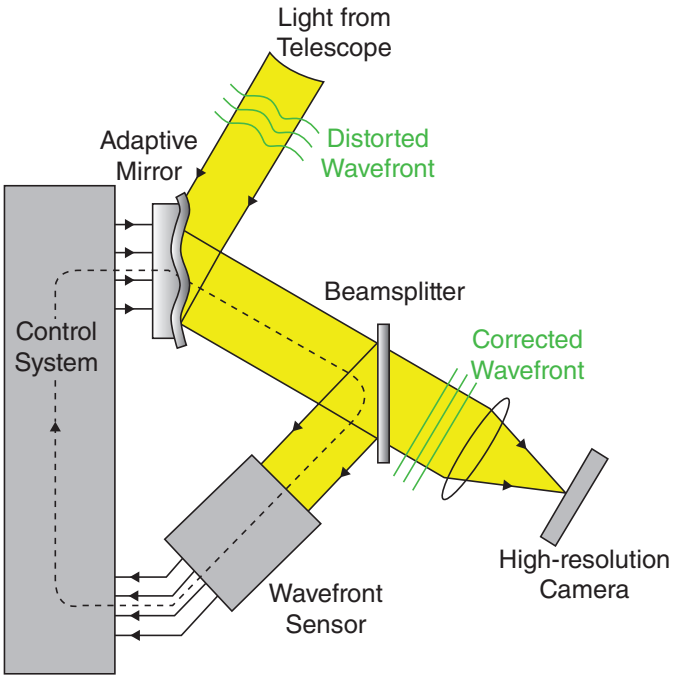

It is thus opening a new frontier for clinical research in ophthalmology, providing new information on the early pathological changes of the retinal microstructures in various retinal diseases. AO systems allow direct visualization of individual rod and cone photoreceptor cells, retinal pigment epithelial (RPE) cells, red and white blood cells, lamina cribrosa and retinal blood vessels. Most of the research published to date is focused on cone photoreceptors which are easily imaged owing to their unique wave-guiding properties, whereas inbuilt software helps in analysing the counts and the spacing between them (see Figure 4).

Figure 4. The cone counts and spacing in the sampling window

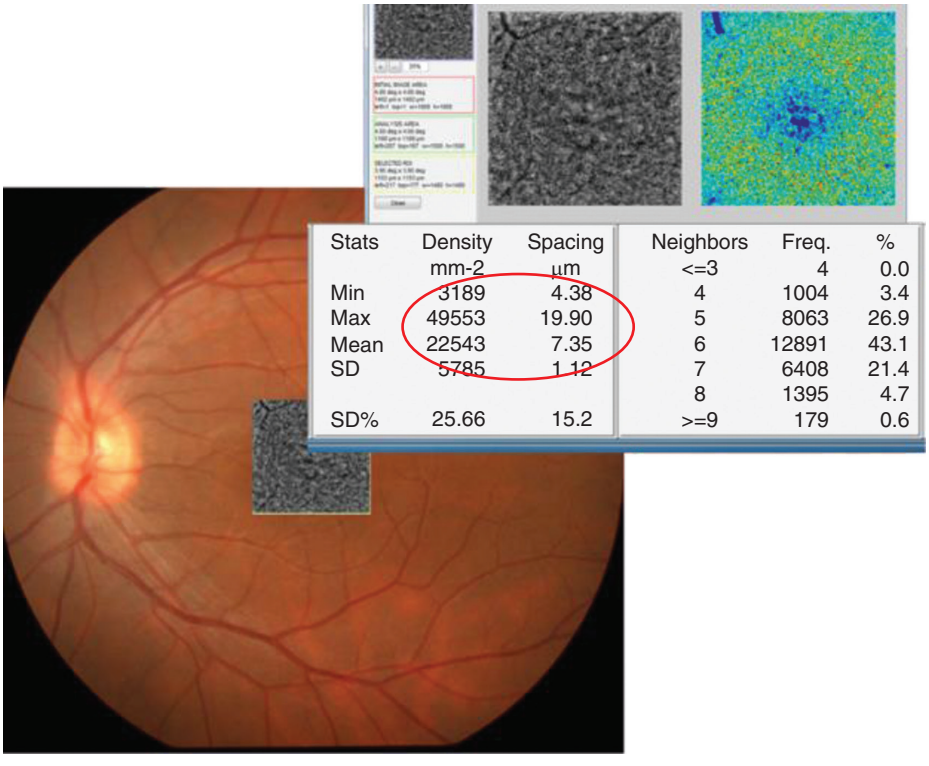

Imaging rods is more tedious given their small diameter (~2 µm) and their significantly reduced wave-guiding properties compared to cones. Considering that structural damage of these microstructures precedes their functional impairment, the detection of pathological variations of photoreceptors at the pre-clinical stage of the disease will help us not only understand the pathogenesis of diseases but also pave way for the exciting possibility of early treatment for these diseases.

Various studies have demonstrated the correlation of cone parameters on AO images with measures of central visual function including visual acuity, foveal threshold and multifocal electroretinogram (ERG) in patients with retinitis pigmentosa (RP) and cone-rod dysfunction. Cone spacing measures were also seen to be reproducible suggesting that these can be useful in monitoring disease progression and response to treatment. Similarly, it's use in various inherited retinal diseases and drug-related retinopathy is being evaluated.[13]

(B) OPTICAL COHERENCE TOMOGRAPHY ANGIOGRAPHY

Study of vasculature is critical to understanding the systemic status of the body. The retina is an end organ and subtle changes in the capillaries are a sign of degeneration, either in the systemic status like diabetes mellitus or age-related changes.

Fluorescein angiography (FA) and indocyanine green angiography (ICGA) are both invasive tests that require intravenous administration of dye and imaging for up to 10–30 minutes. They provide two-dimensional image sets that allow for dynamic visualization of blood flow with a wide field of view.[14]

Figure 5. The Angioplex OCTA: (a) Acquisition of data and processing. (b) Superficial, deep and avascular maps from sequential scans with B scans showing layers that define the maps and a schematic of the vasculature of the eye

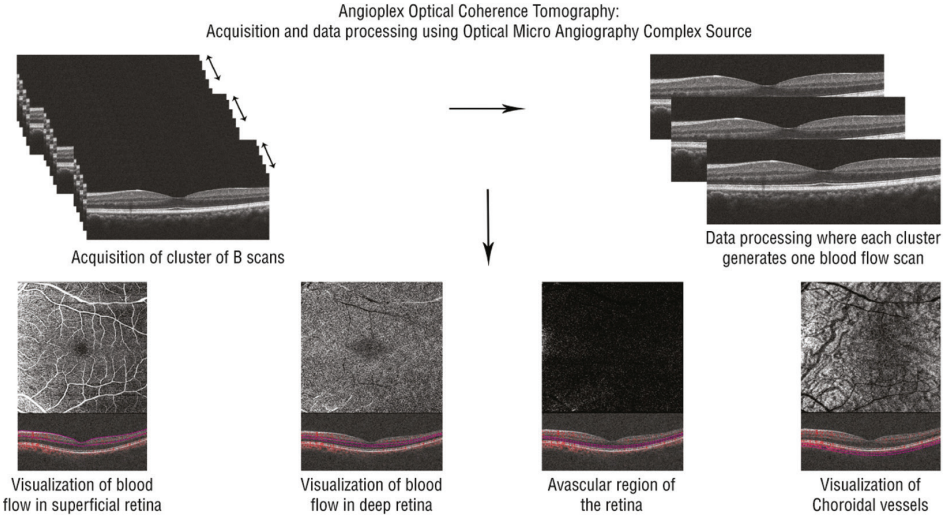

FA and ICGA have other drawbacks that can limit their widespread use. Since they are invasive, relatively expensive and time-consuming, they are not ideal techniques to use on a regular basis in a busy clinical setting. Although considered safe, the dyes pose risks ranging from nausea to allergic reactions, including anaphylaxis in rare instances. Aside from allergic reactions of which the likelihood increases with frequency of use, indocyanine green dye is contraindicated in pregnancy and kidney disease. For the

evaluation of patients requiring frequent follow-up exams or of those that may not tolerate injection of intravenous dye, a rapid non-invasive technique to visualize retinal and choroidal vessels would be beneficial.[14]

Optical coherence tomography angiography (OCTA) is a new non-invasive imaging technique that employs motion contrast imaging to high-resolution volumetric blood flow information generating angiographic images in a matter of seconds. The angiographic images are generated using a complex algorithm that analyses differences in both intensity and phase information from repeated B-scans at the same position. This process is repeated at multiple adjacent positions to generate an en-face flow volume, as seen in Figure 5.[14,15]

Each three-dimensional scan set takes approximately six seconds to obtain. The en-face images (OCT angiograms) can then be scrolled outward from the internal limiting membrane (ILM) to the choroid to visualize the individual vascular plexus and segment the inner retina, outer retina, choriocapillaris or other areas of interest. The en-face acquisition areas currently range from 2×2 mm to 12×12 mm with the scan quality greatly decreased with a widened field of view since the same number of OCT B-scans is used for all scanning areas. Use of the montage technique allows for a larger field of view much like FA/ICGA while maintaining this improved resolution. Full-thickness scans are manually segmented into the superficial (plexus at the RNFL), intermediate (plexus at the GCL) and deep (plexuses at IPL/INL and INL/OPL borders) inner retinal vascular plexuses, outer retina, choriocapillaris and choroidal layers.[14,15]

Various studies have been done to analyse the vascular pattern using OCTA in diabetic macular oedema, choroidal neovascular membrane, polypoidal choroidal vasculopathy, macular telangiectasia, vascular occlusions etc.[15] OCTA has been used to classify the diseases, assess severity, monitor treatment responses and prognosticate the macular pathologies.

OUTLINE OF THE THESIS

The aim of this thesis is to study two high-resolution imaging modalities, namely, adaptive optics and optical coherence tomography angiography, analyse their data in normal and pathological retina to help aid in diagnosis, prognosis and treatment of retinal diseases.

CHAPTER TWO involves a review of literature on AO. Here, we describe the basic principles of AO, clinical applications of AO in photoreceptor analysis in retinal degenerations and dystrophies and in retinal vascular analysis.

CHAPTER THREE presents normative data for cone density in emmetropic Indian eyes. It also discusses the parafoveal cone arrangement, their variations with eccentricity and interocular symmetry.

CHAPTER FOUR looks at the variations in the cone mosaic in a population of young myopic adults in relation to the axial length and extent of the refractive error.

CHAPTER FIVE describes the structure-function correlation by correlating the cone-packing with the retinal sensitivity utilizing microperimetry in emmetropes at different eccentricities.

CHAPTER SIX is a single case report where AO is described in a case of melanoma-associated retinopathy (MAR). This chapter describes the role of AO in assessing the extent of pathology in MAR.

CHAPTER SEVEN is a case report describing improvement in perfusion of the superficial capillary plexus immediately after anterior chamber paracentesis in acute central retinal artery occlusion.

CHAPTER EIGHT discusses the role of OCTA in detecting an increment in the macular perfusion and vascularity indices at 1 month after uneventful phacoemulsification surgery, independent of improvement in signal strength.

CHAPTER NINE characterizes the morphology of retinal microvasculature in patients with diabetic macular oedema and its correlation with visual acuity after treatment with Ranibizumab injections.

CHAPTER TEN elucidates the superiority of manual segmentation over automated segmentation to identify choroidal neovascular membrane in age-related macular degeneration.

CHAPTER ELEVEN shows the superficial capillary plexus of an isolated racemose angioma in an asymptomatic young girl without any systemic associations.

CHAPTER TWELVE is a general discussion in which the findings of the research presented in this thesis are put into perspective.

CHAPTER THIRTEEN summarizes the main findings of the preceding chapters.

CHAPTER FOURTEEN reflects on the scientific impact of the results of the research described in this thesis and its social impact.

REFERENCES

1. Parts of the Eye. American academy of ophthalmology. https://www.aao.org/eye-health/anatomy/parts-of-eye. Accessed December 21, 2018.
2. Khurana A, Khurana I, Khurana AK, Khurana B. *Anatomy and Physiology of Eye*. CBS Publishers & Distributors Pvt Limited; 2017.
3. Curcio CA, Sloan KR, Kalina RE, Hendrickson AE. Human photoreceptor topography. *J Comp Neurol.* 1990;292(4):497–523.
4. Williams RW. The human retina has a cone-enriched rim. *Vis Neurosci.* 1991;6(4): 403–406.
5. Fu Z, Sun Y, Cakir B, et al. Targeting neurovascular interaction in retinal disorders. *Int J Mol Sci.* 2020;21(4):1503.
6. Colenbrander A, Tasman W, Jaeger EA. *Principles of Ophthalmoscopy Duane's Ophthalmology*. Vol 1. 2013 ed. 2012: chap 63.
7. Atebara NH, Miller D, Thall EH. Ophthalmic instruments. In: Yanoff M, Duker JS, eds. *Ophthalmology*. 5th ed. Philadelphia, PA: Elsevier; 2019: chap 2.5.
8. Meyer-Schwickerath GR. Ophthalmology and photography: the 20th Arthur J. Bedell Lecture. *Am J Ophthalmol.* 1968;66(6):1011–1019.
9. Lombardo M, Lombardo G. Wave aberration of human eyes and new descriptors of image optical quality and visual performance. *J Cataract Refract Surg.* 2010;36(2):313–331.
10. Lombardo M, Serrao S, Devaney N, Parravano M, Lombardo G. Adaptive optics technology for high-resolution retinal imaging. *Sensors.* 2013;13(1):334–366.
11. Puliafito CA, Hee MR, Lin CP, et al. Imaging of macular diseases with optical coherence tomography. *Ophthalmology.* 1995;102(2):217–229.
12. Rosander F. Detection of Pathological lesions in high resolution retinal images [master's thesis]. Linköping, Sweden: Linköping University; 2013.
13. Godara P, Dubis AM, Roorda A, Duncan JL, Carroll J. Adaptive optics retinal imaging: emerging clinical applications. *Optom Vis Sci.* 2010;87(12):930.
14. De Carlo TE, Romano A, Waheed NK, Duker JS. A review of optical coherence tomography angiography (OCTA). *Int J Retin Vitr.* 2015;1(1):5.
15. Bandello F, Souied EH, Querques G. *OCT Angiography in Retinal and Macular Diseases*. Karger Medical and Scientific Publishers; 2016.

CHAPTER 2

ADAPTIVE OPTICS IMAGING OF THE RETINA

Rajani Battu, Supriya Dabir, Anjani Khanna,
Anupama Kiran Kumar, Abhijit Sinha Roy

INDIAN JOURNAL OF OPHTHALMOLOGY 2014; 62:60–65

ABSTRACT

Adaptive optics is a relatively new tool that is available to ophthalmologists for study of cellular level details. In addition to the axial resolution provided by the spectral-domain optical coherence tomography, adaptive optics provides an excellent lateral resolution, enabling visualization of the photoreceptors, blood vessels and details of the optic nerve head. We attempt a mini review of the current role of adaptive optics in retinal imaging in normal subjects, myopes and inherited retinal diseases.

PubMed search was performed with key words Adaptive optics OR Retina OR Retinal imaging. Conference abstracts were searched from the Association for Research in Vision and Ophthalmology (ARVO) and American Academy of Ophthalmology (AAO) meetings. In total, 261 relevant publications and 389 conference abstracts were identified.

Keywords: Adaptive optics, cone count, cone spacing, retinal imaging.

2.1. INTRODUCTION

The invention of the direct ophthalmoscope gave a boost to the study of retinal diseases, with the knowledge of reversibility of rays and paraxial viewing. A further development was the indirect ophthalmoscope, which allowed rays to form real images using the same system that converged the light into the eye. Unlike imaging of everyday objects, imaging of the retina is limited by the size of the entrance pupil, and the outgoing rays being imaged are restricted by the size of the same exit pupil.[1,2]

The ability to retrieve these outgoing rays and form an image was possible with the development of the fundus camera. Although limited initially by the film, its resolution and image characteristics were significantly enhanced with charge-coupled devices (CCD cameras) producing a digital image.[3]

The scanning laser ophthalmoscopy (SLO) marked a change in photographic capture technique which utilized the principle of illuminating only a small spot of the retina with collimated laser light directed through the very centre of the pupil and capturing the reflections from its entire surrounds within the pupil confines.[4] This reversed the optics of entrance and exit imaging and allowed usage of much lower levels of light energy with better images. However, the small spot imaged at each instant, necessitated a scanning system to allow a large area of the fundus to be scanned and produce an image after collating the scans with appropriate software; this was done with a series of rotating polygonal mirrors and galvanometric mirrors to produce a 'raster scan'. This resulted in two effects on the viewing of the image. Axial resolution was further addressed by using a simple, but ingenious principle of "confocal scanning" where a pinhole of a sufficient diameter interposed before the photodetector system allowed scattered light in front of and behind "the plane of focus" to be reflected off and only the 'confocal rays' finding their way through the pinhole and onto the photodetector. This allowed micrometer precision axial resolution at an image 'plane' combined with the lateral resolution offered by the SLO.

Optical Coherence tomography (OCT) added a new dimension to retinal imaging with the ability to develop cross sectional images of retinal tissue to a submicron axial resolution and millimeter penetration using a low coherence interference technique combined with a broadband light source.[5] Time domain initially and later Fourier domain OCT techniques have further improved axial resolution of tissue cross-section.

Despite technological advancements, imaging of the retina was limited by the 'optical aberrations' of the eye, also expressed as 'wave aberrations'. Wavefront distortions of incoming light limit the cones' resolution capacity. Conversely, wave front distortions of light emerging from the eye, limit the capacity of optical systems' lateral resolution.

Wavefront aberrations may be Low order (LOA - defocus or astigmatism) or High order (HOA-coma, trefoil and spherical aberration).[6] The LOA aberrations constitute about 90% of all aberrations of the human eye and have been addressed effectively in many optical imaging devices including the fundus camera. However, HOAs still pose a limit to the lateral resolution capability, as they are unstable; recognition and correction has to be continuous to allow for excellent resolution.

Adaptive optics (AO) technology aims to correct these ocular aberrations and enhance performance of the optical systems. AO was first used in astronomical telescopes to allow for correction of atmospheric aberrations on wavefronts entering telescopes leading to significant loss of resolution and contrast.[7]

The three principal components of such an AO system include a wavefront sensor (typically Hartman-Shack), a deformable mirror and software to control the interaction between these two components. The wavefront sensor measures the native aberrations of the eye in vivo. The deformable mirror uses a complex system of actuators to adjust several small mirrors to compensate for the aberrations measured. The interaction between the two is controlled by specialized software (Figure 1).[6,8]

Adaptive optics in retinal imaging could be used with flood illumination or combined with both the SLO and the OCT to produce high quality images whose lateral resolution permits cone discrimination and also allows the study of blood vessels and cells.[9,10] By compensating for the aberrations caused by irregularities of the optics of the eye, lateral (transverse) resolutions to the order of 2 µm can be achieved, thereby allowing for the visualization of individual cone photoreceptors.[11]

Figure 1. Schematic outline of adaptive optics imaging system. A beam of light enters the eye, and a small amount is reflected back out of the eye and into the optical system. Reflected light is altered by the deformable mirror for optical aberrations based on measurements made by the wave-front senor. Information about the aberrations of the wave front is processed by the control system that provides feedback to the deformable mirror

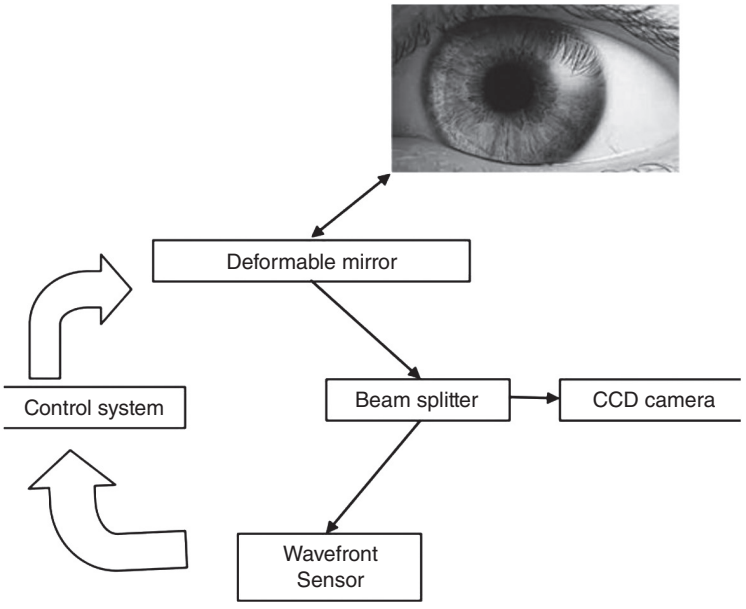

With the rapidly increasing potential for adaptive optics imaging, we herein provide a mini-review of the current status of AO in retinal imaging.

2.2. APPLICATIONS

AO system allows direct visualization of individual rod and cone photoreceptor cells, retinal pigment epithelial (RPE) cells, red and white blood cells, lamina cribrosa and retinal blood vessels. Cone photoreceptors are easily imaged owing to their unique wave-guiding properties, and most of the research published to date is focused on this.[12–16] Imaging rods is more tedious given their small diameter (~2 μm), and their significantly reduced wave-guiding properties compared to cones.[17]

2.2.1. AO IMAGING IN NORMAL SUBJECTS

Data from the AO imaged in healthy eyes is necessary in establishing a baseline of the cone characteristics in vivo, to enable detection of retinal diseases at a very early stage.

One of the AO prototypes (rtx1, Imagine Eyes, Orsay, France) operates at a wavelength of 750 nm to measure and correct aberrations while maintaining focus at different retinal layers. Another light source of 850 nm is used to illuminate the retina and capture an image of 4° × 4°. For fixation, the device has a yellow cross, which can be moved by the investigator. A sequence of 40 frames (frame rate, 9.5 fps) is acquired on overlapping regions of the posterior pole (Figure 2).

Figure 2. Raw image before analysis from the rtx1 (from a normal subject). Note the multiple white dots corresponding to the cones

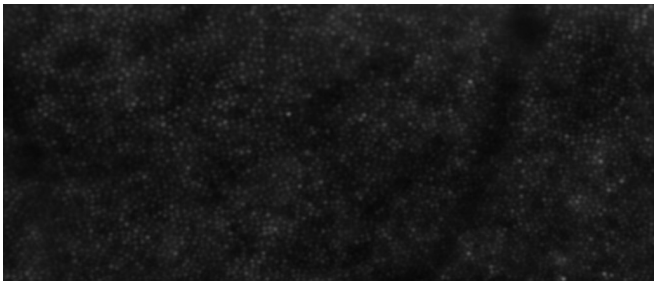

After acquisition, a program provided by the manufacturer is used to produce a final image with enhanced signal-to-noise ratio. Frames exhibiting large motion artifacts owing to eye movement or blinking are manually removed before processing. Before analysis, the retinal magnification factor is calculated in each eye using the Gullstrand schematic eye as a model.

Image analysis of the acquired image is then performed using Image J (version 1.45a, NIH, Bethesda, MD). Once the region of interest (ROI) is selected, analysis of the region provides three parameters, mainly cone-packing density, cone spacing and the Voronoi analysis. The Voronoi analysis assesses the regularity of the photoreceptors and the percentage of hexagonal polygons. The ROI can be selected as specific areas in the posterior pole, for comparison with various structural pathologies. The possible range of spherical correction on the rtx1 is −12DS to +6DS. Some AO systems are unable to resolve the central foveal cones due to the high foveal cone-packing density (Figures 3–5).

Figure 3. Cone-packing density in a normal subject on the rtx1. The encircled area shows the mean and standard deviation of cone density and cone spacing in the central 4x4 deg

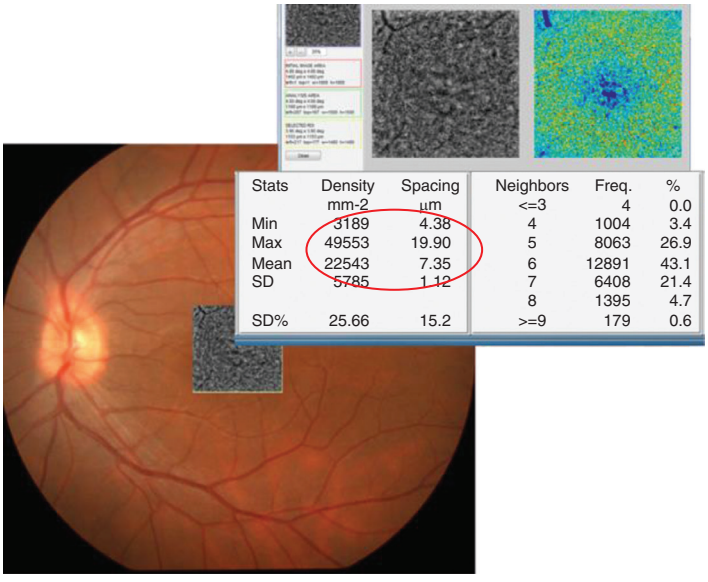

Figure 4. Voronoi tessellation of photoreceptors (cones) in a normal subject on the rtx1. The colour scale shows the packing density in the central 4 × 4 deg. The apparent low cone density depicted in the foveal centre is due to a lack of adequate resolution of the device in that region. In this patient, the mean cone count was 17428 ± 6743/mm^2.

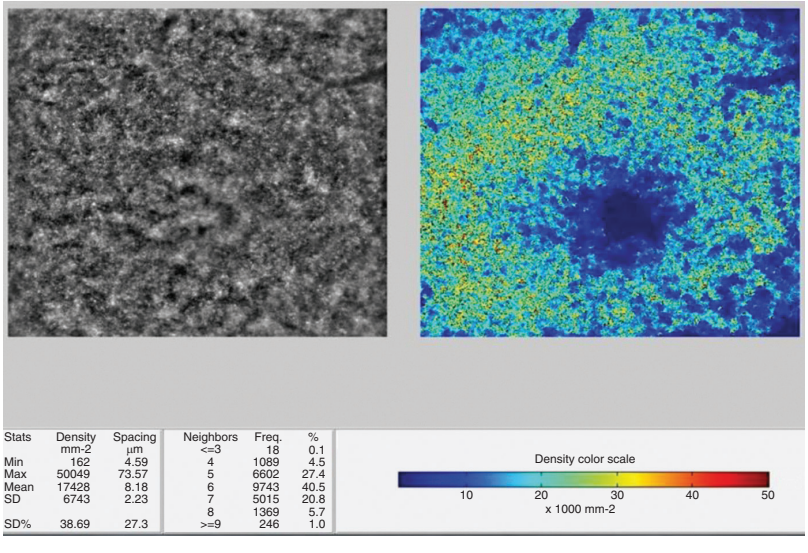

Figure 5. Voronoi teselation of cones in a 4 × 4 deg square of a normal subject. The colour scale shows the Voronoi legend

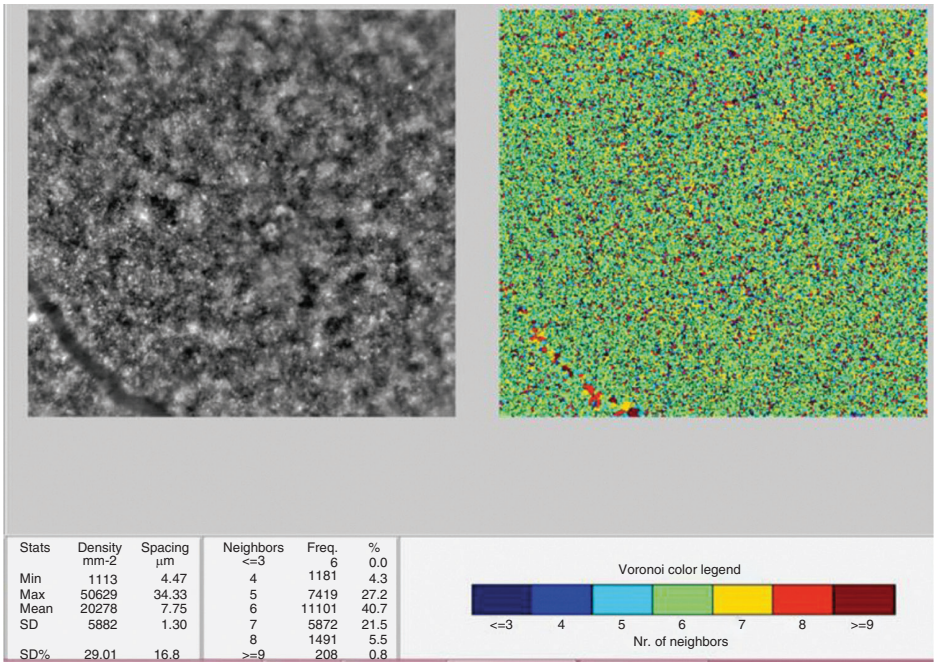

In a study by Chui et al., cone densities ranged from approximately 40,000 cones/mm^2 at 1° to 10,000 cones/mm^2 at 7° from the fovea. They also indicated that the human cone photoreceptors are arranged hexagonally near the fovea with the cones becoming more irregular as the retinal eccentricity increases, perhaps due to rod intrusion.[18] A study by Park et al. using a Canon prototype AO-SLO showed a cone density of 32,200 cells/mm^2 at 0.5 mm from the fovea, which decreased to 11,600 cells/mm^2 at 1.5 mm from the fovea.[19] They did not find demographic and clinical factors, such as gender, ocular dominance, and race/ethnicity to be determinants of cone-packing density. Only retinal eccentricity and axial length were significantly associated with measured cone-packing density.

Lombardo et al. using the rtx1 AO observed that with the exception of the central fovea (<160 µm), the photoreceptor structure was well resolved in most of the eyes. The inter-individual variation in cone density was 16%, between 260 µm and 600 µm eccentricity from the foveal center.[9] Song et al. reported that cone-packing density in the living human retina decreased as a function of age.[20]

2.2.2. AO IN MYOPIA

Axial length (AL) measurements are an important consideration in the analysis of cone-packing density. Although the mechanisms are not completely understood, it has been shown that the eye continues to grow into early adulthood, while the cones reach their final number early in development.[21] It therefore stands to reason that cone density varies across eyes with varying axial lengths.

In a population of 18 eyes of 18 healthy subjects (age range 23 to 43 years; AL range 22.86 to 28.31 mm), Li et al. found that cone density decreased significantly with increasing AL at eccentricities between 100 mm and 300 mm from the foveal center.[22]

Chui et al. reported cone-packing density variations with refractive error; they found that the cone-packing density was lower in highly myopic eyes than in emmetropic eyes at both 1.0 mm and 2.0 mm eccentricity from the foveal center.[18] They also compared differences between eyes based on simple angular density of the cones—that is, using the visual angle rather than retinal size, which required correcting the data for the axial length of the eye. They found that the cone-packing density was much more constant with axial length when expressed in cells per square degree of visual subtense than when expressed as cells per mm^2 of retinal surface area.[18]

Park et al. also found a statistically significant negative correlation between axial length and cone-packing density (decrease of 341 cell/mm^2 per 1 mm) increase in axial length.[19] Lombardo et al. also detected a higher amount of intraocular higher order aberrations in myopic eyes. The retinal stretching resulting from the increased AL in the eye has been postulated to cause the lower cone density estimated in myopic eyes.[18]

2.2.3. INHERITED RETINAL DISEASES

Inherited retinal degenerations affect about 1:2000 to 1:7000 people worldwide.[23] These are a group of disorders like Retinitis Pigmentosa (RP), Stargardt disease, Usher's syndrome and cone-rod dystrophies that are characterized by slow progressive death of rod and cone photoreceptors and relentless vision loss.[24] There is presently no definitive treatment for most of these; several therapeutic trials that are underway include stem cells, gene therapy, neuroprotective drugs and retinal prosthesis.[25–27] One limitation to the development of these modalities has been lack of sensitive outcome measures of

disease progression and response to therapy. Tests of visual function cannot be used as outcome measures as significant photoreceptor loss must have occurred before reliable significant differences are measurable in visual function. Objective sensitive measures of photoreceptor survival may reduce the time to identify treatment effect of an experimental therapy; studying surviving photoreceptors using adaptive optics may be one step in this direction. It is therefore not surprising that the majority of scientific work on the AO is dedicated to the study of photoreceptors, mostly cones (Figure 6).

Figure 6. Voronoi tessellation of photoreceptors (cones) in a patient with rod-cone dystrophy on the rtx1. The colour scale shows the packing density in the superior 100 x 100 µ (0.34x0.34 deg). In this patient, the mean cone count was 2683 ± 4006/mm^2

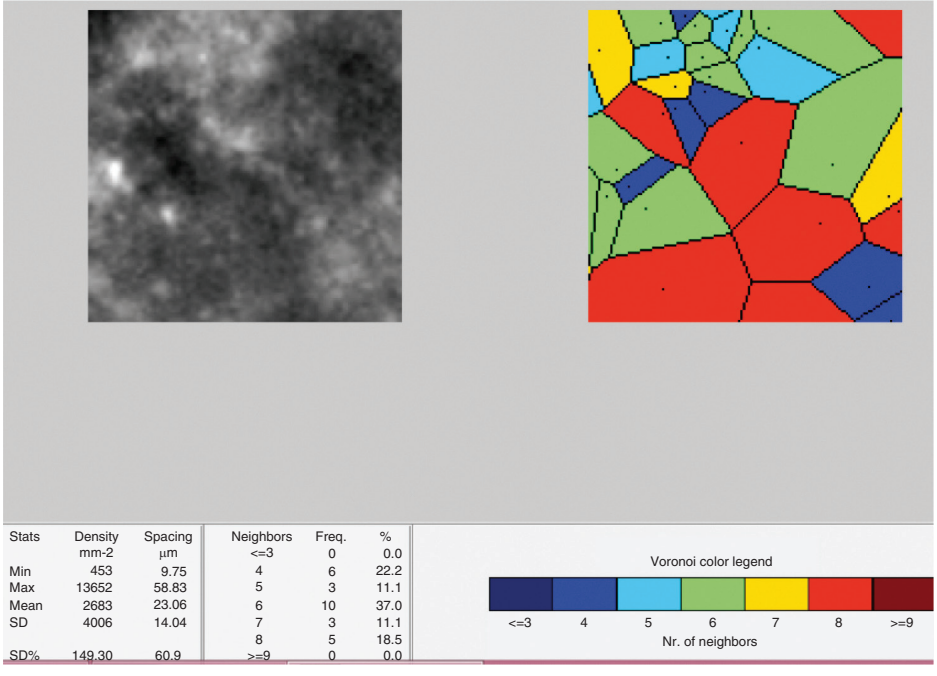

AO has been used in the following instances in the study of photoreceptors:

1) To study photoreceptor density and structure in patients with inherited retinal degenerations:

Various groups have studied the cone photoreceptor structure and their functional correlation in inherited retinal disorders. Chen et al. used AO-SLO, SD-OCT and fundus guided microperimetry to study macular cone structure, lipofuscin deposition and visual function in patients with Stargardt disease and found a correlation with abnormal autofluorescence and abnormalities of cone morphology and packing on AO with corresponding impaired function.[28]

Tojo et al. found a correlation between AO images, OCT and fundus autofluorescence (FAF) images in 2 patients with RP. They demonstrated that the edge of the high-density FAF ring (that corresponded to the border of external limiting membrane and inner segment-outer segment (IS-OS) line on OCT) showed blurring of cone photoreceptors at the ring as compared to controls on AO. They attributed this to loss of photoreceptor outer segments in patients with RP.[29]

Other studies have demonstrated the correlation of cone parameters on AO images with measures of central visual function including visual acuity, foveal threshold and multifocal electroretinogram (ERG) in patients with RP and cone-rod dysfunction. Cone spacing measures were also seen to be reproducible suggesting that these can be useful in monitoring disease progression and response to treatment.[30, 31]

Rod photoreceptors have also recently been imaged with AO-SLO and the emergence of first rods has been demonstrated at 190 µ from foveal centre as seen in histopathological studies.[32] The rod mosaic can be focused best at 10 microns, shallower than cones, at retinal eccentricities more than 8 degrees. This can open new insights into the study of rod disorders.

2) Assessment of photoreceptor function

Variations in photoreceptor reflectivity have been observed in different disease states. Photoreceptor reflectivity in AO appears to represent an optical biomarker of photoreceptor integrity. In patients with achromatopsia the remaining cones are sparse and have been shown to reduce reflectivity. Similar cone phenotype is also seen in patients with opsin mutations, acute macular neuroretinopathy (AMN) and closed globe blunt ocular trauma.[33]

Rod and cone photoreceptors have been also shown to vary in intensity over time and by developing methods to quantify this temporal variability, more insight into the health of photoreceptors may be available.[34]

3) To decide which patients will benefit the most from treatment

AO imaging of achromatopsia has revealed varying degrees of retained cone structure. Studying the structure and function of retained cones can set a baseline to assess those patients who may benefit from gene therapy (as has been successful in dog and mouse models) and to anticipate the degree of functional improvement that can be expected based on the patient's baseline cone count.[14] Hence, it can help prioritize those patients who can undergo trial of gene therapy (i.e. those with certain number of retained cones) over patients who may not benefit from therapy (those with absent cones).

4) Monitoring response to treatment

In a study by Talcott et al., AOSLO was used to longitudinally study the cone spacing and density in 3 patients implanted with Ciliary Neurotrophic Factor (CNTF) encapsulated implant.[35] While other modalities like visual field sensitivity and electroretinography responses did not show significant changes at 24 months, AOSLO images showed significantly reduced rates of cone loss in CNTF-treated eyes. Longitudinal imaging and monitoring of individual cones was also done and they concluded that AOSLO provided a sensitive measure of disease progression and treatment responses in patients with retinal degenerations.

2.2.4. VASCULAR ANALYSIS ON AO

Imaging and analysis of the retinal vasculature can be a surrogate marker for systemic vascular health. Correlations between vascular abnormalities in the retina and elsewhere in the body have been demonstrated in a diverse array of conditions including diabetes, hypertension, stroke and migraine. The earliest change in disease begins at the level of the microvasculature; however, current imaging methods lack the lateral resolution to track blood flow at the capillary level.[36] Imaging retinal capillaries

is difficult because of their small size, low contrast and arrangement in multiple planes of varying retinal depth.

Due to its high-magnification, resolution, and real time visualization, it is possible to observe details of vascular wall and contents using AO (Figure 7). Lombardo et al. used an AO flood-illumination retinal camera and described a characteristic pattern of the lumen of a blood vessel, consisting of a central high-intensity channel and two peripheral darker channels. They attributed this difference in intensity to the curvature of the vessel wall and the different shear rate of erythrocytes.[37] In a subset of diabetics, they showed the capillary lumen caliber to be significantly narrower in non-proliferative diabetic retinopathy eyes than age matched controls.[34]

Figure 7. High-resolution image of the venule and arteriole. The black arrow points to the vessel wall (venule). Note the defocused retinal nerve fibre layer in the background

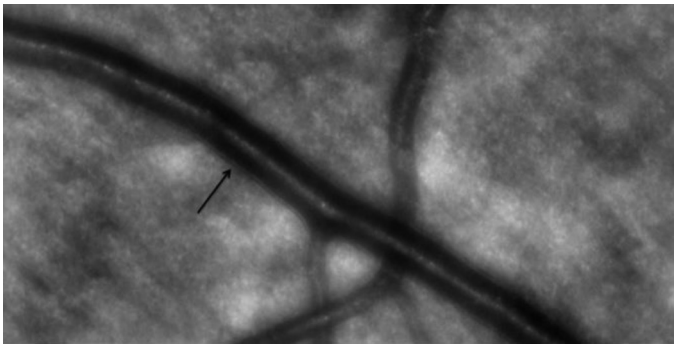

Martin and Roorda imaged parafoveal capillary leukocyte movement and measured their velocity without contrast dyes. A follow-up study investigated the possible role of the cardiac cycle on capillary leukocyte velocity by directly measuring capillary leukocyte pulsatility.[38]

The detection of preclinical abnormalities of retinal microcirculation may potentially represent an additional advantage of AO retinal imaging in patients with diabetes and cardiovascular diseases. Tam et al. evaluated the parafoveal capillary network in patients with Type 2 diabetes. They showed a capillary dropout and a higher tortuosity of the arteriovenous channels in patients with no retinopathy compared to healthy controls.[39] Popovic et al. imaged the foveal capillary networks of five healthy subjects with no previous history of ocular or neurologic disease or surgery with a novel high-resolution, wide-field dual-conjugate adaptive optics (DCAO) imaging instrument.[39]

Their results showed a mean foveal avascular zone (FAZ) area of 0.302 ± 0.100 mm^2 and mean equivalent diameter of 612±106 µm.[40]

2.3. CLINICAL LIMITATIONS AND FUTURE PROSPECTS OF ADAPTIVE OPTICS

As adaptive optics imaging finds more clinical applications, normative databases need to be developed for different populations as a reference for disease states. Universally acceptable standards and protocols need to be defined for image acquisition and analysis to ensure reproducibility and comparability worldwide. Acquisition of AO images of sufficient quality to perform quantitative cone spacing measures is difficult in patients with unstable fixation, dense cataracts and other media opacities. The use of AO may be limited owing to costs and lack of expertise.

In summary, AO is an innovative new tool in the extensive armamentarium of ophthalmologists to explore the cellular details of the retina. It may help us understand the pathogenesis of diseases at a subclinical stage, thus paving way for the exciting possibility of early treatment for these diseases. It is possible that as more detailing of cellular structures becomes possible, we may need to develop better analytical tools. As treatment paradigms for inherited retinal diseases evolve, it is likely that AO systems will play a major role in early diagnosis and monitoring therapies.

REFERENCES

1. Colenbrander A. Principles of ophthalmoscopy. In: Tasman W, Jaeger EA, eds. *Duane's Ophthalmology.* Vol 1. 2013:chap 63.
2. Atebara NH, Miller D, Thall EH. Ophthalmic instrumentation. In: Yanoff M, Duker JS, eds. *Ophthalmology.* Philadelphia, PA: Elsevier; 2008:chap 2.10.
3. Meyer-Schwickerath GR. Ophthalmology and photography. *Am J Ophthalmol.* 1968;66:1011–1019.
4. Mainster MA, Timberlake GT, Webb RH, Hughes GW. Scanning laser ophthalmoscopy: clinical applications. *Ophthalmology.* 1982;89(7):852–857.
5. Puliafito CA, Hee MR, Lin CP, et al. Imaging of macular diseases with optical coherence tomography. *Ophthalmology.* 1995;102(2):217–229.
6. Lombardo M, Lombardo G. Wave aberration of human eyes and new descriptors of image optical quality and visual performance. *J Cataract Refract Surg.* 2010;36(2):313–331.
7. Babcock HW. Adaptive optics revisited. *Science.* 1990;249(4966):253–257.
8. Lombardo M, Serrao S, Ducoli P, Lombardo G. Eccentricity dependent changes of density, spacing and packing arrangement of parafoveal cones. *Ophthalmic Physiol Opt*. 2013;33(4):516–526.
9. Duncan JL, Zhang Y, Gandhi J, et al. High-resolution imaging with adaptive optics in patients with inherited retinal degeneration. *Invest Ophthalmol Vis Sci.* 2007;48(7):3283–3291.
10. Torti C, Považay B, Hofer B, et al. Adaptive optics optical coherence tomography at 120,000 depth scans/s for non-invasive cellular phenotyping of the living human retina. *Opt Express*. 2009;17(22):19382–19400.
11. Zhang Y, Roorda A. Evaluating the lateral resolution of the adaptive optics scanning laser ophthalmoscope. *J Biomed Opt.* 2006;11(1):014002.
12. Godara P, Dubis AM, Roorda A, Duncan JL, Carroll J. Adaptive optics retinal imaging: emerging clinical applications. *Optom Vis Sci.* 2010;87(12):930–941.
13. Lombardo M, Lombardo G, Ducoli P, Serrao S. Adaptive optics photoreceptor imaging. *Ophthalmology.* 2012;119(7):1498–1498e2.

14. Carroll J, Kay DB, Scoles D, Dubra A, Lombardo M. Adaptive optics retinal imaging–clinical opportunities and challenges. *Curr Eye Res.* 2013;38(7):709–721.

15. Kim JE, Chung M. Adaptive optics for retinal imaging: current status. *Retina*. 2013;33:1483–1486.

16. Lombardo M, Serrao S, Devaney N, Parravano M, Lombardo G. Adaptive optics technology for high-resolution retinal imaging. *Sensors.* 2013;13(1):334–366.

17. Alpern M, Ching C, Kitahara K. The directional sensitivity of retinal rods. *J Physiol*. 1983;343(1):577–592.

18. Chui TYP, Song H, Burns SA. Adaptive-optics imaging of human cone photoreceptor distribution. *J Opt Soc Am A Opt Image Sci Vis.* 2008;25(12):3021–3029.

19. Park SP, Chung JK, Greenstein V, Tsang SH, Chang S. A study of factors affecting the human cone photoreceptor density measured by adaptive optics scanning laser ophthalmoscope. *Exp Eye Res.* 2013;108:1–9.

20. Song H, Chui TYP, Zhong Z, Elsner AE, Burns SA. Variation of cone photoreceptor packing density with retinal eccentricity and age. *Invest Ophthalmol Vis Sci.* 2011;52(10):7376–7384.

21. Grosvenor T, Scott R. Role of the axial length/corneal radius ratio in determining the refractive state of the eye. *Optom Vis Sci*. 1994;71(9):573–579.

22. Li KY, Tiruveedhula P, Roorda A. Intersubject variability of foveal cone photoreceptor density in relation to eye length. *Invest Ophthalmol Vis Sci.* 2010;51(12):6858–6867.

23. Fasiuddin A. Inherited retinal degenerations. *Int Ophthalmol Clin*. 2010;50(4):45–56.

24. Hartong DT, Berson EL, Dryja TP. Retinitis pigmentosa. *Lancet.* 2006;368(9549):1795–1809.

25. Stone EM. Progress toward effective treatments for human photoreceptor degenerations. *Curr Opin Genet Dev*. 2009;19(3):283–289.

26. Huang Y, Enzmann V, Ildstad ST. Stem cell-based therapeutic applications in retinal degenerative diseases. *Stem Cell Rev.* 2011;7(2):434–445.

27. Farrar G, Millington-Ward S, Chadderton N, Humphries P, Kenna P. Gene-based therapies for dominantly inherited retinopathies. *Gene Ther.* 2012;19(2):137–144.

28. Chen Y, Ratnam K, Sundquist SM, et al. Cone photoreceptor abnormalities correlate with vision loss in patients with Stargardt disease. *Invest Ophthalmol Vis Sci.* 2011;52(6):3281–3292.

29. Tojo N, Nakamura T, Fuchizawa C, Oiwake T, Hayashi A. Adaptive optics fundus images of cone photoreceptors in the macula of patients with retinitis pigmentosa. *Clin Ophthalmol.* 2013;7:203.

30. Wolfing JI, Chung M, Carroll J, Roorda A, Williams DR. High-resolution retinal imaging of cone–rod dystrophy. *Ophthalmology.* 2006;113(6):1014–1019.e1.

31. Choi SS, Doble N, Hardy JL, et al. In vivo imaging of the photoreceptor mosaic in retinal dystrophies and correlations with visual function. *Invest Ophthalmol Vis Sci.* 2006;47(5):2080–2092.

32. Dubra A, Sulai Y, Norris JL, et al. Noninvasive imaging of the human rod photoreceptor mosaic using a confocal adaptive optics scanning ophthalmoscope. *Biomed Opt Express.* 2011;2(7):1864–1876.

33. Genead MA, Fishman GA, Rha J, et al. Photoreceptor structure and function in patients with congenital achromatopsia. *Invest Ophthalmol Vis Sci.* 2011;52(10):7298–7308.

34. Cooper RF, Dubis AM, Pavaskar A, Rha J, Dubra A, Carroll J. Spatial and temporal variation of rod photoreceptor reflectance in the human retina. *Biomed Opt Express.* 2011;2(9):2577–2589.

35. Talcott KE, Ratnam K, Sundquist SM, et al. Longitudinal study of cone photoreceptors during retinal degeneration and in response to ciliary neurotrophic factor treatment. *Invest Ophthalmol Vis Sci.* 2011;52(5):2219–2226.

36. Bedggood P, Metha A. Direct visualization and characterization of erythrocyte flow in human retinal capillaries. *Biomed Opt Express.* 2012;3(12):3264–3277.

37. Lombardo M, Parravano M, Serrao S, Ducoli P, Stirpe M, Lombardo G. Analysis of retinal capillaries in patients with type 1 diabetes and nonproliferative diabetic retinopathy using adaptive optics imaging. *Retina*. 2013;33(8):1630–1639.

38. Martin JA, Roorda A. Direct and noninvasive assessment of parafoveal capillary leukocyte velocity. *Ophthalmology.* 2005;112(12):2219–2224.

39. Tam J, Martin JA, Roorda A. Noninvasive visualization and analysis of parafoveal capillaries in humans. *Invest Ophthalmol Vis Sci.* 2010;51(3):1691–1698.

40. Popovic Z, Knutsson P, Thaung J, Owner-Petersen M, Sjöstrand J. Noninvasive imaging of human foveal capillary network using dual-conjugate adaptive optics. *Invest Ophthalmol Vis Sci.* 2011;52(5):2649–2655.

CHAPTER 3

VARIATIONS IN THE CONE-PACKING DENSITY WITH ECCENTRICITY IN EMMETROPES

Supriya Dabir, Shwetha Mangalesh, Anupama Kiran Kumar,
Mathew Kurian Kummelil, Abhijit Sinha Roy, Rohit Shetty

EYE (LONDON) 2014;28:1488–1493

ABSTRACT

AIM

To describe the parafoveal cone arrangement in emmetropic subjects and it's variations with eccentricity, meridians and change in axial length in Indian eyes.

METHODS

We imaged 25 subjects using compact adaptive optics (AO) retinal camera prototype, the rtx1 (Imagine Eyes, Orsay, France). Imaging was done at 1, 2 and 3 degrees eccentricity from the fovea in 4 meridians: nasal, temporal, superior and inferior.

RESULTS

A statistically significant drop of the cone-packing density was observed from 2 degrees to 3 degrees [2 degrees eccentricity = 25350/mm^2 (5300/mm^2, 8400/mm^2 –34800/mm^2) 3 degrees eccentricity = 20750/mm^2 (6000mm^2, 9000/mm^2–33670/mm^2)] $P<0.05$. The spacing correspondingly increased with increase in distance from the fovea (2 degrees eccentricity = 6.9 µm (0.70 µm, 5.95–11.6 µm) and 3 degrees eccentricity= 7.80 µm (1.00 µm, 6.5–13.5 µm) $P<0.05$. As the axial length increases, the cone density significantly decreased. Interocular variations were noted.

CONCLUSION

With the advent of adaptive optics, visualization at cellular level in now possible. Understanding the photoreceptor mosaic in the parafoveal space in terms of its density, spacing and arrangement is crucial so as to detect early pathology and intervene appropriately. Newer therapeutic modalities that are targeted at the cellular level like yellow micropulse laser, stem cells, gene therapy etc. may be better monitored in terms of safety and efficacy.

Keywords: Cone density, parafovea, adaptive optics, emmetropia, axial length.

3.1. INTRODUCTION

Retinal imaging is challenging because of aberrations caused by the tear film, cornea, lens and internal reflections of eye. Fundus cameras eliminate spherical aberrations, however, adaptive optics (AO) technology has made it possible to correct lower- and higher-order aberrations, allowing better visualization of microscopic structures.[1,2]

Understanding the normal lattice arrangement of photoreceptors' aids in detecting early signs of disease and initial assessment of therapeutic regimes like yellow laser, gene therapy, stem cell therapy etc.[1]

The scope of our article is to describe the parafoveal cone arrangement, their variations with eccentricity and interocular symmetry in emmetropic Indian eyes.

3.2. MATERIALS AND METHODS

3.2.1. SUBJECTS

Twenty-five healthy subjects were included in the prospective study. The study was approved by the institutional review board of the hospital and adhered to the tenets of Helsinki declaration. An informed consent was obtained from all subjects to whom the nature of study was explained. They underwent a comprehensive ophthalmic examination. Normal eyes were defined as emmetropic subjects or those with best correct visual acuity of 20/20 or better with astigmatism less than 2 diopters. Subjects with ocular or systemic diseases or previous eye surgery were excluded from the study. All subjects underwent assessment with the Tonoref RKT-7000 autorefractometer, Nidek, non-contact biometry (IOL master; Carl Zeiss Meditec, Germany) for axial length, I trace (Tracey technologies Corp., Houston, TX, USA) for corneal aberrations and spectral-domain optical coherence tomography (Spectralis, Heidelberg) for central foveal thickness. A compact AO retinal camera prototype, the rtx1 (Imagine Eyes, Orsay, France), was used to image the photoreceptor layer. Core components of the apparatus include a Shack–Hartmann wave front sensor (HASO 32-eye; Imagine Optics, Orsay, France), a deformable mirror (MIRAO 52; Imagine Optics) and a low-noise high-resolution camera (Roper Scientific, Tucson, AZ, USA).

3.2.2. METHODS

In this study, the AO imaging sessions were conducted after dilating the pupils with 1 drop each of 0.5% tropicamide and 10% phenylephrine hydrochloride to achieve mid-dilated pupils. Aberrations induced by pupil dilation are negated by the AO system. Stable fixation was maintained by having the patient look at the system's inbuilt target and then as

moved by the investigator to pre-determined coordinates. The patient was instructed to fixate at 0°, 1°, 2° and 3° eccentricity along all the four quadrants, superior, inferior, nasal and temporal retina. A video (i.e. a series of 40 frames; 4° field size) was captured at each of the above retinal locations. After the acquisition, a program provided by the manufacturer correlated and averaged the captured image frames to produce a final image.[3]

Cone density (cones/mm^2) was measured at 1°, 2° and 3° eccentricity along all the four quadrants, superior, inferior, nasal and temporal retina. There has been no standardized protocol on which areas to image and size of the sampling window to choose the region of interest. The sampling window we choose was 100 µm and we placed it at specific coordinates calculated by a prefixed formula intentionally avoiding blood vessels. Our rationale was that the size of the sampling window correlates with the size of the retinal area stimulated by a Goldman size III target, so as to be able to correlate structure-function in the future. Eccentricity was computed as the distance between the center of each window and the foveal center reference point (identified as the point with fixation coordinates: x = 0°, y = 0°). The images were captured at temporal (–3°, 0°), superior (0°, 3°), nasal (3°, 0°) and inferior (0°, –3°), as seen in Figure 1. The cone counting software AO detect created on MATLAB by Imagine Eyes was used to process the images and calculate the cone density, spacing and Voronoi. The cone density was verified by three investigators (SD, SM and AK) in order to minimize the possible error in cone identification of the automated software. The inter-observer variability was tested by three observers. The images of all the 25 subjects were analysed using the AO detect (Imagine Eyes, Orsay, France) by each observer separately and the results were noted. The variability in choosing the region of interest (ROI) and the value of the cone counts was noted between the observers and the closest two values were considered for the interpretation of the results. The subjects were imaged twice at two different time intervals and were analyzed separately. The variation in the cone count was assessed.

Figure 1. Sampling windows showing the cone mosaic at (a) 1° eccentricity (b) 2° eccentricity and (c) 3° eccentricity respectively

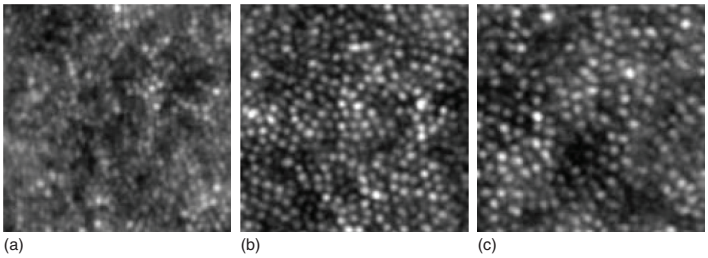

3.2.3. STATISTICAL ANALYSIS

Statistical analysis was performed using the SPSS 17 statistics software program (SPSS Inc., Chicago, IL, USA). The Shapiro-Wilk Test was applied to note the distribution of data. We applied the Friedman's analysis of variation in packing density, spacing and voronoi at different eccentricities and quadrants and a post hoc test with Bonferroni correction was applied to the significance level. Mann-Whitney *U* test was applied to check for interocular variability in the cone-packing density. A simple linear regression was applied to analyze the variation in cone density with axial length.

3.3. RESULTS

The study group comprised of 14 females and 11 males between the ages of 20–40 years, as seen in Table 1. The axial length and spherical equivalent ranged between 21.53–24.9 mm and –0.24 to + 0.13D respectively. The cone count, spacing and Voronoi D (50) p = 0.000 were significantly non-normal in distribution.

Cone-packing density, spacing and Voronoi were analyzed for the 4 quadrants and the eccentricities separately, as seen in Figure 2. The cone density was found to be significantly different among all the four quadrants (temporal = 25900/mm^2 (6100/mm^2, 15000/mm^2–34800/mm^2), superior = 21600/mm^2 (7400/mm^2, 12200/mm^2–33700/mm^2), nasal = 23100/mm^2 (4400/mm^2, 9000/mm^2–32700/mm^2) and inferior = 20400/mm^2 (6900/mm^2, 8400/mm^2–30200/mm^2). A statistical significance (P<0.008) was found between the orthogonal meridians i.e. temporal, nasal > superior, inferior (temporal + nasal= 49000/mm^2 > superior + inferior = 42000/mm^2).

Table 1. Demographics of the study group

Demographics	Values
Total no. of eyes	25 eyes of 25 volunteers
Age group	20–40 years
Sex (male: female)(%)	11: 14 (44: 56%)
Axial length (range)	21.53–24.9 mm
Spherical equivalent (range)	-0.24D- +0.13D

A similar result was observed in the spacing between the cones in the various quadrants temporal = 6.90 µm (0.80 µm, 5.95–8.8 µm), superior = 7.60 µm (1.1 µm, 5.95–13.5 µm), nasal = 7.20 µm (0.90 µm, 6.05–11.20 µm) and inferior = 7.80 µm (0.90 µm, 6.30–11.60 µm). Temporal, nasal < superior, inferior (temporal + nasal = 14.1 µm < superior + inferior = 15.40 µm) was found to be statistically significant (P<0.008).

Figure 2. Box plots showing the (a) average cone density distribution in the 4 quadrants, inferior, nasal, superior and temporal; (b) average cone density distribution at different retinal eccentricities; (c) Voronoi analyses at different retinal eccentricities

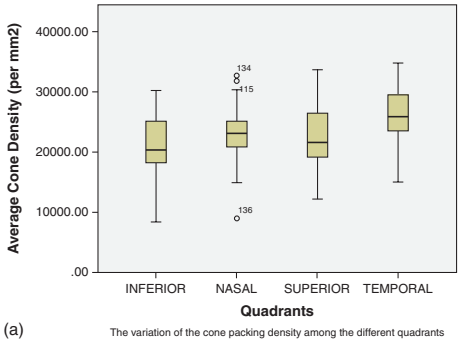

(a) The variation of the cone packing density among the different quadrants

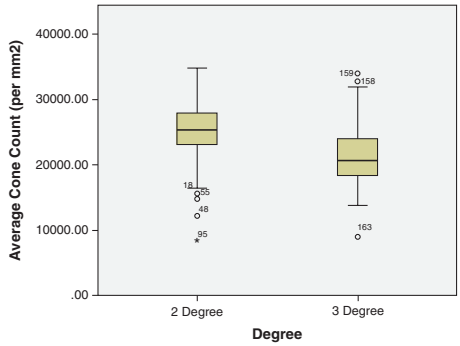

(b) Variation in the Average Cone Count at different eccentricities

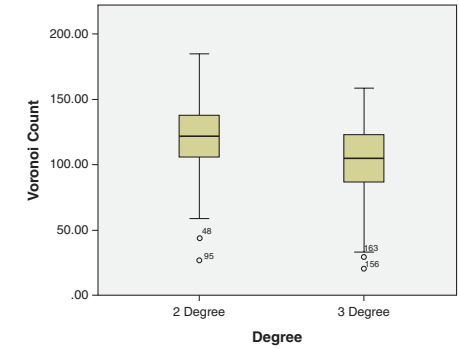

(c) The number of hexagonal cones at different retinal eccentricities

A statistically significant drop of the cone-packing density was observed from 2 degrees to 3 degrees (2 degrees eccentricity = 25350/mm^2 (5300/mm^2, 8400/mm^2–34800/mm^2) 3 degrees eccentricity = 20750/mm^2 (6018/mm^2, 9000/mm^2–33670/mm^2) P<0.05. The spacing correspondingly increased as we moved away from the fovea (2 degrees eccentricity = 6.9μm (0.73μm, 5.95μm–11.6μm) and 3 degrees eccentricity = 7.80μm (1.00μm, 6.5μm–13.5μm) P<0.05.

Voronoi analysis was done to assess if the cone-packing was regular. The number of hexagonal cones were counted and analyzed at the various quadrants and degrees. It was observed that the number of hexagonal cones decreased from 2 degrees to 3 degrees (2 degrees eccentricity =122 and 3 degrees eccentricity = 105) and this observation was found to be statistically significant (P<0.05).

Table 2. Variation in cone-packing density and spacing in the 4 meridians at different retinal eccentricities

	Cone Count		Spacing		P-value
	2° Eccentricity	3° Eccentricity	2° Eccentricity	3° Eccentricity	
Temporal	29500	24500	6.4	8.1	P=0.000 (P<0.008)
Superior	25700	19300	7.0	8.0	P=0.000 (P<0.008)
Nasal	24000	23000	7.1	7.3	P=0.000 (P<0.008)
Inferior	24600	18400	7.0	8.1	P=0.000 (P<0.008)

Table 3. Interocular variability in the cone-packing density

	2° Eccentricity	3° Eccentricity	P-value[a]
Right eye	25200	21100	P=0.534 (P<0.05)
Left eye	21400	20600	

[a]Mann-Whitney *U* test.

Difference was also noted in the number of hexagonal cones between the four quadrants (P<0.05). The agreement between the three observers was found to be 0.57. The difference was found to be in the selection of the ROI between the observers and hence a difference of ± 2000/mm^2. The subjects were imaged at two different intervals in the same locations to note the variability in the cone count.

The difference in the cone counts between the images was found, although the difference was not statistically significant (p=0.453).

We also noted the mean cone count at 1 degree [23000/mm^2 (2800/mm^2–32000/mm^2)]. However, counts at or closer than one degree to the foveal center was not considered for statistical analysis due to the unreliable values obtained from images near the fovea.

Interocular variability was analyzed at the different retinal eccentricities in all the quadrants, as seen in Table 3. No statistically significant difference was found in the cone-packing density between the two eyes (p=0.534).

A negative correlation was observed between cone density and axial length at both 2 and 3 degrees, which was found to be statistically significant (R^2 = 0.147 p=<0.05 and R^2 = 0.236 P<0.05), as seen in Figure 3.

Figure 3. Scatter plot depicting the relation between cone-packing density and axial length at (a) 2° eccentricity and (b) 3° eccentricity respectively

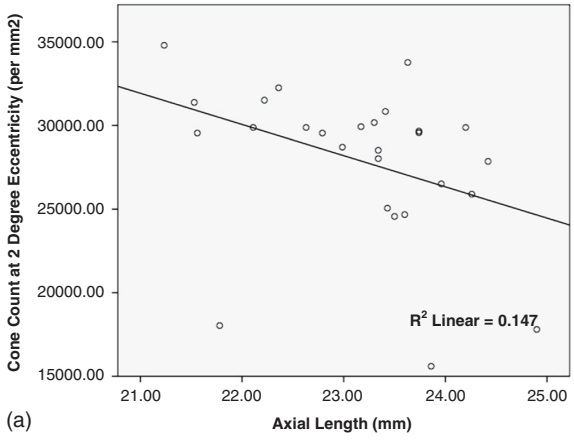

(a)

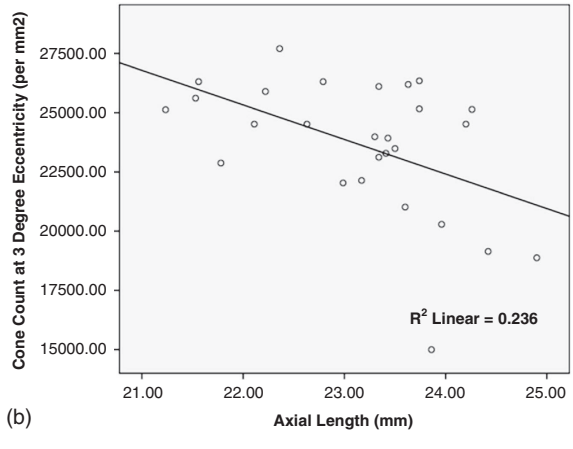

(b)

3.4. DISCUSSION

The average human retina contains 4.6 million cones (4.08–5.29 million). Peak foveal cone density averages 199,000 cones/mm^2 and is highly variable between individuals (100,000–324,000 cones/mm^2).[4]

Curcio et al. (1990)[4] studied the histology of eight eyes and found individual variations in cone density differ with retinal region, highest being near the fovea, least in the midperiphery and an increase again towards the ora serrata.

In our current study, we found the average cone-packing densities at 1, 2 and 3 degrees from the fovea. At 1 degree, the counts were erroneous due to dense packing of the cones and hence the software was unable to count the cones which were smaller than 2 µm, or the spacing was less than 2 µm, leading to a gross under sampling of the cone density. Hence they were not utilized for statistical analysis. The counts at 2 and 3 degrees were approximately 25,350/mm^2 (5,300/mm^2, 8,400/mm^2–34,800/mm^2) to 20,750/mm^2 (6,018/mm^2, 9,000/mm^2–33,670/mm^2) $P<0.05$. Park et al. (2013)[5] in their study found the cone density decreased from 32,200 to 11,600 cells/mm^2 with retinal eccentricity (0.5 mm to 1.5 mm from the fovea, $P < 0.001$). Lombardo et al. (2013)[6] found an average decline of cone density from 51,000 cones/mm^2 at 250 mm eccentricity to 14,000 cones/mm^2 at 1,300 mm eccentricity along the horizontal meridian.

The numerical variation between the published western literature and our study could be because of various factors such as eyes with different axial lengths, the location of the foveal reference point, the difference in the sampling window size and the non-standardized approach used to calculate cone distribution among the various studies.[5,6] Some have a manual addition to the automated software and a few have used special tools with MATLAB software.[5]

Lombardo et al. (2013)[1] have discussed the various technical differences between the Voronoi maps created using images of the photoreceptor mosaic acquired using different systems, i.e. flood-illumination and SLO-based. Some of them are due to differences in the brightness and contrast of the various types of cone mosaics, effect of rods and retinal vessels and image processing tools.

We have described the distribution of density, spacing and the hexagonal-packing arrangement of the cone photoreceptors at different retinal eccentricities across the

parafovea in emmetropic young adults. It is essential to establish normative data so as to be able to detect early onset of pathology at cellular level and accordingly intervene early.

Park et al. (2013)[5] compared cone-packing density in the 4 meridians at different eccentricities of 0.5 mm, 1 mm and 1.5 mm and found no significant difference, with the exception of 1.0 mm eccentricity. At 1.0 mm eccentricity, there were significant differences in cone-packing density between the orthogonal meridians ($P < 0.001$; nasal, temporal > superior, inferior). We found the highest density to be in the temporal meridian followed by superior, nasal and inferior at both the eccentricities of 2 and 3 degrees. Our pattern describes the horizontal packing of cones to be denser than the vertical meridian, as noted by the various histological studies.[4,7]

As cone density decreases with increasing distance from fovea, the spacing will accordingly increase. We found the average spacing increase from a mean of 7.08 µm at 2 degrees to 7.86 µm at 3 degrees. Lombardo et al. (2013)[3] found the eccentricity increase from an average of 4.50 to 8.20 µm from 250 to 1100 µm, which is similar to our data.

Axial length played a significant role in our study as has been proved by multiple studies[5,8,9] so far. As the axial length increased, the cone count significantly decreased, following the hypothesis of posterior pole being stretched and the cones getting distributed along a larger surface area. The coefficient of variation between the two eyes of each patient was 30.7% at 2 degrees and 21% at 3 degrees.

The limitation of our study was the absence of a manual addition to the existing automated software to count missed cones, small sample size and the data presented was limited to 3 degrees eccentricity.

3.5. CONCLUSION

There has been no literature published thus far from the Indian population and our work may help in the development of normative database of individual variations in emmetropic subjects. This allows us to understand early pathology at the cellular level and intervene appropriately. Newer therapeutic modalities that are targeted at the cellular level like yellow micropulse laser, stem cells, gene therapy etc. may be better monitored in terms of safety and efficacy.

REFERENCES

1. Lombardo M, Serrao S, Devaney N, Parravano M, Lombardo G. Adaptive optics technology for high-resolution retinal imaging. *Sensors*. 2013;13(1):334–366.
2. Chui TY, Song H, Burns S. Adaptive-optics imaging of human cone photoreceptor distribution. *J Opt Soc Am A Opt Image Sci Vis*. 2008;25(12):3021–3029.
3. Lombardo M, Serrao S, Ducoli P, Lombardo G. Eccentricity dependent changes of density, spacing and packing arrangement of parafoveal cones. *Ophthalmic Physiol Opt.* 2013;33(4):516–526.
4. Curcio C, Sloan K, Kalina R, Hendrickson A. Human photoreceptor topography. *J Comp Neurol.* 1990;292(4):497–523.
5. Park S, Chung J, Greenstein V, Tsang S, Chang S. A study of factors affecting the human cone photoreceptor density measured by adaptive optics scanning laser ophthalmoscope. *Exp Eye Res.* 2013;108:1–9.
6. Lombardo M, Lombardo G, Schiano Lomoriello D, Ducoli P, Stirpe M, Serrao S. Interocular symmetry of parafoveal photoreceptor cone density distribution. *Retina*. 2013;33(8):1640–1649.
7. Curcio C, Sloan K. Packing geometry of human cone photoreceptors: variation with eccentricity and evidence for local anisotropy. *Vis Neurosci*. 1992;9(2):169–180.
8. Lombardo M, Serrao S, Ducoli P, Lombardo G. Variations in image optical quality of the eye and the sampling limit of resolution of the cone mosaic with axial length in young adults. *J Cataract Refract Surg.* 2012;38(7):1147–1155.
9. Chui T, Song H, Burns S. Individual variations in human cone photoreceptor packing density: variations with refractive error. *Invest Ophthalmol Vis Sci.* 2008;49(10):4679–4687.

CHAPTER 4

AXIAL LENGTH AND CONE DENSITY AS ASSESSED WITH ADAPTIVE OPTICS IN MYOPIA

Supriya Dabir, Shwetha Mangalesh, Jan S A G Schouten,
Tos T J M Berendschot, Mathew Kummelil Kurian,
Anupama Kiran Kumar, Naresh K Yadav, Rohit Shetty

INDIAN JOURNAL OF OPHTHALMOLOGY 2015; 63:423–426

ABSTRACT

AIM

To assess the variations in cone mosaic in myopia and its correlation with axial length (AL).

SUBJECTS AND METHODS

Twenty-five healthy myopic volunteers underwent assessment of photoreceptors using adaptive optics retinal camera at 2° and 3° from the foveal center in four quadrants superior, inferior, temporal and nasal. Data were analyzed using SPSS version 17 (IBM). Multivariable regression analysis was conducted to study the relation between cone density and AL, quadrant around the fovea and eccentricity from the fovea.

RESULTS

The mean cone density was significantly lower as the eccentricity increased from 2° from the fovea to 3° (18,560 ± 5455 to 16,404 ± 4494/mm^2 respectively). There was also a statistically significant difference between four quadrants around the fovea. The correlation of cone density and spacing with AL showed that there was a significant inverse relation of AL with the cone density.

CONCLUSION

In myopic patients with good visual acuity, cone density around the fovea depends on the quadrant, distance from the fovea as well as the AL. The strength of the relation of AL with cone density depends on the quadrant and distance.

Keywords: Adaptive optics, axial length, cone density, myopia.

4.1. INTRODUCTION

Myopia is a common visual imperfection mostly due to an increase in the axial length (AL) of the eye. It can lead to severe visual loss when myopic degeneration develops. It may also cause both lower as well as higher-order aberrations.[1] In a less severe stage, its vision loss can be corrected with glasses or contact lenses. Even with glasses the quality of vision with best-corrected visual acuity of 20/20 between myopes and emmetropes is not the same, and this may be due to multiple anatomical and physiological factors.[2–6] These could include the spatial distribution and orientation of the photoreceptors stretched along the posterior pole of the retina due to a larger AL in a myopic eye. It is to be expected that the cone density decreases with increasing myopia.[7–9] However, to what extent this occurs in relation to changes in the AL or extent of the refractive error is largely unknown. With the advent of adaptive optics (AO) technology in vision science, it is now feasible to determine the photoreceptor cone distribution.[7–9] In this study, we measured the variations in the cone mosaic in a population of young myopic adults in relation to the AL and extent of the refractive error. This may help to understand the missing link between increasing severity of myopia and changes in the visual acuity or quality of vision in patients with myopia and enhance the opportunity to monitor essential anatomic changes in myopia.

4.2. SUBJECTS AND METHODS

4.2.1. SUBJECTS

Twenty-five consecutive patients who, visited the comprehensive out-patient and the refractive out-patient departments, with myopia within the age group of 20–40 years, were included in the prospective study. An informed consent was obtained from all subjects, and the nature of the study was explained to them. The study adhered to the tenets of the declaration of Helsinki and was approved by the Ethics Committee and review board of the hospital. The patients in the study group were those who presented with myopia with the spherical equivalent between −1D and −12D and best corrected visual acuity of 20/20. Pathological myopia, and those with any ocular or systemic pathology were not included in the study and all patients enrolled had a clinically normal fundus. We grouped the myopes as low, moderate and high based on their spherical equivalent (mild being 1D–3D, moderate = 3D–6D and high >6D) for analysis.

All the subjects underwent a comprehensive ophthalmic examination including an assessment with the Tonoref RKT-7000 autorefractometer, Nidek, non-contact biometry (IOL master; Carl Zeiss Meditec, Germany) for AL and spectral-domain optical coherence tomography (Spectralis, Heidelberg) for central foveal thickness. A compact AO retinal camera prototype, the rtx 1 (Imagine Eyes, Orsay, France), was used to image the photoreceptor layer.

4.2.2. ADAPTIVE OPTICS IMAGING

As mentioned in our previous study on emmetropes,[10] the AO imaging sessions were conducted after dilating the pupils with 1 drop each of 0.5% tropicamide and 10% phenylephrine hydrochloride to achieve mid-dilated pupils. Aberrations induced by pupil dilation are negated by the AO system. Stable fixation was maintained by having the patient look at the system's inbuilt target and then as moved by the investigator to predetermined coordinates. The patient was instructed to fixate at 0°, 1°, 2° and 3° eccentricity along all the four quadrants, superior, inferior, nasal and temporal retina. A video (i.e. a series of 40 frames; 4° field size) was captured at each of the above retinal locations. After the acquisition, a program provided by the manufacturer correlated and averaged the captured image frames to produce a final image. Cone density (cones/ mm^2) was measured at 1°, 2° and 3° eccentricity along all the four quadrants, superior, inferior, nasal and temporal retina. There has been no standardized protocol on which areas to image and size of the sampling window to choose the region of interest. The sampling window we choose was 100 μ and we placed it at specific coordinates calculated by a prefixed formula intentionally avoiding blood vessels. Eccentricity was computed as the distance between the center of each window and the foveal center reference point (identified as the point with fixation coordinates: x = 0°, y = 0°). The images were captured at temporal (−3°, 0°), superior (0°, 3°), nasal (3°, 0°) and inferior (0°, −3°).[10] The cone counting software AO detect created on MATLAB by Imagine eyes was used to process the images and calculate the data. The repeatability has been mentioned in our previous study.

4.2.3. DATA ANALYSIS

The statistical analysis was performed using the IBM SPSS version 20 (SPSS Inc. Chicago, ILa, USA) and MedCalc version 11. The Shapiro–Wilk test was performed to determine

whether the continuous data were parametric or non-parametric in distribution. We first described the values of cone density and spacing with AO per quadrant and per eccentricity, 2° and 3° from the fovea. Secondly, we tested by means of dependent t-test whether there was a difference in these parameters between the four quadrants per degree of eccentricity. Thirdly, we tested whether there was a difference between the degrees of eccentricity per quadrant. We finally studied the relation between either AL or degree of myopia expressed as spherical equivalents and AO parameters per quadrant and per degree of eccentricity. A linear regression analysis was conducted and a multivariable model was developed with the interaction of AL with the quadrant and degree of eccentricity. In both models the cone density was the dependent variable. The same analyses were conducted with refractive error instead of AL as the dependent variable.

4.3. RESULTS

Fifty eyes of 25 myopic subjects (10 female, 15 male) between the ages of 20 and 40 years, refractive error of −1D to −12D and an AL of 22.68–28.20 mm were included in the study. The mean cone count and spacing the four quadrants (temporal, superior, nasal, inferior to the fovea) and at different eccentricities (2° and 3° from the fovea) are represented in Table 1. The mean cone density was found to be significantly lower in the myopic group when compared to the age-matched emmetropic group as reported in our previous study.[10]

Table 1. The mean and SD of the cone density and spacing at the 4 quadrants (temporal, superior, nasal, inferior) and at 2° and 3° retinal eccentricities

	Temporal		Superior		Nasal		Inferior	
	2°	3°	2°	3°	2°	3°	2°	3°
Cone count (/mm^2)	18,410±5790	18,650±4370	19,600±5080	15,495±3854	17,030±5892	16,845±4953	19,193±4780	14,625±3759
Spacing (μm)	8.44±1.53	8.30±1.25	8.14±1.47	9.14±1.63	8.83±1.61	8.51±2.28	8.17±1.14	9.30±1.27

SD: Standard deviation

Table 2. Mean and SD of cone density and cone spacing between 2° and 3° retinal eccentricity among myopic subjects

	2°	3°	Significance (P)
Cone count (/mm^2)	18,560 ± 5,455	16,404 ± 4,494	<0.001
Spacing (µm)	8.40 ± 1.4	8.81 ± 1.7	0.010

SD: Standard deviation

There was a significant decrease in the mean cone density from 18560/mm^2 ± 5455 to 16,404/mm^2 ± 4,494 respectively and a significant increase in spacing from 8.40 µm ± 1.4 to 8.81 µm ± 1.7 with increase in eccentricity from 2° to 3° from the fovea respectively in the myopic group, as seen in Table 2, a mirror trend similar to that of the emmetropes (decrease in cone density and increase in cone spacing as the distance from fovea increases).

Table 3. The effects of fixed factors on the cone count by LMM

Parameter	Parameter estimate	Significant	95% CI	
				Upper limit
Intercept	32,307	0.010	7,845	56,770
Degree=2	16,986	0.022	2,423	31,549
Degree=3$^+$	0			
Site=I	28,465	0.007	7,870	49,061
Site=N	25,416	0.016	4,821	46,011
Site=S	12,930	0.218	−7,665	33,525
Site=T$^+$	0			
Axial length	−600	0.231	−1,588	387
Degree=2×AL	−599	0.046	−1,187	−11
Degree=3×AL$^+$	0			
Site=I×AL	−1,216	0.004	−2,047	−384
Site=N×AL	−1,091	0.010	−1,923	−260
Site=S×AL	−562	0.184	−1,394	269
Site=T×AL$^+$	0			

$^+$Factors set to zero, since they are redundant. Dependent variable: Cone count, AL: Axial length, CI: Confidence interval, LMM: Linear mixed models

Table 4. The correlation between AL and refractive error

Degree	Quadrant	AL		Refractive error	
		R^2	P	R^2	P
2	Temporal	–0.195	0.174	–0.131	0.365
2	Superior	–0.492	<0.001	–0.245	0.086
2	Nasal	–0.404	0.004	–0.197	0.171
2	Inferior	–0.619	<0.001	–0.284	0.046
3	Temporal	–0.223	0.12	–0.211	0.142
3	Superior	–0.239	0.094	–0.58	0.689
3	Nasal	–0.46	0.001	–0.174	0.226
3	Inferior	–0.53	<0.001	–0.203	0.157

AL: Axial length

The linear regression test performed to relate the cone density and spacing with AL showed that there was significant relation of AL with the cone density in all separate quadrants, at 2° as well as at 3° eccentric from the fovea [Figures 1 and 2] and is lower when AL is higher. The results for cone spacing showed an increase in the spacing between adjacent cones as eccentricity from the fovea increased. Moreover, there is an interaction between AL on one hand and quadrant and degrees on the other implying that the strength of the relation between AL and cone density depends on the degree and quadrant, as seen in Table 3. The relation strength was not different for the square of the radius (= half AL), a measure directly related to the surface area. Figure 3 shows the variation in the cone density between the mild-, moderate- and high-myopia groups. There was no statistically significant difference between these groups. When refractive error was used as the independent variable instead of AL, the strength of the relation in all analyses was lower, as seen in Table 4. The Pearson's coefficient, used to find the correlation between refractive errors versus ALs, was significant ($R^2 = 0.352$, $P = 0.012$ [$P < 0.05$]).

Figure 1. (a–d) Scatter plots showing the variation in cone density with axial length in the 4 quadrants (temporal, superior, nasal and inferior) at 2° eccentricity

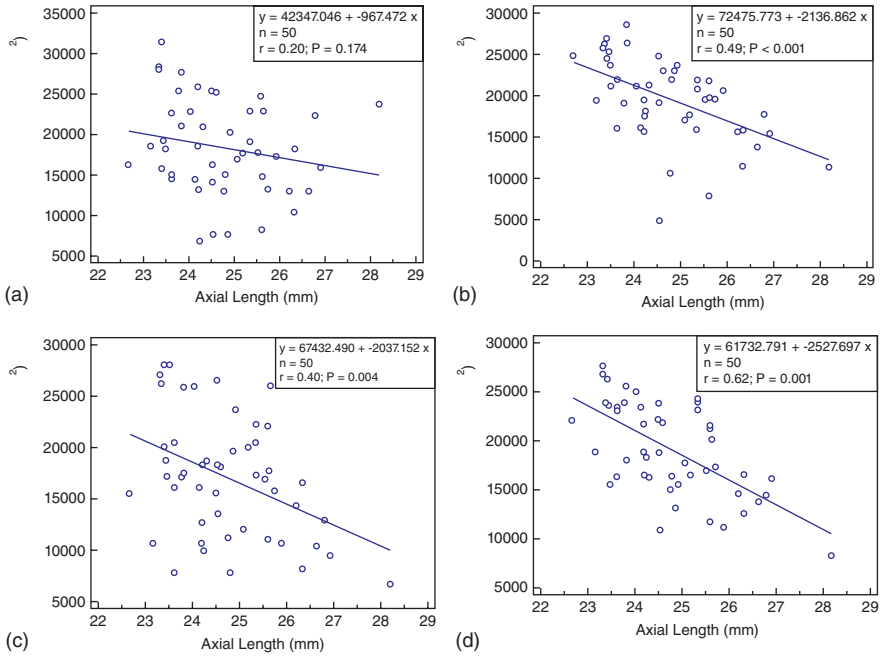

Figure 2. (a–d) Scatter plots showing the variation in cone density with axial length in the 4 quadrants (temporal, superior, nasal and inferior) at 3° eccentricity

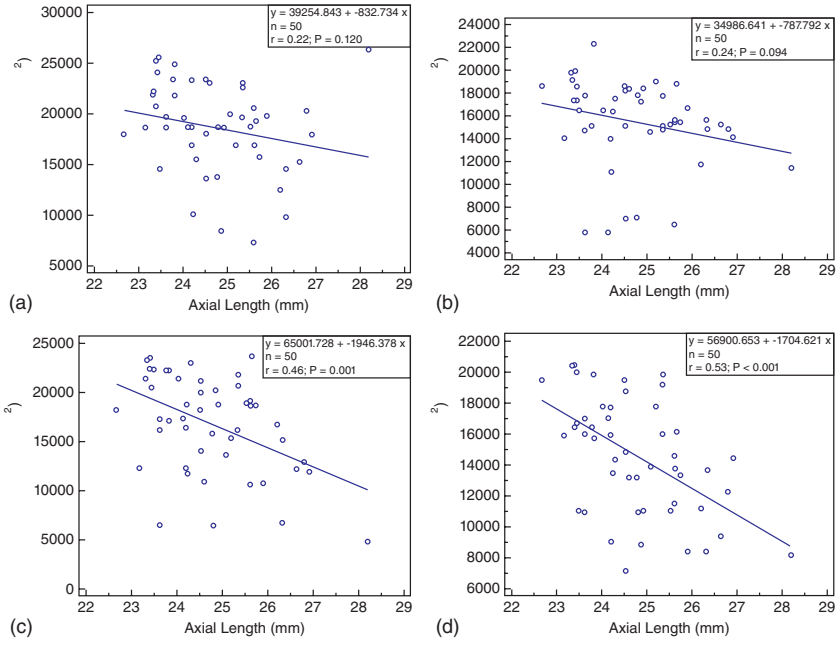

Figure 3. Box plot showing the difference in the cone density between the subgroups (mild, moderate and high) in the myopic subjects

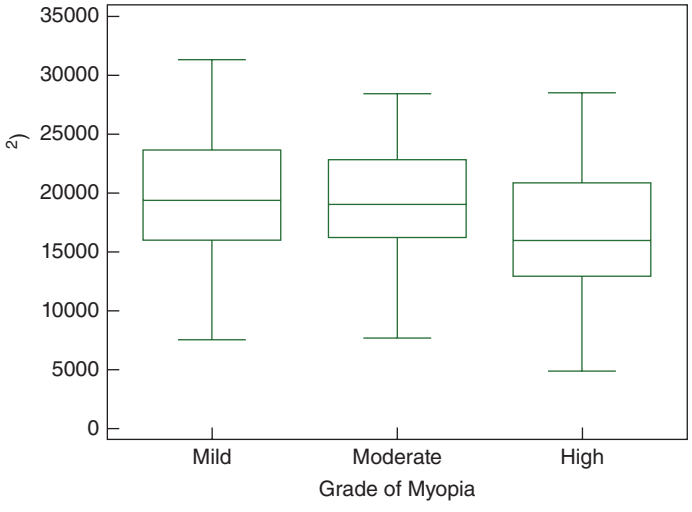

4.4. DISCUSSION

There have been multiple studies that have looked at the axial elongation of the eye in myopia, rather than the equatorial elongation.[11] This is because it is easier to study changes in the photoreceptor mosaic at the posterior pole than at the equator.[3,12] It is well-established that the cones do not get distributed evenly as the expansion occurs non-uniformly. The retinal vasculature is said to restrict the cone migration along the entire surface.[13,14] Curcio et al. in his histological analysis found the density at 1 mm in the parafoveal retina to be 16,000 cells/mm^2, corresponding to a cone spacing of 7.4 mm.[15] In our previous study on emmetropes, we found a statistically significant difference in the cone density from 2° to 3°. At 2° eccentricity the mean was 25,350/mm^2 (5,300/mm^2, 8,400–34,800/mm^2), and at 3° eccentricity the mean was 20,750/mm^2 (6,000 mm^2, 9,000–33,670/mm^2) $P < 0.05$.

The spacing correspondingly was lower at 2° of eccentricity as compared to 3°. At 2° the mean was 6.9 mm (0.70 mm, 5.95–11.6 mm) and at 3° the mean was 7.80 mm (1.00 mm, 6.5–13.5 mm) $P < 0.05$.[10] In our current study, we found similar difference in the counts as the eccentricity increased from 2° from the fovea to 3° (18,560 ± 5,455–16,404 ± 4,494/mm^2 respectively).

When we used the variable as refractive error, the relation with cone density was less strong as compared to AL as a variable.

Lombardo et al. studied 11 eyes and found cone density in moderately myopic eyes (up to −7.50 D) was significantly lower than in emmetropic eyes within (or at) 2.0 mm from the fovea, similar to our results. They reported the spatial vision and the Nyquist limit of resolution of the retinal cone mosaic to reduce with increasing AL from 22.60 to 26.60 mm.[9]

Kitaguchi et al. reported the cone spacing in the moderate- to high-myopic group to be larger than that in the emmetropic and low-myopic group. They found the cone spacing in a −15D myopic eye was 5.92 µm, which is 1.48 times the cone spacing in emmetropic eyes (4.00 µm), unlike a mathematical model where it would be 1.26-fold. We grouped the myopes as low, moderate and high based on their spherical equivalent (mild being 1D–3D, moderate = 3D–6D and high >6D) and evaluated the cone density at different eccentricities from the fovea to understand local anisotropia in correlation to increase in AL. The cone count and spacing between the mild and moderate group was not found to be significantly different but statistically significant variation was found between the mild and the moderate group with the high myopes (Figure 3). This adds to the theory that the expansion is non-uniform.[7]

The limitations of our study were the cone mosaic at the fovea could not be assessed due to their dense arrangement[9] and absence of a correction factor due to the retinal magnification factor.[7]

4.5. CONCLUSION

The variables affecting vision in myopes are multifactorial. The higher-order aberrations, size of the pupil, stretching of the photoreceptors, reduced retinal sampling and the contribution of postreceptor neural factors play a role. With AO we are now able to understand the placement of the photoreceptors with respect to the AL in myopes. In myopic patients with good visual acuity, cone density around the fovea depends on the quadrant, distance from the fovea as well as the AL. The strength of the relation of AL with cone density depends on the quadrant and distance. Further research on the relation between cone density, visual acuity, psychophysical tests and micro-perimetry may help us understand the structural and functional vision of these patients. This may aid us better in counseling our patients, e.g. prior to any refractive or retinal surgical procedure.

REFERENCES

1. Guirao A, Porter J, Williams DR, Cox IG. Calculated impact of higher-order monochromatic aberrations on retinal image quality in a population of human eyes. *J Opt Soc Am A Opt Image Sci Vis.* 2002;19:620-628.
2. Atchison DA, Schmid KL, Pritchard N. Neural and optical limits to visual performance in myopia. *Vision Res.* 2006;46(21):3707–3722.
3. Chui TY, Yap MK, Chan HH, Thibos LN. Retinal stretching limits peripheral visual acuity in myopia. *Vision Res.* 2005;45(5):593–605.
4. Coletta NJ, Watson T. Effect of myopia on visual acuity measured with laser interference fringes. *Vision Res.* 2006;46(5):636–651.
5. Strang NC, Winn B, Bradley A. The role of neural and optical factors in limiting visual resolution in myopia. *Vision Res.* 1998;38(11):1713–1721.
6. Rossi EA, Weiser P, Tarrant J, Roorda A. Visual performance in emmetropia and low myopia after correction of high-order aberrations. *J Vis.* 2007;7(8):14.
7. Kitaguchi Y, Bessho K, Yamaguchi T, Nakazawa N, Mihashi T, Fujikado T. In vivo measurements of cone photoreceptor spacing in myopic eyes from images obtained by an adaptive optics fundus camera. *Jpn J Ophthalmol.* 2007;51(6):456–461.
8. Chui T, Song H, Burns S. Individual variations in human cone photoreceptor packing density: variations with refractive error. *Invest Ophthalmol Vis Sci.* 2008;49:4679-4687.
9. Lombardo M, Serrao S, Ducoli P, Lombardo G. Variations in image optical quality of the eye and the sampling limit of resolution of the cone mosaic with axial length in young adults. *J Cataract Refract Surg.* 2012;38:1147-1155.
10. Dabir S, Mangalesh S, Kumar K, Kummelil M, Roy AS, Shetty R. Variations in the cone-packing density with eccentricity in emmetropes. *Eye.* 2014;28(12):1488–1493.
11. Grossniklaus HE, Green WR. Pathologic findings in pathologic myopia. *Retina.* 1992;12(2):127–133.
12. Atchison DA, Jones CE, Schmid KL, et al. Eye shape in emmetropia and myopia. *Invest Ophthalmol Vis Sci.* 2004;45(10):3380–3386.

13. Marcos S, Burns SA. Cone spacing and waveguide properties from cone directionality measurements. *J Opt Soc Am A Opt Image Sci Vis*. 1999;16(5):995–1004.

14. Williams DR. Topography of the foveal cone mosaic in the living human eye. *Vision Res.* 1988;28(3):433–454.

15. Curcio C, Sloan K, Kalina R, Hendrickson A. Human photoreceptor topography. *J Comp Neurol.* 1990;292:497-523.

CHAPTER 5

STRUCTURAL AND FUNCTION CORRELATION OF CONE-PACKING UTILIZING ADAPTIVE OPTICS AND MICROPERIMETRY

Dabir Supriya, Mangalesh Shwetha, Kumar Kiran Anupama, Kurian Kummelil Mathew, Tos T. J. M. Berendschot, Jan S. A. G. Schouten, Roopa Bharamshetter, Yadav K. Naresh, Shetty Rohit and Bharath Hegde

BIOMED RESEARCH INTERNATIONAL 2015; 968672. doi: 10.1155/2015/968672. Epub 2015 Jun 8

ABSTRACT

AIM

To assess the functional aspects of cone mosaic and correlate cone-packing with retinal sensitivity utilizing microperimetry in emmetropes at different eccentricities.

METHODS

Twenty-four healthy volunteers underwent microperimetry (MAIA Centervue, Italy) and assessment of photoreceptors using adaptive optics retinal camera, rtx1 (Imagine Eyes, Orsay, France), at 2 and 3 degrees from the foveal centre in 4 quadrants: superior, inferior, temporal and nasal. Data were analyzed using SPSS version 17 (IBM). Spearman's correlation tests were used to establish correlation between mean cone-packing density and retinal sensitivity at different quadrants.

RESULTS

Thirteen females and 11 males (age range 20–40 years) were included. The cone density was found to be significantly different among all quadrants (temporal = 25786.68/mm^2 ± 4367.07/mm^2, superior = 23009.35/mm^2 ± 5415.81/mm^2, nasal = 22838.09/mm^2 ± 4166.22/mm^2 and inferior = 21097.53/mm^2 ± 4235.84/mm^2). A statistical significance ($\mu < 0.008$) was found between orthogonal meridians, that is, temporal, nasal (48624.77/mm^2) > superior, inferior (44106.88/mm^2). A drop in retinal sensitivity was observed as the eccentricity increased ($\mu < 0.05$). It was also found that as cone-packing density decreased retinal sensitivity also decreased ($\mu < 0.05$) in all quadrants. This was observed at both 2 and 3 degrees.

CONCLUSION

It is crucial to establish normative variations in cone structure-function correlation. This may help in detection of subtle pathology and in it's early intervention.

5.1. INTRODUCTION

Adaptive optics (AO) is emerging as an objective tool in assessment of the architecture of the photoreceptor layer of retina. It can be used to quantify the cone mosaic including the density and packing arrangements. Studying the cone mosaic shows different reflectance patterns with wide temporal and spatial variations. Multiple AO systems have described this variation in the cone reflectivity to be secondary to differences in the phases of phototransduction, length of the outer segment, disc shedding, wavelength of the light, and so forth.[1–3]

By just studying the cone mosaic, we are unable to assess the functional aspect of a visible cone and correlate whether a visible cone is a functional cone.

Our study aims to assess the functional aspects of the cone mosaic and correlate the cone-packing with the retinal sensitivity utilizing microperimetry (MAIA) in emmetropes at different eccentricities.

5.2. SUBJECTS

Twenty-four healthy volunteers were included in the study after an informed consent was obtained, approved by the institutional review board and in adherence to the tenets of Helsinki declaration. Inclusion criteria were emmetropia or best correct visual acuity of 20/20 or better with astigmatism less than 2 diopters (as assessed by the Tonoref RKT-7000 autorefractometer, Nidek). Subjects with ocular or systemic diseases or previous eye surgery were excluded from the study.

5.3. METHODS

All subjects underwent objective refraction, non-contact biometry (IOL master; Carl Zeiss Meditec, Germany) for axial length, and microperimetry (MAIA Centervue-100809). A compact AO retinal camera prototype, the rtx1 (Imagine Eyes, Orsay, France), was used to image the photoreceptor layer. Core components of the apparatus include a Shack-Hartmann wavefront sensor (HASO 32-eye; Imagine Optics, Orsay, France), a deformable mirror (MIRAO 52; Imagine Optics), and a low-noise high-resolution camera (Roper Scientific, Tucson, AZ, USA). AO imaging sessions were conducted after dilating the pupils with 1 drop each of 0.5% tropicamide and 10% phenylephrine hydrochloride. Stable fixation was maintained by having the patient look at the system's inbuilt target moved by the investigator to predetermined coordinates. The patient was instructed to

fixate at 0°, 2°, and 3° eccentricity along all the four quadrants, superior, inferior, nasal, and temporal retina. A series of 40 frames, 4° field size, was captured at each of the above retinal locations. After acquisition, a program provided by the manufacturer correlated and averaged the captured image frames to produce a final image.[4] At each site, a sampling window square of 100 microns width was chosen avoiding blood vessels. Cone counting software created on MATLAB by Imagine Eyes was used to process the images and calculate the cone density (cones/mm^2) and spacing. The axial length was entered into the automated software to account for differences in magnification.

Macular integrity was tested with MAIA, a non-mydriatic, near infrared, line SLO scanning laser ophthalmoscope with high-frequency eye tracker, a third-generation automated macular perimeter with normative database and a statistical analysis module. An expert or detailed threshold test takes about 4–7 minutes for each eye and was performed. The grid selected was 37-point stimuli covering the central 6 degrees with 25 µm stimulus size, that is, Goldmann III. The threshold values at radius of 2 degrees and 3 degrees from the fovea were considered in all the 4 quadrants: superior, inferior, nasal, and temporal. The Goldmann size III target subtends 0.431° of visual angle and represents 0.123 mm (0.431°* 0.286 mm/°) on the retina and an area of 0.012 mm^2.[5] The sampling window that we have used with the AO image processing is 0.1 mm, and hence the correlation has the potential for fine retinotopic precision, as seen in Figure 1.

Figure 1. The retinal sensitivity on the MAIA image being correlated to the cone-packing density at 1, 2, and 3 degrees from the fovea and 4 quadrants (superior, inferior, temporal, and nasal)

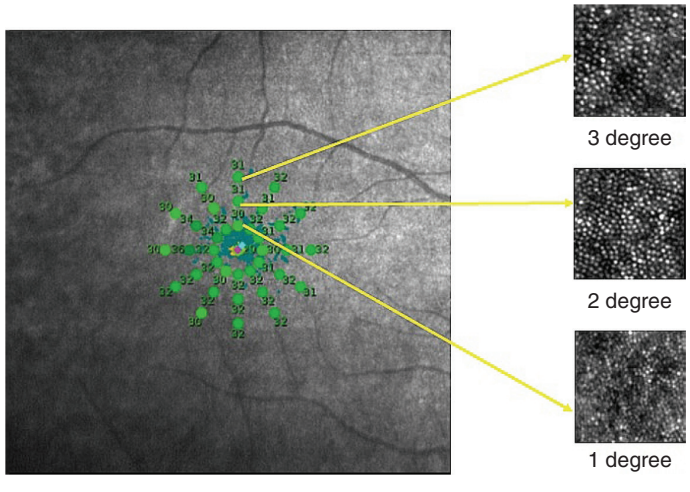

5.4. STATISTICAL ANALYSIS

The data collected was analyzed using SPSS version 17 (IBM). Spearman's correlation tests were used to establish the correlation between the mean cone-packing density and the retinal sensitivity at the different quadrants. To look for possible differences between MAIA threshold values at the different quadrants and eccentricities, a Linear Mixed Models analysis (LMM) was performed with subject ID as grouping factor and cone density, eccentricity, and quadrant and their interaction term as covariates. The LMM procedure expands the general linear model so that the data are permitted to exhibit correlated and non-constant variability. The LMM analysis, therefore, provides the flexibility of modeling not only the means of the data but their variances and covariances as well. LMM handle data where observations are not independent, as in this study. That is, LMM correctly models correlated errors, whereas procedures in the general linear model family usually do not.[6, 7] *P*-values smaller than 0.05 were considered to be significant.

5.5. RESULTS

Twenty-four subjects were included in the study. The study group comprised of 13 females and 11 males between the ages of 20 and 40 years. Figure 2 shows MAIA threshold values as a function of cone density for the different quadrants. The Pearson correlation coefficient, *r*, was significant for all sites ($P < 0.001$). The cone density was found to be significantly different among all the four quadrants (temporal: 25786 ± 4367 mm^{-2}, superior: 23009 ± 5415 mm^{-2}, nasal: 22838 ± 4166 mm^{-2}, and inferior: 21097 ± 4235 mm^{-2}). A statistical significance ($P < 0.008$) was found between the orthogonal meridians, that is, temporal, nasal > superior, inferior (temporal + nasal = 48624 mm^{-2}> superior + inferior = 44106 mm^{-2}). Figure 3 shows mean MAIA thresholds at 2 and 3 degrees for the different quadrants. A drop in the retinal sensitivity was observed as the eccentricity increased. LMM analysis revealed that MAIA threshold values differed significantly between the four quadrants (temporal = 32.2 ± 2.7 dB, superior = 31.2 ± 1.6 dB, nasal: 31.8 ± 1.4 dB, and inferior: 30.5 ± 2.1 dB, $P = 0.001$) and also between the two eccentricities (see Figure 3, $P = 0.01$).

Figure 2. Scatter plot showing correlation between cone density and average threshold at 4 quadrants, both at 2 and 3 degrees

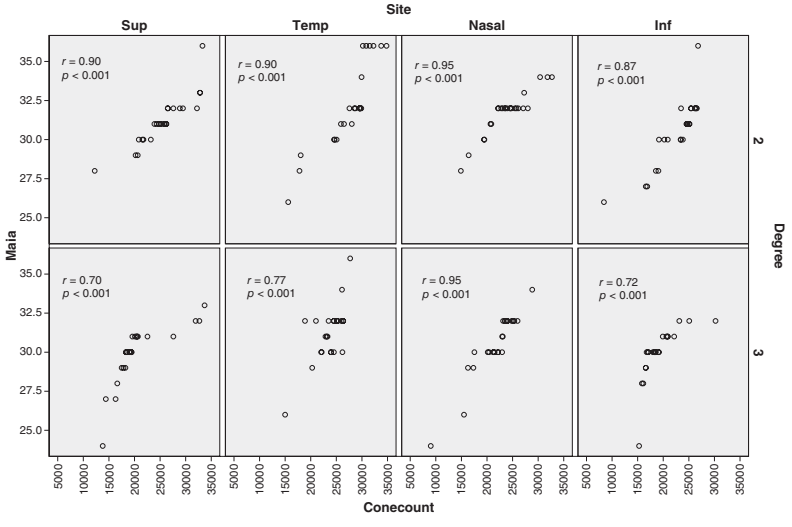

Figure 3. Mean MAIA thresholds at 2 and 3 degrees for the different quadrants

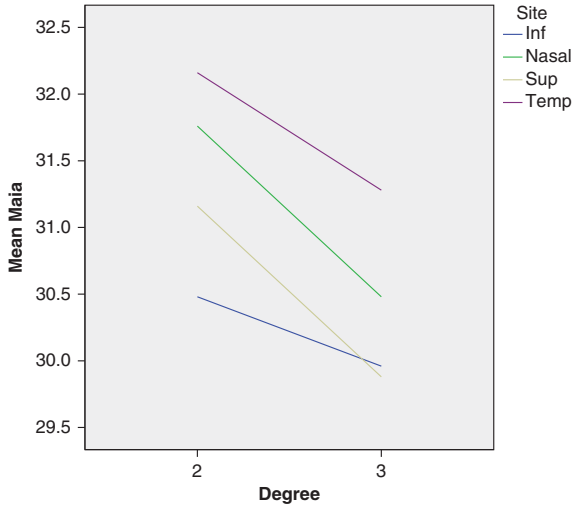

5.6. DISCUSSION

With the advent of adaptive optics leading to compensation of higher-order aberrations, the in-vivo imaging of the photoreceptor mosaic is now a reality. The challenge

now comes in assessing the correlation of the cone mosaic with their function. It is interesting to understand whether areas with dense cone-packing are associated with higher retinal sensitivities. Establishing the normative database in emmetropes is essential before we understand pathology. This may be useful in establishing the functional correlates of photoreceptor mosaic structure in patients with macular disease who develop central scotomas due to various diseases like age-related macular degeneration. They can then be coached to prefer a certain peripheral part of retina to fixate with, depending on the cone density and retinal sensitivity at that area.[8, 9] Even in children after squint surgeries, they may be trained to develop fixation by utilizing the structure-function knowledge of the retinal areas.

There has been a lot of literature on the use of microperimetry alone to find the preferential retinal locus in patients with central macular disease, and they have found it to be differing with respect to the task assigned to the patient.[8–12] This however does not happen in normal adults where the preferential retinal locus is fixed. Hence it may be possible to rehabilitate these patients once we understand the areas in which relative structural photoreceptor loss has led to relative functional loss.

The Goldmann size III target has the diameter which subtends 0.431° of visual angle which corresponds to the sampling window of the adaptive optics, and hence the correlation has the potential for fine retinotopic precision.

Our study shows that when the mean cone-packing density decreased with increasing eccentricity, the corresponding retinal sensitivity also decreased ($P < 0.05$).

The limitations of our study are that we have used a flood-illuminated AO camera and not an AO-SLO-based microperimetry system,[13] which would have better localizing. Also multifocal electrophysiology would have been a more objective tool to analyze the macular function but the costs of tests were a limiting factor.

This study may help establish a sensitive outcome measure to evaluate the safety and efficacy of newer treatment modalities like stem cell therapy and gene therapy in the management of genetic retinal disorders.

5.7. CONCLUSION

Understanding the correlation between the anatomy of a structure and its function is crucial to plan management of any disease. Knowing the variations in a healthy population helps us analyze pathology better.

REFERENCES

1. Jonnal RS, Besecker JR, Derby JC, et al. Imaging outer segment renewal in living human cone photoreceptors. *Opt Express.* 2010;18(5):5257–5270.
2. Pircher M, Zawadzki RJ, Evans JW, Werner JS, Hitzenberger CK. Simultaneous imaging of human cone mosaic with adaptive optics enhanced scanning laser ophthalmoscopy and high-speed transversal scanning optical coherence tomography. *Opt Lett.* 2008;33(1):22–24.
3. Pallikaris A, Williams DR, Hofer H. The reflectance of single cones in the living human eye. *Invest Ophthalmol Vis Sci.* 2003;44(10):4580–4592.
4. Lombardo M, Serrao S, Ducoli P, Lombardo G. Influence of sampling window size and orientation on parafoveal cone-packing density. *Biomed Opt Express.* 2013;4(8):1318–1331.
5. Garway-Heath DF, Caprioli J, Fitzke FW, Hitchings RA. Scaling the hill of vision: the physiological relationship between light sensitivity and ganglion cell numbers. *Invest Ophthalmol Vis Sci.* 2021;41(7):1774–1782.
6. Jansen I, Beunckens C, Molenberghs G, Verbeke G, Mallinckrodt C. Analyzing incomplete discrete longitudinal clinical trial data. *Stat Sci.* 21(1):52–69.
7. Laird NM, Ware JH. Random-effects models for longitudinal data. *Biometrics.* 1982;38(4):963–974.
8. Calabrese A, Bernard J-B, Hoffart L, et al. Wet versus dry age-related macular degeneration in patients with central field loss: different effects on maximum reading speed. *Investig Ophthalmol Vis Sci.* 2011;52(5):2417–2424.
9. Nilsson UL, Frennesson C, Nilsson SEG. Patients with AMD and a large absolute central scotoma can be trained successfully to use eccentric viewing, as demonstrated in a scanning laser ophthalmoscope. *Vision Res.* 2003;43(16):1777–1787.
10. Shima N, Markowitz SN, Reyes SV. Concept of a functional retinal locus in age-related macular degeneration. *Can J Ophthalmol.* 2010;45(1):62–66.
11. Pacella E, Pacella F, Mazzeo F, et al. Effectiveness of vision rehabilitation treatment through MP-1 microperimeter in patients with visual loss due to macular disease. *Clin Ter.* 2012;163(6):e423–428.

12. Fujita K, Yuzawa M. Preferred retinal locus in patients with age-related macular degeneration. *Nippon Ganka Gakkai Zasshi.* 2003;107(10):602–606.

13. Tuten WS, Tiruveedhula P, Roorda A. Adaptive optics scanning laser ophthalmoscope-based microperimetry. *Optom Vis Sci.* 2012;89(5):563–574.

CHAPTER 6

MELANOMA-ASSOCIATED RETINOPATHY: A NEW DIMENSION USING ADAPTIVE OPTICS

Supriya Dabir, Shwetha Mangalesh, Indu Govindraj, Ashwin Mallipatna, Rajani Battu, Rohit Shetty

OMAN JOURNAL OF OPHTHALMOLOGY 2015; 8:125–127

ABSTRACT

We report a 56-year-old male patient, complaining of metamorphopsia in his left eye. Visual acuity, slit lamp, and fundus examinations were within normal limits. Microperimetry (MAIA, Centervue, Italy) revealed central field loss and spectral domain optical coherence tomography (Spectralis, Heidelberg, Germany) showed disrupted cone outer segment tip layer. The patient had a diagnosis of cutaneous melanoma in his foot for which an excision biopsy with lymph node dissection was performed 5 months earlier. Our clinical diagnosis was melanoma-associated retinopathy. Electrophysiology confirmed the diagnosis. Adaptive optics retinal imaging (Imagine eyes, Orsay, France) was performed to assess the cone mosaic integrity across the central retina. This is the first report on the investigation of autoimmune retinopathy using adaptive optics ophthalmoscopy. This case highlights the viability of innovative diagnostic modalities that aid early detection and subsequent management of vision threatening retinal pathology.

Keywords: Adaptive optics, autoimmune retinopathy, cone dysfunction, electrophysiology, melanoma-associated retinopathy.

6.1. INTRODUCTION

Autoimmune retinopathy is a spectrum of immune-mediated degenerations of the retina that occurs in patients, including cancer-associated retinopathy, melanoma associated retinopathy (MAR) and presumed non-paraneoplastic autoimmune retinopathy.

Most commonly, these patients present with night blindness, photopsia and painless, progressive vision loss. Clinically, ocular findings are often unremarkable; nevertheless they include optic nerve pallor, retinal pigment epithelial alterations across the macular area and vascular attenuation.[1] In the absence of clinical findings, high-resolution imaging tools might be of great value to detect pathological alterations of ocular microstructures, even in patients with a history of systemic neoplasm.

We discuss the case of a patient with history of cutaneous melanoma in the foot were combined imaging and functional tools aided in assessment of early pathological retinal alterations.

6.2. CASE REPORT

A 56-year-old man complained of metamorphopsia in his left eye since 1 month. On examination, his best-corrected visual acuity was 20/20 and N6 in both eyes. The anterior segment was normal. Intraocular pressure was 10 and 12 mmHg using applanation tonometry in the right and left eye respectively. The pupils were quickly reacting to light without any relative afferent pupillary defect. Fundus examination was normal, as shown in Figure 1.

He subsequently underwent a few investigations including a 30-2 Humphreys perimetry (Humphrey Field Analyzer; Carl Zeiss Meditec, Dublin, CA, USA), spectral domain optical coherence tomography (SD-OCT; Spectralis, Heidelberg, Germany) and microperimetry (MAIA, Centervue, Italy).

The 30-2 field of vision showed a central scotoma in both eyes, larger in the left eye than right eye. The SD-OCT of the macula was normal. Foveal contour and central foveal thickness were 204 microns in both eyes, as shown in Figure 1.

The microperimetry showed abnormal macular integrity index, 100, in both eyes (normal values = 0–40, suspect = 40–60, abnormal = 60–100). Average threshold was 22.1 decibels (dB) and 0 dB in the right and left eye respectively (normal = 36–25 dB, suspect = 25–24 dB and abnormal <24 dB). Fixation was stable in the right eye and relatively unstable in the left eye, as shown in Figure 2.

Figure 1. Fundus montage of the right (a) and (b) left eye showing normal fundus with normal spectral domain optical coherence tomography and the decreased cone count using adaptive optics at 1.5° eccentricity in all four quadrants

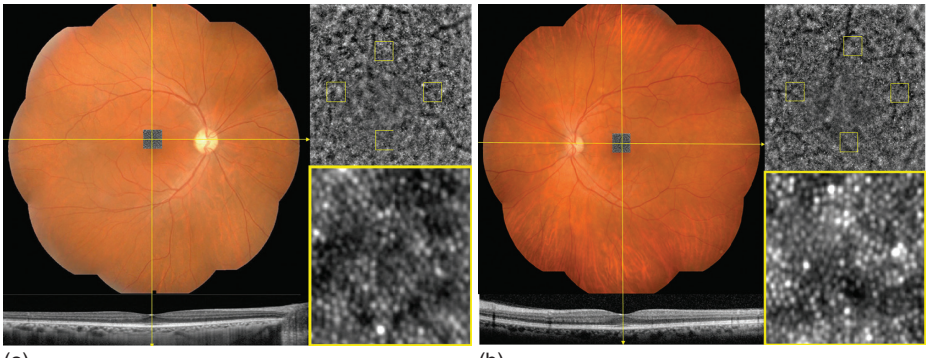

(a) (b)

Detailed systemic history elicited that the patient had a diagnosis of cutaneous melanoma of the foot 5 months earlier for which he had undergone a wide excision of the lesion with block dissection of the ilio-inguinal lymph nodes. The histopathology report clarified it was a histiocytoid variant with tumor-free margins. Positron emission tomography showed metastasis to right iliac, inguinal and popliteal lymph nodes. The patient was free from pulmonary or distant metastasis.

With a provisional diagnosis of MAR, the patient underwent fullfield and multifocal electroretinogram (Full-field electroretinography [ff ERG] and multifocal electroretinography [mf ERG]; Visual Evoked Response Imaging System Science™ 5) for confirmation. The ff ERG showed a central cone photoreceptor dysfunction in the right eye and a reduced scotopic response, with a negative ERG in the combined maximal response in the left eye, as shown in Figure 3. The mf ERG showed reduced responses across the central 0–15° in both eyes.

Adaptive optics retinal imaging was done using the rtx1 instrument (Imagine Eyes, France) and its automated software was used to assess the cone density and their spacing across the central retina, as seen in Figure 1. The central 4° × 4° of the retina was evaluated. His axial length was 24 mm in both eyes. A mean (± standard deviation [SD]) density of 12.923 ± 4218 cones/mm^2 at 1.5° temporal and 18.485 ± 5825 cones/mm^2 at 1.5° nasal from the foveal fixation was detected in the right and left eye respectively (mean cone density of emmetropes with no ocular pathology at 1.5° from the fovea

is 31.707 ± 7149 cones/mm^2 as calculated on 25 age-matched healthy subjects). The mean cone spacing (±SD) was of 9.61 ± 1.75 µm and 8.16 ± 1.52 µm in the right eye and left eye respectively (cone spacing of emmetropes, as seen in 25 age-matched healthy subjects was an average of 6.21 ± 0.85 µm at 1.5° from the fovea. The patient was then sent to his primary oncologist for metastatic work up. All the reports were negative. He was then started on a tapering oral prednisolone 1 mg/kg body weight by the immunologist. At 3 months followup, he remains clinically stable.

Figure 2. Sensitivity map of the right (a) and left eye (b) showing unstable fixation and decreased sensitivity in the left eye only

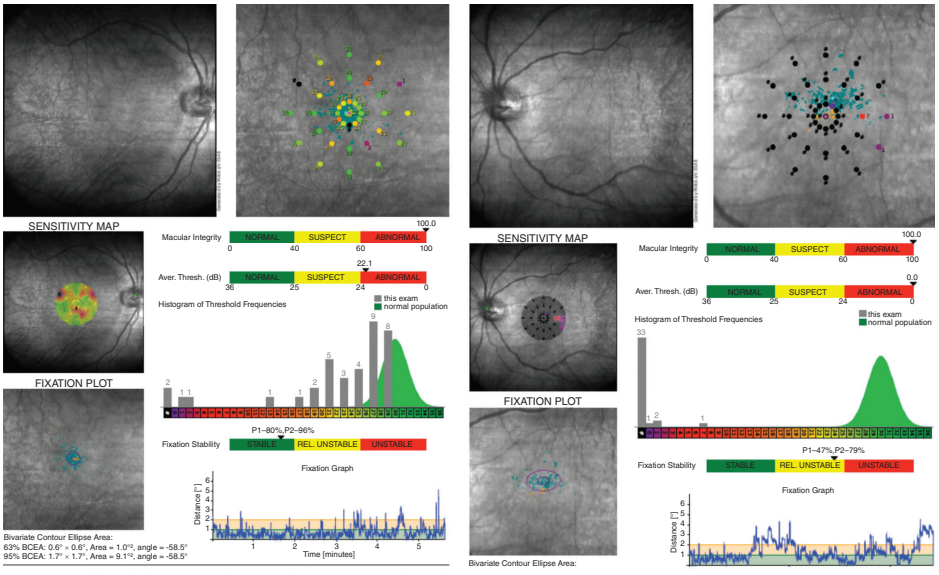

Figure 3. Full-field electroretinography (ff ERG) of the right eye (a) shows normal response in scotopic ERG and subnormal response in photopic ERG; (b) ff ERG Left shows an unrecordable b wave in the dark-adapted 0.01 ERG and a negative 'b' wave in dark adapted 3.0 ERG; the photopic response is also subnormal

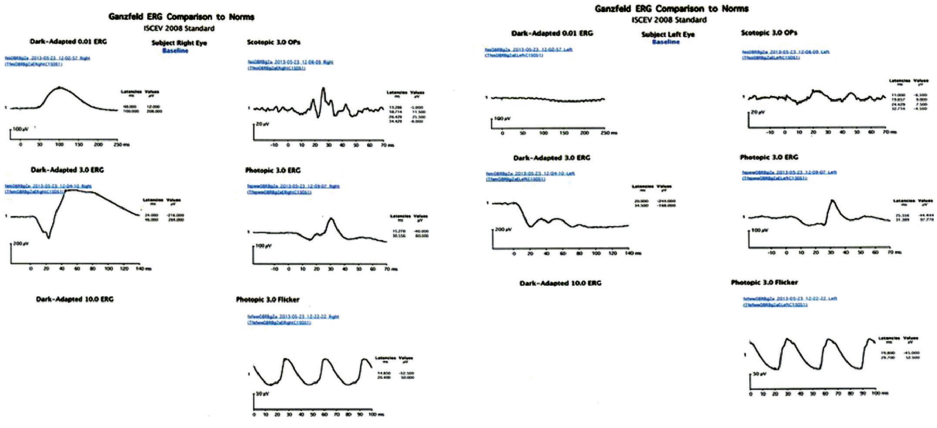

6.3. DISCUSSION

The diagnosis of MAR is always a clinical dilemma since most of the patients have very subtle clinical findings. Hence, the use of highly accurate investigative modalities plays a main role in the management of these patients. Identification of antiretinal antibodies might not be often feasible because of the costs and the reagents availability in the laboratory in developing countries. There is no definitive treatment of MAR.[1] Audemard et al. discuss a rare case of melanoma and MAR treated with ipilimumab, taking into account the fact that it can be effective on tumor burden, but can also increase autoimmunity.[2]

Pepple et al. have evaluated the use of SD-OCT and auto fluorescence in patients with autoimmune retinopathy and reported the presence of a hyperautofluorescence ring

that corresponded with disruptive changes seen in outer retinal layers on SD-OCT.[3] ERG changes were inconclusive of the diagnosis too. In our patient the structural damage was not severe enough to be picked up on SD-OCT, but was easily detected on the adaptive optics camera where the cone density was reduced. Furthermore, functional changes were appreciated on Humphrey fields and microperimetry.

With the advent of new technology such as adaptive optics, we can image as near-histology as possible with the high-resolution scans, allowing us to quantify the extent of cone degeneration. Thus far, adaptive optics has been used to study eyes with early retinal degenerations and dystrophies and proved to be a good tool to study early onset of subtle pathology.[4, 5]

This new imaging modality may be useful in establishing the diagnosis of this rare disease, monitoring disease progression and evaluating response to therapy. It may help in monitoring the patient's response to immunotherapy by quantifying the cone density and hence revolutionize the way these patients are managed in the future.

REFERENCES

1. Braithwaite T, Vugler A, Tufail A. Autoimmune retinopathy. *Ophthalmologica.* 2012;228(3):131–142.
2. Audemard A, de Raucourt S, Miocque S, et al. Melanoma-associated retinopathy treated with ipilimumab therapy. *Dermatology.* 2013;227(2):146–149.
3. Pepple KL, Cusick M, Jaffe GJ, Mruthyunjaya P. SD-OCT and autofluorescence characteristics of autoimmune retinopathy. *Br J Ophthalmol.* 2013;97(2):139–144.
4. Lombardo M, Lombardo G, Schiano Lomoriello D, Ducoli P, Stirpe M, Serrao S. Interocular symmetry of parafoveal photoreceptor cone density distribution. *Retina.* 2013;33(8):1640–1649.
5. Lombardo M, Serrao S, Ducoli P, Lombardo G. Eccentricity dependent changes of density, spacing and packing arrangement of parafoveal cones. *Ophthalmic Physiol Opt.* 2013;33(4):516–526.

CHAPTER 7

SPECTRAL DOMAIN OPTICAL COHERENCE TOMOGRAPHY ANGIOGRAPHY FEATURES IN A PATIENT OF CENTRAL RETINAL ARTERIAL OCCLUSION BEFORE AND AFTER PARACENTESIS

Devanshi R. Bhanushali, Naresh K Yadav, Supriya Dabir, Lavanya Chidambara, Priya Srinivasan, Rohit Shetty

RETINA 2016; 36:E36–38

ABSTRACT

An 80-year-old Asian Indian man presented with sudden painless loss of vision in the right eye since 7 days. Best-corrected visual acuity at presentation was hand movements in the right eye and 20/20 in the left eye with normal intraocular pressure. Fundus examination revealed central retinal arterial occlusion in the right eye. Fundus fluorescein angiography revealed filling of the cilioretinal artery in early phase and delayed filling of the retinal arteries (Figure 1). Optical coherence tomography angiography (OCTA) revealed perfusion in the cilioretinal artery with nonperfusion of vessels in the superficial and deep plexus, however, the choroid capillaries remained unaffected (Figure 2). The patient underwent anterior chamber paracentesis. OCTA performed immediately after paracentesis showed return of the blood flow in superficial and deep vasculature (Figure 2) but with no vision improvement.

OCTA works on principle of split-spectrum amplitude decorrelation algorithm (SSADA) which detects motion in blood vessel lumen by measuring variation in reflected OCT signal amplitudes between consecutive scans. An 8 mm × 8 mm scan was acquired by the angiovue protocol (ReVue, version 2014.2.0.15; Optovue Inc.).[1] The image thus acquired shows the retinal layers into four slabs: the superficial-internal limiting membrane to internal plexiform layer, deep-outer internal plexiform layer to outer plexiform layer, outer retina-outer plexiform layer to retinal pigment epithelium, and the choroid-basement membrane of retinal pigment epithelium to 20 micron posteriorly.

Keywords: Spectral domain-optical coherence tomography, angiography, central retinal artery occlusion, paracentesis

Figure 1. Fundus fluorescein angiography (Heidelberg retinal tomography, HRT; Heidelberg Engineering, Heidelberg, Germany) at 20 seconds showing filling of the cilioretinal artery with retro grade flow into the veins. The area perfused by the cilioretinal artery does not involve the fovea. At 3.25 minutes, angiogram shows delayed filling of the arteries.

Figure 2. Optical coherence tomography angiography (OptoVue RTVue XR AVANTI, Inc, Fremont, CA, USA) (SSADA algorithm) performed before and immediately after paracentesis. Optical coherence tomography angiography performed before paracentesis (a–c) showing no perfusion in the superficial plexus (a) except a localized area supplied by the cilioretinal artery that is perfused; deep plexus (b) shows disruption in the vascular areas with coarse texture and the choriocapillaris are not affected. An altered area at choroidal level (c) can be noticed which may be due to the overlying retinal edema in the superficial layers. The OCTA changes correspond very precisely to the early frames of fundus fluorescein angiography. The brighter areas on choroid capillary layer correspond to the better contrast of the fovea and perfused cilioretinal artery in comparison with the dark arc-like area seen in the outer retina and choroid as this dark area is the representation of the retinal edema due to central retinal arterial occlusion itself. Optical coherence tomography angiography performed after paracentesis (d–f) reveals increased perfusion of the retinal vasculature in both superficial and deep layers. The superficial layer (d) shows reperfusion quite clearly with an established centripetal pattern. The deep layer (e) shows artifacts of the vessels

present in the superficial plexus. The choroidal layer (f) shows no alteration.

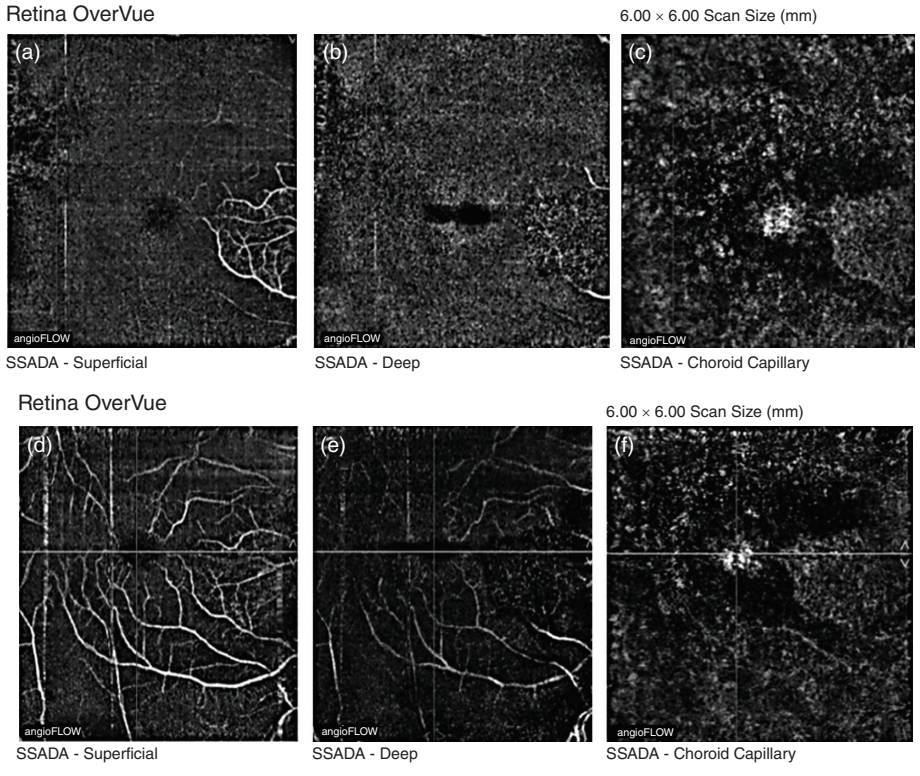

DISCUSSION

Vascular changes in central retinal arterial occlusion documented on fundus fluorescein angiography were comparable with OCTA. Optical coherence tomography angiography after paracentesis showed a prompt re-perfusion in the superficial layers despite the 7-day-old event. The repeatability constraints of invasive fundus fluorescein angiography can thus be overcome by the non-invasive OCTA. To the best of our knowledge, there are no reports of OCTA findings of central retinal arterial occlusion in the literature. Optical coherence tomography angiography can be an efficient and promising alternative in acute vascular episodes due to its non-invasiveness, repeatability, and nil systemic side effects.

REFERENCES

1. Spaide RF, Klancnik JM Jr, Cooney MJ. Retinal vascular layers imaged by fluorescein angiography and optical coherence tomography angiography. *JAMA Ophthalmol.* 2015;133(1):45–50.

CHAPTER 8

ASSESSMENT OF MICROVASCULAR CHANGES USING OPTICAL COHERENCE TOMOGRAPHY ANGIOGRAPHY AFTER PHACOEMULSIFICATION SURGERY IN AN INDIAN POPULATION

Supriya Dabir, Mohan Rajan, Sujatha Mohan, Vaidehi Bhatt, M. Ravishankar, Sowmya Sunil, Deepak Bhatt, Preetam Samant, Berendschot TTJM, Webers CAB

JOURNAL OF CLINICAL & EXPERIMENTAL OPHTHALMOLOGY 2021; 12: 1–6

ABSTRACT

PURPOSE

To identify changes in superficial retinal capillary microvasculature before and after cataract surgery using optical coherence tomography angiography (OCTA).

SETTING

Rajan eye care, Tertiary care center in Chennai, India.

DESIGN

Prospective observational study.

METHODS

Patients above 40 years who underwent uncomplicated cataract surgery had 6 × 6 mm OCTA fovea-centered scans using Zeiss Angioplex 5000 OCTA before and 4 weeks postoperatively. Signal strength and automated values obtained for perfusion density (PD) and vascular density (VD) were recorded.

RESULTS

Fifty-eight eyes of 33 patients aged 67 ± 5 years were enrolled. Signal strength (3.9 ± 2.3 vs. 5.7 ± 2.1, P < 0.001), PD (16.4 ± 10.4 vs. 26.6 ± 10.3, p < 0.001) and VD (7.4 ± 4.5 vs. 11.4 ± 4.0, P < 0.001) increased significantly after surgery. Strong positive correlation was seen between signal strength and PD (r=0.86, P < 0.001) and VD (r=0.79, P < 0.001). Linear-mixed model analysis with eye as grouping factor, time (i.e. pre- and post-surgery) and signal strength as covariates showed, surgery independently caused an increase in PD (ß= 3.63 increment in PD after surgery, P < 0.001) and VD (ß = 1.61 increment in VD after surgery, p=0.003). After adjusting for signal strength, a 20% increment in macular PD and VD was observed in central 1 mm area around fovea. Foveal avascular zone (FAZ) area, perimeter and circularity, did not change after surgery.

CONCLUSION

Macular perfusion and vascularity indices increase immediately after cataract surgery independent of improvement in signal strength, though FAZ is not influenced.

Keywords: OCT angiography, microvascular changes, phacoemulsification, superficial retinal capillary layer, vascular density, perfusion density.

8.1. INTRODUCTION

Cataract surgery is the most commonly performed intraocular procedure worldwide. There have been paradigm shifts to improve the safety of surgery and ensure excellent refractive outcomes. However, cataract surgery has been known to induce transient inflammation leading to increased retinal circulation and clinically significant cystoid macular edema in a minority of cases.[1,2] Evaluation of retinal morphology has shifted from the routine use of fluorescein angiography to optical coherence tomography (OCT) over the past decade. Studies have shown a slight increment in the macular thickness after uncomplicated cataract surgery using automated OCT measurements, thereby providing surrogate evidence of an increase in retinal perfusion after cataract surgery.[3,4] However, quantitative measurements of the retinal vascular density and perfusion status after cataract surgery have not been studied extensively.

Optical coherence tomography angiography (OCTA) is an exciting and new imaging modality that has revolutionized our understanding of the retinal and choroidal vasculature in a non-invasive manner in normal as well as diseased states.[5] This technology has been recently used to study changes in retinal circulation following cataract surgery with most authors confirming an increment in circulation at the level of the superficial and deep capillary plexus.[6–8] However, there is controversy regarding whether OCTA measurements denote a true increment in blood flow or whether a mere improvement in signal strength post cataract removal gives a pseudo impression of enhanced blood flow.[9] This potential source of error is compounded by the fact that OCTA scans are prone to motion artifacts and segmentation errors, are influenced by signal strength[10] and every OCTA machine uses different software algorithms to automatically denote vascularity indices.

In view of this, it is important to statistically adjust for variability in signal strength and re-evaluate the OCTA parameters to understand whether cataract surgery has a truly pro-inflammatory influence on retinal circulation. We performed a study to understand the changes in the superficial retinal capillary microvasculature before and after cataract surgery using the OCTA in an Indian population.

8.2. MATERIALS AND METHODS

This was a prospective observational study on consecutive consenting patients undergoing uncomplicated cataract surgery for routine age-related cataracts. The study was approved by the institutional ethics committee and was carried out as per the tenets of the declaration of Helsinki and good clinical practice guidelines. Informed consent was obtained from all patients before undertaking the cataract surgery.

All patients above the age of 40 who presented to our institution with senile cataracts without any coexisting ocular or systemic comorbidity were offered participation and consenting patients were enrolled. Eyes with posterior polar, brown, black or mature cataracts, those with poor mydriasis, pseudoexfoliation, zonular weakness and eyes that experienced a surgical complication such as posterior capsular rupture were excluded from the analysis. All patients underwent a routine preoperative work up including evaluation of the best corrected visual acuity (BCVA), intraocular pressure (IOP), dilated slit lamp evaluation of the anterior segment and thorough evaluation of the posterior segment followed by optical biometry for intraocular lens power estimation.

Patients also underwent preoperative OCTA assessment in the eye to be operated using the Zeiss Angioplex – 5000 OCTA system (Carl Zeiss Meditec, Dublin, CA, USA). The scans were acquired by a technician well-trained in obtaining OCTA. A 6 × 6 mm scan centered on the fovea was acquired and en-face retinal angiograms were created using the proprietary Optical Microangiography (OMAG) algorithms from the manufacturer that utilizes amplitude and phase OCT signal data to deliver the angiography images. A preoperative signal strength of minimum of 3/10 was required to register the scan for analysis without any motion artifacts. The technician checked for segmentation errors as well before admitting the scan for automated analysis. A postoperative signal strength of minimum 5/10 was required for the scan to be admissible. After acquisition, automated measurements from the superficial capillary plexus were used for study purposes. Parameters used were perfusion density, vascular density and the size of the foveal avascular zone (FAZ). These parameters from the central (circle with a diameter of 1 mm), parafoveal (circle with a diameter of 3 mm) and perifoveal (circle with a diameter of 6 mm) regions, as described previously by Zhao et al.[6], were used for analysis.

All patients underwent routine clear corneal phacoemulsification with intraocular lens implantation and received topical prednisolone acetate eye drops in a tapering fashion for 4 weeks. At the end of 4 weeks, the OCTA measurements were again performed by the same technician using the same protocols described above. The primary outcome measures were changes in perfusion density, vascular density and size of the FAZ at 4 weeks post cataract surgery compared to preoperative values.

8.2.1. STATISTICAL ANALYSIS

All continuous variables were described as means with standard deviation and categorical variables were described as proportions (n, %). Differences between pre and postoperative measurements were done using the paired t-test. To study changes of perfusion and vascularity density as well as FAZ in time we performed a linear mixed model analysis with these dependent variables and with time (i.e. pre- and post-surgery) and signal strength as covariates. Data were recorded using Microsoft Excel and statistical analyses were done with SPSS statistical software (version 25, IBM Corp, Armonk, NY, USA). A p-value of <0.05 was considered significant.

8.3. RESULTS

Table 1. OCTA parameters acuity pre- and post-surgery.

	VA pre	VA post	P*
Signal Strength	3.9 ± 2.3	5.7 ± 2.1	< 0.001
PD Central	3.4 ± 3.3	6.9 ± 5.3	< 0.001
PD Inner	14.1 ± 10.6	25.2 ± 11.7	< 0.001
PD Outer	17.5 ± 10.8	27.8 ± 10.3	< 0.001
PD Full	16.4 ± 10.4	26.6 ± 10.3	< 0.001
VD Central	1.8 ± 1.5	3.3 ± 2.5	< 0.001
VD Inner	6.6 ± 4.7	10.9 ± 4.7	< 0.001
VD Outer	8.2 ± 4.5	11.8 ± 4.0	< 0.001
VD Full	7.4 ± 4.5	11.4 ± 4.0	< 0.001
FAZ area	0.23 ± 0.18	0.20 ± 0.21	0.32
FAZ perimeter	2.04 ± 1.00	1.57 ± 0.61	0.62
FAZ circularity	0.65 ± 0.14	0.62 ± 0.09	0.59

*Paired t-test. PD: perfusion density; VD: vascular density; FAZ: foveal avascular zone.

In this study, we included 58 eyes of 33 subjects (21 female, 12 male), aged 67 ± 5 years. Table 1 shows pre- and post-surgery values for the perfusion density, vascular density, and FAZ in the central, perifoveal and parafoveal zones. The signal strength improved significantly after surgery. Similarly, the perfusion density and vascular density also increased significantly after surgery (P<0.001). Figure 1a & b shows OCTA images of an eye before and after surgery showing increased perfusion and vascular density.

Figure 1. (a) The OCTA of a patient before cataract surgery. (b) The OCTA of a patient after cataract surgery

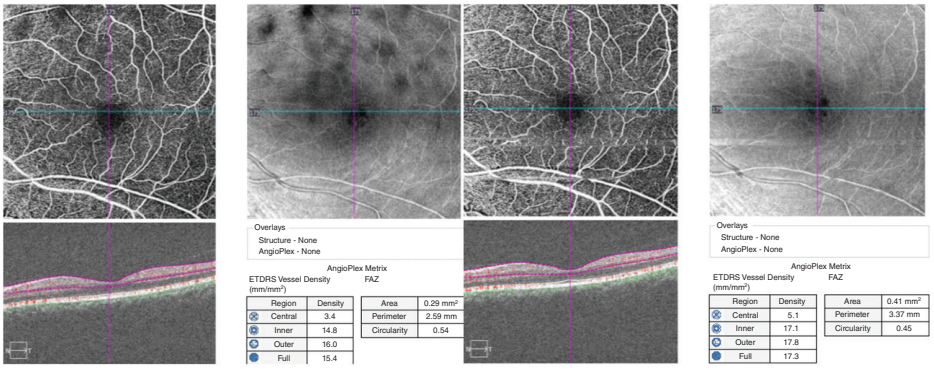

(a) (b)

Table 2. Pearson correlation, *r*, between signal strength and the different OCTA parameters.

	r	P
PD Central	0.56	< 0.001
PD Inner	0.83	< 0.001
PD Outer	0.86	< 0.001
PD Full	0.86	< 0.001
VD Central	0.49	< 0.001
VD Inner	0.75	< 0.001
VD Outer	0.80	< 0.001
VD Full	0.79	< 0.001
FAZ area	-0.029	0.84
FAZ perimeter	-0.069	0.63
FAZ circularity	-0.082	0.57

PD: perfusion density; VD: vascular density; FAZ: foveal avascular zone

Figure 2. (a) Perfusion density vs signal strength. (b) Vascular density vs signal strength

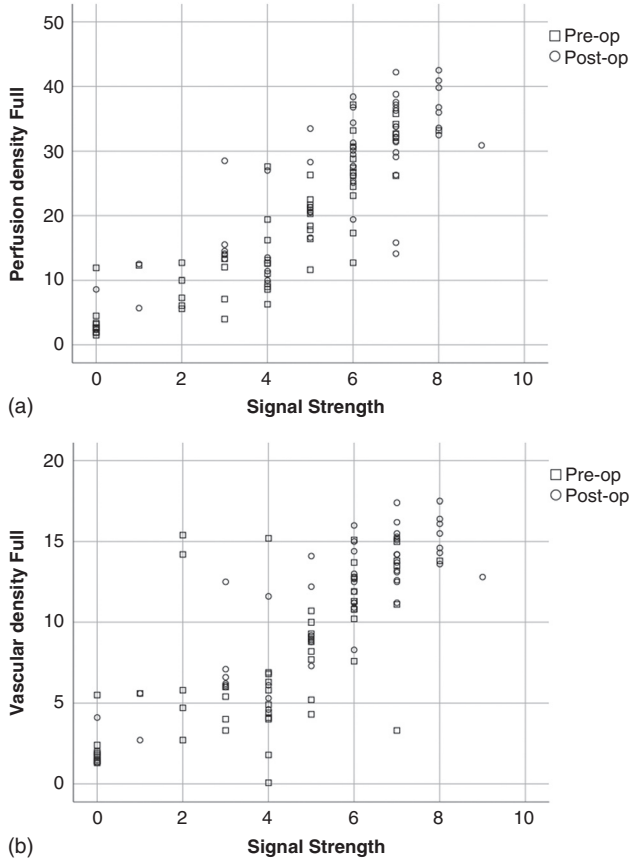

A strong positive correlation was found between signal strength and the perfusion and vascular density (Table 2). The scatter plots in Figure 2 show the association between signal strength and perfusion and vascular density.

A linear mixed model analysis with eye as grouping factor, the different OCTA parameters as dependent variable and time (i.e. pre- and post-surgery) and signal strength as covariates showed that both signal strength and surgery independently caused an increase in perfusion density and vascular density (Table 3). Assuming a constant signal strength of 8, associated with an excellent signal, this would imply an increment in perfusion density of 20% in the central zone, of 12% in the inner zone and of 10% in the outer zone. For the vascular density this would be 11%, 12% and

8% respectively. The FAZ parameters i.e. area, perimeter and circularity, did not change after surgery and showed no correlation with the signal strength. None of the patients showed any changes of cystoid macular edema at the study end point of 4–6 weeks.

Table 3. Pearson correlation, *r*, between signal strength and the different OCTA parameters.

	constant	signal strength		post- versus pre-surgery	
	β	β	P	β	P
PD Central	1.42	0.97	< 0.001	1.85	0.012
PD Inner	2.98	3.94	< 0.001	4.20	0.001
PD Outer	6.18	3.93	< 0.001	3.64	< 0.001
PD Full	5.28	3.79	< 0.001	3.63	< 0.001
VD Central	1.17	0.83	< 0.001	0.85	0.023
VD Inner	2.61	1.50	< 0.001	1.78	0.009
VD Outer	3.77	1.45	< 0.001	1.27	0.020
VD Full	3.41	1.44	< 0.001	1.61	0.003

PD: perfusion density; VD: vascular density

8.4. DISCUSSION

In this prospective study, measuring OCTA parameters before and after cataract surgery, in a cohort of patients who underwent routine uncomplicated cataract surgery, we found that there was a significant increment in retinal capillary perfusion and vascular density in the superficial capillary plexus. This relation persisted even after adjusting for the proportionally increased signal strength due to cataract removal. The maximum increment in vascular parameters was seen in the central zone and least in the perifoveal zone between 3 and 6 mm from center of fovea. The FAZ dimensions did not show any change on OCTA parameters after the cataract surgery and was not affected by the signal strength.

In a recent study with a similar methodology, Zhao et al. evaluated the macular vasculature of 32 consecutive eyes undergoing uncomplicated cataract surgery using a split-spectrum amplitude-decorrelation angiography algorithm (RTVue-XR Avanti

(Optovue, Inc.).[11] They reported that the mean vessel density increased by 6% and 3% in the parafoveal and perifoveal area at 3 months after surgery.

The authors also reported a 27% reduction in the size of the FAZ. Contrary to these results, we did not find any change in the FAZ and also found greatest increment in vascularity on the central 1 mm zone of about 20% from baseline. These differences could be explained on the basis of different algorithms used to analyze the OCTA data with different machines, and importantly, adjustment for signal strength done in our study as opposed to unadjusted measures reported by Zhao et al.[11] Tan et al.[9] have pointed out this ambiguity of unadjusted values presented by Zhao et al. and have cast doubts on the results published.

Similarly, Yu et al. have demonstrated the influence of cataract density and grade on the OCTA measurements using a swept source OCTA in 12 eyes.[8] Authors showed increment in the perfusion and vessel densities in both the superficial and deep capillary plexus after cataract surgery within the 3 × 3 mm images obtained. Authors also observed significantly better distinguishability of FAZ border postoperatively, however, FAZ area and perimeter measurements did not significantly change after cataract surgery, a finding similar to ours. Lim et al. have also shown signal strength as an important factor in the analysis of microvascular density using OCTA.[10] In view of these publications, we thought it was prudent to evaluate changes in the macular vascularity after adjustment of the increase in signal strength. Age is another factor known to influence these measurements.[12] However, given the small range of age in our study and the limited numbers, we did not include age as a covariate in our statistical modeling when adjusting for signal strength.

We observed maximum increment in vascularity in the central 1 mm zone around the FAZ. This could be because of the way the algorithm computed the thickness with maximum averaging done at the macula, or it could be because the pro-inflammatory cytokines produced after cataract surgery gravitate to the centre of the fovea and lead to increased vascular density and permeability. However, none of the eyes developed cystoid macular edema, making it difficult to provide a direct clinical application to these findings. Yet, it may be prudent to perform OCTA before cataract surgery, especially in eyes with diabetic retinopathy and other diseases prone to developing macular edema postoperatively. Also, these findings may be transient and studies with longer follow up are required to determine this.

The drawbacks of the study are the lack of assessment of the deep capillary plexus and lack of correlation with macular thickness values using the structural OCT. The merits are the adequate number of eyes studied and the statistical adjustment done to compensate for the influence of signal strength on macular vessel density.

8.5. CONCLUSION

In conclusion, even after adjusting for changes in signal strength, we observed a near 20% increment in the macular perfusion and vascular density in the central 1 mm area around the fovea. These increments were slightly lower but still statistically significant in the parafoveal and perifoveal regions. FAZ was not influenced by cataract surgery. The clinical relevance of these findings needs to be studied further with larger samples and longer follow-up periods.

What was known

1. Signal strength while obtaining OCT images improves after cataract surgery due to media clarity.
2. Studies have shown a slight increment in the macular thickness after uncomplicated cataract surgery using automated OCT measurements, thereby providing surrogate evidence of an increase in retinal perfusion after cataract surgery.
3. Quantitative measurements of the retinal vascular density and perfusion status after cataract surgery have shown slight increment after surgery, however, there is controversy regarding whether OCTA measurements denote a true increment in blood flow.

What this paper adds

1. There is significant increment in retinal capillary perfusion and vascular density in the superficial capillary plexus after cataract surgery and this relation persisted even after adjusting for the proportionally increased signal strength due to cataract removal.
2. The maximum increment in vascular parameters was seen in the central zone within 1 mm of fovea and least in the perifoveal zone between 3–6 mm from center of fovea.
3. The FAZ dimensions did not show any change on OCTA parameters after the cataract surgery and was not affected by the signal strength.

REFERENCES

1. Flach AJ. The incidence, pathogenesis and treatment of cystoid macular edema following cataract surgery. *Trans Am Ophthalmol Soc.* 1998;96:557–634.
2. Hilton EJ, Hosking SL, Gherghel D, Embleton S, Cunliffe IA. Beneficial effects of small-incision cataract surgery in patients demonstrating reduced ocular blood flow characteristics. *Eye*. 2005;19(6):670–675.
3. Perente I, Utine CA, Ozturker C, et al. Evaluation of macular changes after uncomplicated phacoemulsification surgery by optical coherence tomography. *Curr Eye Res.* 2007;32(3):241–247.
4. Guliani BP, Agarwal I, Naik MP. Effect of uncomplicated cataract surgery on central macular thickness in diabetic and non-diabetic subjects. *J Ophthalmic Vis Res.* 2019;14(4):442–447.
5. Gao SS, Jia Y, Zhang M, et al. Optical coherence tomography angiography. *Invest Ophthalmol Vis Sci.* 2016;57(9):27–36.
6. Zhao Y, Yang K, Li J, Zhu S. Comparison between the prechopping method with a reverse chopper and the routine stop-and-chop method in treating cataract with grade IV hard nucleus. *J Fr Ophtalmol.* 2018;41(4):315–320.
7. Alnawaiseh M, Müller V, Lahme L, Merté RL, Eter N. Changes in flow density measured using optical coherence tomography angiography after istent insertion in combination with phacoemulsification in patients with open-angle glaucoma. *J Ophthalmol.* 2018;2018:2890357.
8. Yu S, Frueh BE, Steinmair D, et al. Cataract significantly influences quantitative measurements on swept-source optical coherence tomography angiography imaging. *PLoS One*. 2018;13(10):e0204501.
9. Tan CS, Lim LW, Ting DS. Changes in retinal vasculature after phacoemulsification evaluated using optical coherence tomography angiography. *J Cataract Refract Surg*. 2018;44(10):1297–1298.
10. Lim HB, Kim YW, Nam KY, Ryu CK, Jo YJ, Kim JY. Signal strength as an important factor in the analysis of peripapillary microvascular density using optical coherence tomography angiography. *Sci Rep.* 2019;9(1):16299.

11. Zhao Z, Wen W, Jiang C, Lu Y. Changes in macular vasculature after uncomplicated phacoemulsification surgery: optical coherence tomography angiography study. *J Cataract Refract Surg.* 2018;44(4):453–458.

12. Iafe NA, Phasukkijwatana N, Chen X, Sarraf D. Retinal capillary density and foveal avascular zone area are age-dependent: quantitative analysis using optical coherence tomography angiography. *Invest Ophthalmol Vis Sci.* 2016;57(13):5780–5787.

CHAPTER 9

EARLY VISUAL FUNCTIONAL OUTCOMES AND MORPHOLOGICAL RESPONSES TO ANTI-VASCULAR GROWTH FACTOR THERAPY IN DIABETIC MACULAR EDEMA USING OPTICAL COHERENCE TOMOGRAPHY ANGIOGRAPHY

Supriya Dabir, Mohan Rajan, Liji Parasseril, Vaidehi Bhatt, Preetam Samant, CAB Webers, TTJM Berendschot

CLINICAL OPHTHALMOLOGY 2021; 15:331–339

ABSTRACT

PURPOSE

Diabetic macular oedema (DME) is a vision threatening complication of diabetic retinopathy. Spectral domain optical coherence tomography angiography (SD-OCTA) is useful for assessing DME. We performed serial OCTA measurements before and after 3 monthly intravitreal anti-vascular endothelial growth factor (anti-VEGF) injections to understand its relation with best corrected visual acuity (BCVA), central macular thickness (CMT) and vascular indices.

METHODS

OCTA assessment consisting of 6 × 6 mm scans centred on fovea and en-face retinal angiograms were obtained. Scans were done at baseline and at 1 month following each of the 3 intravitreal injections of anti-VEGF (Ranibizumab- Lucentis®).

RESULTS

Our prospective study included 24 eyes of 24 subjects, aged 63.0 ± 5.0 years. There was a mean gain of 0.07 log MAR (3 letters) and reduction of CMT, vessel density (VD) and perfusion density (PD) by end of 3rd month. CMT was independently associated with improvement in BCVA. There were significant reductions in FAZ area, VD and PD over 3 months from baseline.

CONCLUSION

At 3 months, intravitreal anti-VEGF therapy is associated with visual function recovery in DME, with reduction in CMT being the most reliable predictor of response. OCTA shows a reduction in VD and PD suggestive of reduced macular perfusion in the short term. Simultaneous reduction in FAZ size can be due to reversal of manual displacement of the retinal capillaries resulting from resolution of intraretinal edema.

Keywords: Diabetic macular oedema, superficial capillary plexus, vascular density, perfusion density, foveal avascular zone, optical coherence tomography angiography, macular ischemia.

9.1. INTRODUCTION

Diabetic retinopathy (DR) is a common cause for acquired loss of vision in adults worldwide and is known to be a progressive microvascular complication of diabetes mellitus. India alone is estimated to have 72 million people with diabetes mellitus (DM) and potentially 33% of them are at risk of developing retinopathy.[1] With a prevalence and a rising trend in diagnosis of DM at a younger age, the incidence of retinopathy is expected to rise. In fact, the risk of developing sight threatening DR is 2 times higher in people who develop DM earlier in life (<40 years) and nearly 6.5 times higher in individuals with long-standing DM (>16 years).[2]

Diabetic macular oedema (DME) is the most common vision threatening complication of DR and is estimated to be affecting ~9% of all patients with any form of DR in India.[1] A metabolic cascade secondary to systemic hyperglycaemia results in the disruption of the blood retinal barrier (BRB) and is a consequent cause of macular oedema. Although inflammatory dysregulation of the vascular endothelium could be a critical pathway, it is also found that the swelling and subsequent apoptosis of pericytes activates the cascade of vasoconstriction, followed by disruption resulting in vasculopathy and fluid collection.[3,4] Hypoxia caused by the microvascular disease stimulates the release of vascular endothelial growth factor (VEGF), leading to increased vascular permeability and resultant retinal oedema.[3] In recent years, the use of intravitreal anti-VEGF injections have become the standard of care in managing diabetic macular oedema.[5] Intravitreal steroids are used as an alternative in patients who fail to respond to anti-VEGF, elderly individuals with pseudophakia, or when they are unable to take monthly injections. These therapies are also best used with routine monitoring and measurements of the retinal vasculature as frequently as possible to obtain safe and effective patient outcomes. While fluorescein angiography had been the established gold standard for assessing retinal vasculature, it is limited by its invasiveness, use of contrast, and limited ability to obtain quantifiable measurements of avascular area and vessel density.[6]

Newer non-invasive modalities such as spectral domain optical coherence tomography (SD-OCT) have paved a way for assessing the effectiveness of intravitreal anti-VEGF treatment in patients with DME and is the current gold standard in care.[6] Spectral domain optical coherence tomography angiography (SD-OCTA) has added a new dimension to understanding the disease as it gives the vascular pattern of the different layers of the retinal capillaries. It was limited in its use till late because of being predominantly qualitative, time-consuming and lack of an applicable software.

Now with the automated software built into the machine, it is easier to quantify the vascular features. Studies in the past have described the various changes that occur on OCT in diabetic retinopathy. However, more studies are needed in the Indian setting to understand the relation between the OCTA markers and improvement in the visual acuity following anti-VEGF therapy, given the high burden of cases and resource poor setting to tailor optimal strategies. To understand the recovery in retinal microvasculature and treatment responses to anti-VEGF agents, in this study our objective was to perform serial OCTA measurements before and after monthly intravitreal anti-VEGF injections (Ranibizumab-Lucentis®). Our aim was to understand the changes in central macular thickness (CMT), vascular indices, and foveal avascular zone (FAZ). We also explored the relationship between the change in the best-corrected visual acuity (BCVA) with OCTA measures including CMT, FAZ, vessel density (VD), and perfusion density (PD).

9.2. PATIENTS AND METHODS

This prospective study at Rajan Eye Care Hospital Pvt Limited, a tertiary eye care centre in Chennai, South India, included patients with type 2 diabetes who were diagnosed with diabetic macular oedema, defined as central retinal thickness greater than 300 mm. The clinical severity of DR in each patient was classified using the International Clinical Diabetic Retinopathy Disease Severity Scale. Eyes with moderate-severe DR, were included in this study. We included both treatment-naïve eyes and eyes that received previous anti-VEGF or focal photocoagulation treatments more than 6 months before the base-line. We excluded patients with retinal vascular diseases, uveitis, glaucoma. Any media opacities like dense cataracts and patients with OCTA scans with signal strength less than 6 were not enlisted in the study. Patients with systemic history of recent cerebrovascular accident/ischemic heart disease in the last 6 months were also excluded. The methodology adhered to the tenets of the Declaration of Helsinki and the Rajan eye care ethical Committee. Informed consent was obtained from all patients.

All patients underwent a comprehensive ophthalmic evaluation including SD-OCT, OCTA, best-corrected visual acuity (BCVA), tonometry, slit lamp bio microscopy and indirect fundus examination at baseline,1 month, 2 months, and 3 months. The

patients received loading monthly injections for a period of 3 months irrespective of the fluid status on SD-OCT (fixed dosage regimen). Physician clearance was obtained if the patient had a recent history of systemic thromboembolic event within the past 3 months. One-week variation in dosing was allowed. The procedure was done by an experienced retina surgeon in the Operation Theatre, under aseptic precautions. OCTA assessment was done using the Zeiss Angioplex – 5000 OCTA system (Carl Zeiss Meditec, USA). The scans were acquired by a technician well-trained in obtaining OCTA. Only scans with signal strength more than 6 were considered. A 6 × 6 mm scan centred on the fovea was acquired and en-face retinal angiograms were created using the proprietary Optical Microangiography (OMAG) algorithms from the manufacturer that utilizes amplitude and phase OCT signal data to deliver the angiography images. After acquisition, automated measurements from the superficial capillary plexus were used for study purposes. Parameters used were central macular thickness, perfusion density, vascular density and the size of the foveal avascular zone (FAZ). The scan was done 4 times in total for each patient, at baseline and at 1 month after each of the 3 injections.

9.2.1. STATISTICAL ANALYSIS

Statistical calculations were done with SPSS statistical software (version 25, IBM Corp, Armonk, NY, USA). To study changes in time, we used a general linear model repeated analysis and performed a linear mixed model analysis. Results are expressed as mean ± standard deviation. To analyse visual acuity, we used LogMar values. A p-value of <0.05 was considered significant.

9.3. RESULTS

In this study we included 24 eyes of 24 subjects (9 female, 15 male), aged 63.0 ± 5.0 years and of which 9 were pseudophakic. Eleven patients had moderate NPDR and 13 had severe NPDR with a mean duration of diabetes mellitus around 16.2 ± 4.0 years. Twenty-one eyes were treatment-naïve while 3 eyes had previously received treatment with anti-VEGF injections ± laser minimum 6 months prior to the study. We treated 14 right eyes and 10 left eyes. Visual acuity improved in time. Vessel density and PD decreased significantly in time, as seen in Figure 1, for all four areas as well as the area and perimeter of the FAZ and the CMT. We found no differences in time in the circularity of the FAZ (Table 1).

Figure 1. The SCP with the vessel density and perfusion density at baseline and 1 month after the 3rd injection of a study patient. It shows the superficial capillary plexus (a) with vessel density calculated at baseline (b) with vessel density calculated at the end of 3 months (after 3 consecutive injections of anti-VEGF) (c) with perfusion density calculated at baseline (d) with perfusion density calculated at the end of 3 months (after 3 consecutive injections of anti-VEGF)

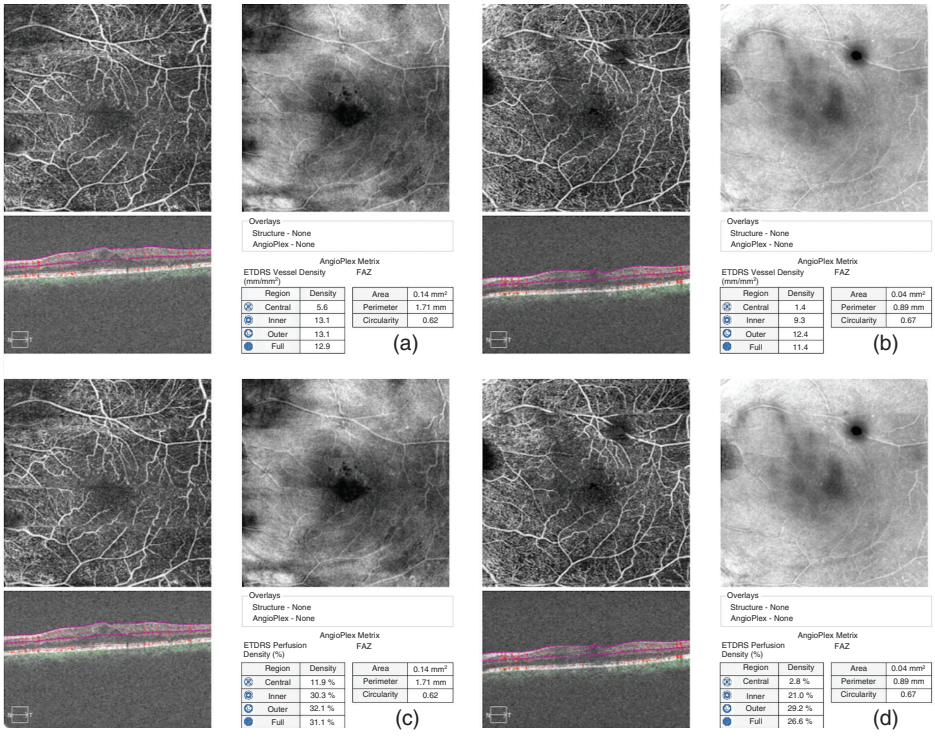

Table 1. Visual acuity, central macular thickness and different OCTA parameters at baseline and follow-ups.

	Baseline	1 month	2 months	3 months	P[a]	P[b]
LogMar	0.27 ± 0.18	0.25 ± 0.12	0.25 ± 0.18	0.20± 0.17	0.017*	0.028*
Snellen[c]	0.54 ± 0.22 (20/37)	0.56 ± 0.16 (20/36)	0.56 ± 0.23 (20/36)	0.63± 0.25 (20/32)		< 0.001
CMT	450 ± 94	409 ± 81	382 ± 81	331 ± 69	< 0.001*	< 0.001*
VD Central	7.0 ± 3.1	5.4 ± 2.4	5.2 ± 2.9	4.0 ± 2.3	< 0.001*	< 0.001*
VD Inner	13.2 ± 1.8	11.9 ± 2.1	10.8 ± 3.4	9.7 ± 2.4	< 0.001*	< 0.001*
VD Outer	13.5 ± 2.1	12.2 ± 1.8	11.1 ± 2.4	10.4 ± 2.2	< 0.001*	< 0.001*
VD Full	13.2 ± 1.9	11.9 ± 1.7	10.9 ± 2.6	10.1 ± 2.0	< 0.001*	< 0.001*
PD Central	14.8 ± 7.2	11.3 ± 6.4	11.2 ± 6.7	9.1 ± 5.7	< 0.001*	0.001*
PD Inner	31.0 ± 4.3	27.5 ± 5.5	25.6 ± 8.8	23.7 ± 6.5	< 0.001*	< 0.001*
PD Outer	32.2 ± 4.7	29.3 ± 5.0	26.9 ± 6.5	26.5 ± 5.4	< 0.001*	0.001*
PD Full	31.5 ± 4.3	28.4 ± 4.7	26.2 ± 6.9	25.4 ± 5.6	< 0.001*	< 0.001*
FAZ area	0.21 ± 0.15	0.17 ± 0.12	0.17 ± 0.14	0.19 ± 0.14	0.002*	0.012*
FAZ perimeter	2.13 ± 1.13	1.80 ± 0.78	1.82 ± 0.95	1.95 ± 0.95	0.004*	0.024*
FAZ circularity	0.56 ± 0.14	0.61 ± 0.10	0.61 ± 0.15	0.57 ± 0.15	0.15	0.31

[a] General linear model repeated model analysis; [b] Linear trend in a general linear model repeated model analysis; [c] Determined from LogMAR values; *P-value which is statistically significant; Abbreviations: CMT: Central macular thickness; VD: vascular density; PD: perfusion density; FAZ: foveal avascular zone

We performed a Pearson correlation between LogMAR, CMT, area, and perimeter of the FAZ on one hand and VD and PD on the other hand (Table 2). It showed that the vessel and perfusion densities at the different areas all correlated with each other significantly (r>0.97, P<0.001). Thus, a decrease in VD and PD was significantly correlated with reduction in CMT and decrease in area and perimeter of FAZ. Since VD and PD correlated with CMT, area and perimeter of the FAZ, which changed over time, the observed decreases in both may just be, attributable to the decrease in the latter three.

Table 2. Pearson correlation between LogMAR, CMT, area, and perimeter of the FAZ on one hand and VD and PD on the other hand.

	LogMar		CMT		FAZ area		FAZ perimeter	
	r	P	r	P	r	P	r	P
LogMar			0.57	< 0.001*	0.089	0.42	0.090	0.42
CMT	0.57	< 0.001*			0.13	0.22	0.14	0.22
VD Central	0.42	< 0.001*	0.60	< 0.001*	0.33	0.003*	0.30	0.005*
VD Inner	0.22	0.030*	0.30	0.003*	0.45	< 0.001*	0.44	< 0.001*
VD Outer	0.075	0.47	0.27	0.008*	0.57	< 0.001*	0.55	< 0.001*
VD Full	0.15	0.15	0.31	0.002*	0.56	< 0.001*	0.54	< 0.001*
PD Central	0.49	< 0.001*	0.57	<0.001*	0.31	0.005*	0.28	0.009*
PD Inner	0.19	0.060	0.29	0.004*	0.48	< 0.001*	0.47	< 0.001*
PD Outer	0.029	0.78	0.21	0.042*	0.58	< 0.001*	0.57	< 0.001*
PD Full	0.095	0.36	0.25	0.013*	0.59	< 0.001*	0.57	< 0.001*
FAZ area	0.089	0.42	0.13	0.22			0.97	<0.001*
FAZ perimeter	0.090	0.42	0.14	0.22	0.97	<0.001*		
FAZ circularity	–0.11	0.32	–0.10	0.36	–0.62	<0.001*	–0.74	<0.001*
FAZ circularity	0.56 ± 0.14	0.61 ± 0.10	0.61 ± 0.15	0.57 ± 0.15	0.15			

Abbreviations: CMT: Central macular thickness; VD: vascular density; PD: perfusion density; FAZ: foveal avascular zone; *P-value which is statistically significant

We therefore performed a linear mixed model analysis with eye as the grouping factor, the vessel or perfusion density as the dependent variable and time, central macular thickness and area and perimeter of the fovea avascular zone as covariates (Table 3). It showed that the central macular thickness and the area of the avascular zone independently contributed to the vessel and perfusion density changes. To be precise, a decrease in the CMT and FAZ size was positively correlated with a reduction in VD and PD, respectively.

Neither did the perimeter of the foveal avascular zone contribute additionally nor did we find an additional independent change in time. For LogMAR, central macular thickness appeared to be the only predictor in this approach.

Table 3. β-coefficients from a linear mixed model analysis

	Intercept	CMT		FAZ area	
		β	p	β	p
LogMar	0.073	0.00037	0.011*	0.12	0.22
VD Central	–3.13	0.019	< 0.001*	5.09	0.003*
VD Inner	6.14	0.0092	0.005*	9.33	< 0.001*
VD Outer	8.44	0.0046	0.041*	8.69	< 0.001*
VD Full	7.62	0.0062	0.005*	8.25	< 0.001*
PD Central	–6.58	0.041	< 0.001*	11.96	0.004*
PD Inner	14.41	0.021	0.009*	25.31	< 0.001*
PD Outer	21.07	0.0091	0.123	23.15	< 0.001*
PD Full	18.81	0.012	0.033*	23.45	< 0.001*

Abbreviations: CMT: Central macular thickness; VD: vascular density; PD: perfusion density; FAZ: foveal avascular zone; *p-value which is statistically significant

9.4. DISCUSSION

The current study aimed at measuring longitudinal changes in the functional (BCVA) and anatomical markers following 3 monthly intravitreal anti-VEGF injections in patients with moderate to severe NPDR, and DME based on OCTA. Early responses to anti-VEGF injections reflected a significant visual function recovery as noted by a mean gain of 0.7 log MAR (3 letters) within the group, as well as the reduction of the central CMT, VD and PD by the end of 3rd month. Most of the individuals can be considered to have responded to the anti-VEGF in terms of resolution of macular oedema, and the average reduction of CMT observed was ~120 µm at the end of 3rd month (Table 1).[7] A similar reduction in the CMT has been observed in past studies as well.[8, 9] Although, individual variability did exist in the extent of response amongst the individuals, given the small numbers we were unable to perform any sub-group analysis to explore the potential predictors of good and poor response. Past studies also indicated significant variability in the resolution of macular oedema to anti-VEGF therapy, and up to 50% of the treated individuals have been noted to show significant reduction, and at times, the remainder of them respond poorly to the anti-VEGF therapy.[10]

The analyses also highlighted that the reduction in the CMT was independently associated and predicted the improvement in the BCVA (Table 3). Indeed, oedema reduction and subsequent neural activation could promote synergistically the recovery in the microvascular dysfunction too. Previous studies indicated persistent macular oedema to be a negative prognostic factor in achieving desired visual acuity both in the short- and long-term.[9, 11]

Additionally, the study also demonstrates a significant reduction in the FAZ area, the VD and PD measures over 3 months from baseline (Table 1).

We found that the FAZ area correlated with the reduction in the CMT, however, the model did not attribute any significant contribution of it in the apparent improvement in BCVA (Table 3). With the advent of the OCTA and automated analyses, FAZ estimation has been noted to be reliable, even in comparison to the gold standard fluorescein angiography.[12] Other studies have reported a strong negative correlation between FAZ size and visual acuity and a larger FAZ size to be associated with poor BCVA.[13] Reduction in FAZ following anti-VEGF therapies has been reflective of improved outcomes, and in fact non-reduction to be a predictor of recurrence of oedema.[9,14] Anti-VEGF agents modulate vasculogenesis in the FAZ and supports the optimization of optical path in the cone dense mosaic of the macula, resulting in improved retinal sensitivity.[15–17]

OCTA, unlike the dye-based angiography methods, allows one to quantify the retinal and choroidal vasculature non-invasively, based on the principle of measuring the scattered signals by the moving erythrocytes within the vessels. The VD is one such feature of interest and demonstrably differentiates between the healthy eyes and eyes with diabetic retinopathy. Eyes with DR particularly are noted to have a lower VD in the superficial retinal layer as compared to their healthy matches.[18,19] Also, most studies indicated the VD to be lower in eyes with macular oedema than those without and baseline VD to be a predictor of good treatment response.[8, 14, 20–22] In the study reported by Atta Allah et al., it is particularly of interest to note that the VD differences between the eyes with and without macular oedema was not significantly different, suggesting a differential axis of regulation and possibly non-VEGF mediated mechanisms at play.

In specific view of the VD measurements following anti-VEGF therapy, current reportage of studies indicates a bi-directional response.[23] While most of the studies have shown either a neutral or a positive change in VD[14, 20, 24–26] following anti-VEGF injections, a few have also reported a reduction in VD following anti-VEGF.[27] At the same time Tomita et al., reported a lower VD to be a predictor of recurrence of oedema. The

precise nature of the changes in VD as well as its relation to characterizing macular perfusion specifically following anti-VEGF therapy remains unclear and considerable variability continues to exist, although few long-term follow-up studies have noted a stable or no change in VD following anti-VEGF. [28] In our study, a significant reduction in VD and PD was seen, which is indicative of progression of ischemia. At the same time, we noted a simultaneous reduction in FAZ size which is paradoxical, as it is indicative of improvement in macular perfusion. Nonetheless, a reduction in FAZ size can also occur because of a decrease in manual displacement of retinal capillaries secondary to improvement in macular oedema. This reduction in macular fluid or the central CMT was evidently seen in our series. Hence, we postulate that the primary reason for a reduction in FAZ size seen in our study is due to a concurrent decrease in capillary displacement secondary to resolution of intraretinal oedema, rather than an improvement in macular perfusion. The FAZ circularity too remained unaltered during the 3-month period, indicating no change in the configuration of the FAZ capillary margins. This outcome also corroborates the mechanical displacement theory of changes seen in FAZ size rather than an ischemic cause. Nonetheless, studies continue to report differential responses of the retinal microvasculature measurements in the wake of DME, even with the OCTA. Although comparability amongst the studies are noted to be presently very low, more harmonization in the future could aid better and meaningful comparisons.

It appears that the macular vessel density in DME has a multifactorial origin, role of the pericyte and its modelling of the autoregulatory function of retinal capillaries could be a supplementary axis of dysfunction in addition to the VEGF mediated vascular changes. While the loss of retinal pericytes has been well-established in the breakdown of inner BRB, precise mechanisms are not very clear yet.[29] Also, that the neurovascular coupling in the retinal perfusion linked to active relaxation of the capillaries is understood to be regulated in part by the coupling of the endothelial cell-pericyte interaction.[30] It needs to be seen if pericyte dysfunction represents a residual effect following anti-VEGF therapy.

Different studies have chosen different scan protocols. Ho et al. showed that there was clinical utility for both the higher scan resolution obtainable with a smaller (3 × 3 mm) scan, as well as the larger field of view obtained with larger (6 × 6 mm) OCTA scan protocols in assessing patients with diabetic retinopathy. The more diffuse details of capillary non-perfusion and presence of microaneurysms were better delineated with the 6 × 6 mm scans, though FAZ measurements were more reliable with 3 × 3 mm.[31] Excellent results were found for FAZ area interrater reliability for superficial

vascular layers in smaller angiocubes (i.e. 3 × 3 mm and 6 × 6 mm). However less but still satisfactory reliability was disclosed for 12 ×12-mm angiocube at the same plexuses.[32] We chose the 6 × 6 mm scan protocol as a balance between 3 mm and 12 mm angiocubes, and it delineated the capillary non-perfusion details better.

With better adoption of OCTA, further studies are required to understand the temporo-spatial responses in the retinal microvasculature and cone mosaic to anti-VEGF therapy and its resultant effect in improving the visual acuity.

It must be noted that this study has some limitations. We did not control for factors such as axial length, stage of DR and age, which may affect the quantitative OCTA data. While the OCTA method has been noted to be a very reliable and accurate technique to delineate the retinal thickness and FAZ, measures related to the vessel and perfusion density are yet to be perfected, and depend on the availability of suitable software algorithms, the characterization of the effect of oedema and underlying pathology. Also, the current measurements were limited to the measuring the superficial capillary plexus (SCP) alone, as routine deep capillary plexus (DCP) measurements on OCTA are not bereft with poor visualization and low reliability especially in the patients with significant oedema. Even though few earlier studies have noted a differential predictability of the DCP measures on changes in treatment outcomes, it had to be done in retrospect instead of the current method to ascertain OCTA parameters prospectively.[7] In presence of significant edema, there is a possibility of artifacts impacting the accurate measurements of SCP. To overcome this potential limitation, a single trained reader manually segmented the OCTA sections. Also, by utilizing only the scans with SSI > 6 for analysis, we negated the likelihood of inaccurate measurements. Finally, a smaller sample size with short follow-up period is a drawback of the study. Studies with larger sample size and longer follow-up duration would provide better insight into the role of anti-VEGF agents in modifying macular vascularity in DME on OCTA. Furthermore, additional understanding into comparative evaluation of these parameters in treatment-naïve and previously treated eyes, which was lacking in our study due to small sample size, would be recommended.

The current study provides the first real-world data regarding the morphometric parameters on OCTA in an Indian scenario. The current study would be invaluable to assess and compare these OCTA parameters with other ethnic populations to look for any variation in treatment response. Moreover, very limited data exists regarding these OCTA changes in DME management. Limited studies have mostly utilized PRN regimen

and other agents such as aflibercept and bevacizumab.[20, 21, 33] Hence by utilizing a fixed dose regimen of ranibizumab, we aim to provide valuable real-world evidence to the curtailed existing literature. Also, we report a novel finding of reduction in FAZ size with a paradoxical simultaneous decrease in VD and CD in response to anti-VEGF therapy in DME in the short-term.

Finally, the current study demonstrated, with use of intravitreal anti-VEGF therapy, there is significant improvement in visual functions in patients with DME at 3 months. A simultaneous reduction in CMT was the most reliable predictor for visual response. On OCTA, a reduction in FAZ was noted which can by hypothesized as a concurrent reduction in manual displacement of the FAZ due to resolution of diabetic macular edema.

9.5. FUTURE DIRECTIONS

Based on the current study results we propose that OCTA (SCP) markers in a routine clinical scenario could play a good role in measuring and establishing early progress to anti-VEGF therapy. This could help individualize the standard of care in individuals with retinopathy and macular oedema. More studies are needed to address the reliability and characterization of temporo-spatial changes in the OCTA in the long-term.

REFERENCES

1. Rajalakshmi R, Behera U, Bhattacharjee H, et al. Spectrum of eye disorders in diabetes (SPEED) in India. Report # 2. Diabetic retinopathy and risk factors for sight threatening diabetic retinopathy in people with type 2 diabetes in India. *Indian J Ophthalmol.* 2020;68(13):21–26.
2. Raman R, Vaitheeswaran K, Vinita K, Sharma T. Is prevalence of retinopathy related to the age of onset of diabetes? Sankara Nethralaya Diabetic Retinopathy Epidemiology and Molecular Genetic Report No. 5. *Ophthalmic Res.* 2011;45(1):36–41.
3. Romero-Aroca P, Baget-Bernaldiz M, Pareja-Rios A, Lopez-Galvez M, Navarro-Gil R, Verges R. Diabetic macular edema pathophysiology: vasogenic versus inflammatory. *J Diabetes Res.* 2016;2016:1–7.
4. Cunha-Vaz J, Bernardes R, Lobo C. Blood-retinal barrier. *Eur J Ophthalmol.* 2011;21(suppl 6):S3-S9.
5. Virgili G, Parravano M, Evans JR, Gordon I, Lucenteforte E. Anti-vascular endothelial growth factor for diabetic macular oedema: a network meta-analysis. *Cochrane Database Syst Rev.* 2018;10(10):CD007419.
6. Kwan CC, Fawzi AA. Imaging and biomarkers in diabetic macular edema and diabetic retinopathy. *Curr Diab Rep.* 2019;19(10):95.
7. Lee J, Moon BG, Cho AR, Yoon YH. Optical coherence tomography angiography of DME and its association with anti-VEGF treatment response. *Ophthalmology*. 2016;123(11):2368–2375.
8. Sugimoto M, Ichio A, Mochida D, et al. Multiple effects of intravitreal aflibercept on microvascular regression in eyes with diabetic macular edema. *Ophthalmology Retina*. 2019;3(12):1067–1075.
9. Choi K-E, Yun C, Cha J, Kim S-W. OCT angiography features associated with macular edema recurrence after intravitreal bevacizumab treatment in branch retinal vein occlusion. *Sci Rep*. 2019;9(1):14153.
10. Agarwal A, Soliman MK, Sepah YJ, Do DV, Nguyen QD. Diabetic retinopathy: variations in patient therapeutic outcomes and pharmacogenomics. *Pharmgenomics Pers Med.* 2014;7:399–409.

11. Sadda SR, Campbell J, Dugel PU, et al. Relationship between duration and extent of oedema and visual acuity outcome with ranibizumab in diabetic macular oedema: a post hoc analysis of Protocol I data. *Eye*. 2020;34(3):480–490.

12. Enders C, Baeuerle F, Lang GE, et al. Comparison between findings in optical coherence tomography angiography and in fluorescein angiography in patients with diabetic retinopathy. *Ophthalmologica.* 2020;243(1):21–26.

13. Moein HR, Novais EA, Rebhun CB, et al. Optical coherence tomography angiography to detect macular capillary ischemia in patients with inner retinal changes after resolved diabetic macular edema. *Retina*. 2018;38(12):2277–2284.

14. Dastiridou A, Karathanou K, Riga P, et al. OCT angiography study of the macula in patients with diabetic macular edema treated with intravitreal aflibercept. *Ocul Immunol Inflamm.* 2020;1–6.

15. Kozulin P, Natoli R, O'Brien KMB, Madigan MC, Provis JM. Differential expression of anti-angiogenic factors and guidance genes in the developing macula. *Mol Vis.* 2009;15:45–59.

16. Kozulin P, Provis JM. Differential gene expression in the developing human macula: microarray analysis using rare tissue samples. *J Ocul Biol Dis Infor.* 2009;2(4):176–189.

17. Dabir S, Mangalesh S, Kumar KA, Kummelil MK, Sinha Roy A, Shetty R. Variations in the cone-packing density with eccentricity in emmetropes. *Eye.* 2014;28(12):1527–1527.

18. Lei J, Durbin MK, Shi Y, et al. Repeatability and reproducibility of superficial macular retinal vessel density measurements using optical coherence tomography angiography en face images. *JAMA Ophthalmol.* 2017;135(10):1092–1098.

19. Durbin MK, An L, Shemonski ND, et al. Quantification of retinal microvascular density in optical coherence tomographic angiography images in diabetic retinopathy. *JAMA Ophthalmol.* 2017;135(4):370–376.

20. Ghasemi Falavarjani K, Iafe NA, Hubschman JP, Tsui I, Sadda SR, Sarraf D. Optical coherence tomography angiography analysis of the foveal avascular zone and macular vessel density after anti-VEGF therapy in eyes with diabetic macular edema and retinal vein occlusion. *Invest Ophthalmol Vis Sci.* 2017;58(1):30–34.

21. Hsieh YT, Alam MN, Le D, et al. OCT angiography biomarkers for predicting visual outcomes after ranibizumab treatment for diabetic macular edema. *Ophthalmol Retina.* 2019;3(10):826–834.

22. AttaAllah HR, Mohamed AAM, Ali MA. Macular vessels density in diabetic retinopathy: quantitative assessment using optical coherence tomography angiography. *Int Ophthalmol.* 2019;39(8):1845–1859.

23. Wai KM, Singh RP. Changes in macular and peripheral perfusion following anti-vascular endothelial growth factor treatment for patients with diabetic retinopathy. *Am J Ophthalmic Clin Trials.* 2019;2:4.

24. Sorour OA, Sabrosa AS, Yasin Alibhai A, et al. Optical coherence tomography angiography analysis of macular vessel density before and after anti-VEGF therapy in eyes with diabetic retinopathy. *Int Ophthalmol.* 2019;39(10):2361–2371.

25. Fan X, Pristach C, Liu EY, Freudenreich O, Henderson DC, Goff DC. Elevated serum levels of C-reactive protein are associated with more severe psychopathology in a subgroup of patients with schizophrenia. *Psychiatry Res.* 2007;149(1–3):267–271.

26. Michaelides M, Fraser-Bell S, Hamilton R, et al. Macular perfusion determined by fundus fluorescein angiography at the 4-month time point in a prospective randomized trial of intravitreal bevacizumab or laser therapy in the management of diabetic macular edema (Bolt Study): Report 1. *Retina*. 2010;30(5):781–786.

27. Tomita R, Iwase T, Goto K, Yamamoto K, Ra E, Terasaki H. Correlation between macular vessel density and number of intravitreal anti-VEGF agents for macular edema associated with branch retinal vein occlusion. *Sci Rep.* 2019;9(1):16388.

28. Karst SG, Deak GG, Gerendas BS, et al. Association of changes in macular perfusion with ranibizumab treatment for diabetic macular edema: a subanalysis of the RESTORE (Extension) study. *JAMA Ophthalmol.* 2018;136(4):315–321.

29. Klaassen I, Van Noorden CJ, Schlingemann RO. Molecular basis of the inner blood-retinal barrier and its breakdown in diabetic macular edema and other pathological conditions. *Prog Retin Eye Res.* 2013;34:19–48.

30. Trost A, Lange S, Schroedl F, et al. Brain and retinal pericytes: origin, function and role. *Front Cell Neurosci.* 2016;10:20.

31. Ho J, Dans K, You Q, Nudleman ED, Freeman WR. Comparison of 3 mm × 3 mm versus 6 mm × 6 mm optical coherence tomography angiography scan sizes in the evaluation of non-proliferative diabetic retinopathy. *Retina.* 2019;39(2):259–264.

32. Rabiolo A, Gelormini F, Marchese A, et al. Macular perfusion parameters in different angiocube sizes: does the size matter in quantitative optical coherence tomography angiography? *Invest Ophthalmol Vis Sci.* 2018;59(1):231–237.

33. Elnahry AG, Abdel-Kader AA, Raafat KA, Elrakhawy K. Evaluation of changes in macular perfusion detected by optical coherence tomography angiography following 3 intravitreal monthly bevacizumab injections for diabetic macular edema in the IMPACT study. *J Ophthalmol.* 2020;2020:5814165.

CHAPTER 10

NEED FOR MANUAL SEGMENTATION IN OPTICAL COHERENCE TOMOGRAPHY ANGIOGRAPHY OF NEOVASCULAR AGE-RELATED MACULAR DEGENERATION

Supriya Dabir, Vaidehi Bhatt, Deepak Bhatt, Mohan Rajan, Preetam Samant, Sivakumar Munusamy, CAB Webers, TTJM Berendschot

PLOS ONE 2020; 15:E0244828

ABSTRACT

PURPOSE

To compare the characteristics of eyes that had manual vs. automated segmentation of choroidal neovascular membrane (CNVM) using optical coherence tomography angiography (OCTA).

METHODS

All patients with CNVM underwent OCTA using the Zeiss Angioplex Cirrus 5000. Slabs of the avascular outer retina, outer retina to choriocapillaris (ORCC) region and choriocapillaris were generated. Manual segmentation was done when there were significant segmentation artifacts. Presence of activity in CNVM was adjudged by the presence of subretinal fluid (SRF) on structural OCT and was compared to activity detected on en-face OCTA slabs based on well-defined criteria.

RESULTS

Eighty-one eyes of 81 patients were recruited of which manual segmentation was required in 46 (57%). Eyes with automated segmentation had significantly more CNVM in the ORCC (75%) whereas those with manual segmentation had deeper CNVM (sub-RPE=22%, intra-PED=22%) ($P<0.001$). Twenty eyes (25%) were found to have active CNVM on both the structural OCT and OCTA while an additional 19 eyes were presumed to have active CNVM on OCTA alone. There was only modest concordance between disease activity detected using structural OCT and OCTA ($\kappa=0.47$, 95% CI=0.30 to 0.64).

CONCLUSION

Manual segmentation of OCTA is required in more than 50% eyes with CNVM and this progressively increases with increasing depth of CNVM location from the ORCC to below the RPE. There is moderate concordance between OCTA and structural OCT in determining CNVM activity.

Keywords: Optical coherence tomography angiography, age-related macular degeneration, choroidal neovascular membrane, manual segmentation, automated segmentation, subretinal fluid.

10.1. INTRODUCTION

Age-related choroidal neovascular membrane (CNVM) is the leading cause of severe vision loss in the elderly.[1,2] Ancillary testing of CNVM for disease detection as well as activity has undergone paradigm shifts over the past decade, where the non-invasive structural optical coherence tomography (OCT) has almost entirely replaced the more invasive fluorescein angiography (FFA).[2,3] Recent evidence shows that there is a high level of concordance in detecting disease activity between OCT and FFA at baseline, though this concordance drops off once treatment is initiated with anti-VEGF agents.[4] More recently, optical coherence tomography angiography (OCTA) that enables visualization of the different vascular layers of the retina and choroid has been extensively used to detect the presence of CNVM as well as to determine disease activity.[5–8] Both qualitative and qualitative metrics have been developed in the assessment of OCTA images to sharpen its resemblance to disease severity and activity.[9–11] Additionally, OCTA has also enabled us to detect subclinical cases of CNVM where a neovascular complex exists without clinical signs of disease activity.[12] However, the role of OCTA in management of CNVM is still evolving.

There are many different commercially available OCTA machines based on spectral domain and swept source (SS) OCT technology.[6] Each of these uses a different proprietary algorithm to produce automated en-face OCTA slabs of the superficial and deep capillary plexus in the inner retina, avascular outer retina, outer retina to choriocapillaris (ORCC) region and choriocapillaris. Most studies published on use of OCTA in CNVM utilize the automated image analysis algorithms provided by the manufacturer to determine disease characteristics.[6,13] However, improper segmentation commonly introduces artifacts that lead to incomplete visualization of the CNVM in en-face images, especially in active cases.[14,15] Incomplete or inaccurate segmentation has wider implications in management of AMD. There is an increased likelihood of missing small early networks due to this error. Although exudation on SD-OCT in the absence of membrane on OCTA would be usually treated, but there is a distinct possibility of missing a small non-exudative membrane on OCTA due to segmentation errors. In such a scenario, the patient would be diagnosed as dry AMD and followed-up at a longer interval vis-à-vis a closer follow-up if a non-exudative membrane were detected on OCTA. Additionally, the configuration and dimensions of the network are very dependent on the section been evaluated. Automated segmentation slabs may not truly reflect the widest area of network and/or its true configuration. This can be

overcome by manually readjusting the contours of the slabs to target vascular layers of special interest and generate custom en-face images.

A comparison between manual and automated segmentation in eyes with active and inactive CNVM has been done in the past where Siggel et al. show that accuracy of the SS-OCTA in detecting CNVM decreases as we image deeper into the retina.[16] However, there is not enough literature studying this aspect of OCTA. In this study, we therefore compared the characteristics of eyes that had manual vs. automated analysis of CNVM using OCTA.

10.2. METHODS

This was a cross-sectional observational study on consecutive consenting patients with CNVM who were referred to our center, Rajan eye care hospital Pvt Ltd, Chennai, for OCTA between January 2018 and December 2019. The study was approved by the institutional ethics committee and was carried out as per the tenets of the declaration of Helsinki and good clinical practice guidelines. Written informed consent was obtained from all participants before enrollment.

All patients with CNVM, with or without a history of prior anti-VEGF therapy, and willing to participate in the study were recruited. The exclusion criteria were eyes with significant sub-retinal hemorrhage and eyes with senile cataracts or poor mydriasis precluding reliable OCTA, eyes having type 3 CNVM and aneurysmal type 1 CNVM, and eyes with any other ocular comorbidity. Before performing OCTA, all patients underwent a comprehensive eye examination including evaluation of the best corrected visual acuity (BCVA), intraocular pressure (IOP), dilated slit lamp evaluation of the anterior segment and thorough evaluation of the posterior segment. Presence of CNVM was confirmed on clinical examination by a fellowship – trained retina surgeon and its presence was confirmed by visualization of the CNVM on structural OCT.

10.2.1. OPTICAL COHERENCE TOMOGRAPHY ANGIOGRAPHY

Patients then underwent OCTA assessment of the involved eye with CNVM using the Cirrus 5000 Zeiss Angioplex (Carl Zeiss Meditec, Dublin, CA, USA). A well-trained technician acquired 6 × 6 scans centered on the fovea. Automated en-face retinal

angiograms of the superficial and deep retina, avascular outer retina, ORCC and choriocapillaris were created using the proprietary algorithms provided by the manufacturer. All images were interpreted and graded by an experienced clinician (DB). All OCTA images were analyzed for the need of manual vs. automated segmentation by two experienced clinicians (DB and SD). A good inter-grader reliability of 0.93 was obtained.

In cases where segmentation artifacts made it difficult to visualize the entire CNVM complex, manual segmentation was done using tools in the software and custom slabs were created to visualize the CNVM in its entirety, as per protocols described by Siggel et al.[16]

Briefly, we moved the two boundaries of the standard segmentation pattern such that the CNVM was completely visualized. The software was then utilized to analyze the image. Minimum signal strength of 7/10 was required to register the scan for analysis without any motion artifacts. Based on vascular characteristics observed on the en-face OCTA, the CNVM was classified as active as per descriptions given by Coscas et al.[11] In summary, the CNVM was deemed to be active when it was well-defined with numerous tiny branching capillaries, with anastomoses, peripheral loops and arcades at the vessel termini and/or presence of a hypo-intense halo around the CNVM (Figure 1).

In addition to the OCTA, patients also underwent structural OCT in the affected eyes with CNVM (Cirrus HD OCT, Carl Zeiss Meditec, Dublin, CA, USA). Presence of sub-retinal fluid (SRF) with or without intra-retinal fluid and cystoid spaces was considered to be active disease and this was used as gold standard for comparison of disease activity with OCTA. The same experienced examiner (DB) evaluated both the OCTA and OCT images but not simultaneously, such that he was masked for the lesion characteristics in one modality when grading disease activity in the other modality. The primary outcome measure was comparison between OCTA characteristics of eyes graded using the automated algorithm vs. eyes that required a manual segmentation. Concordance about the activity of the CNVM between OCTA and OCT was also assessed.

Figure 1. (a) OCTA and structural OCT from an eye with active CNVM, with the use of automated segmentation, where the outer margins are blurred. (b) OCTA and structural OCT from an eye with active CNVM, with the use of manual segmentation where the peripheral anastomoses (white arrow), which are the hallmark of activity, is well-appreciated

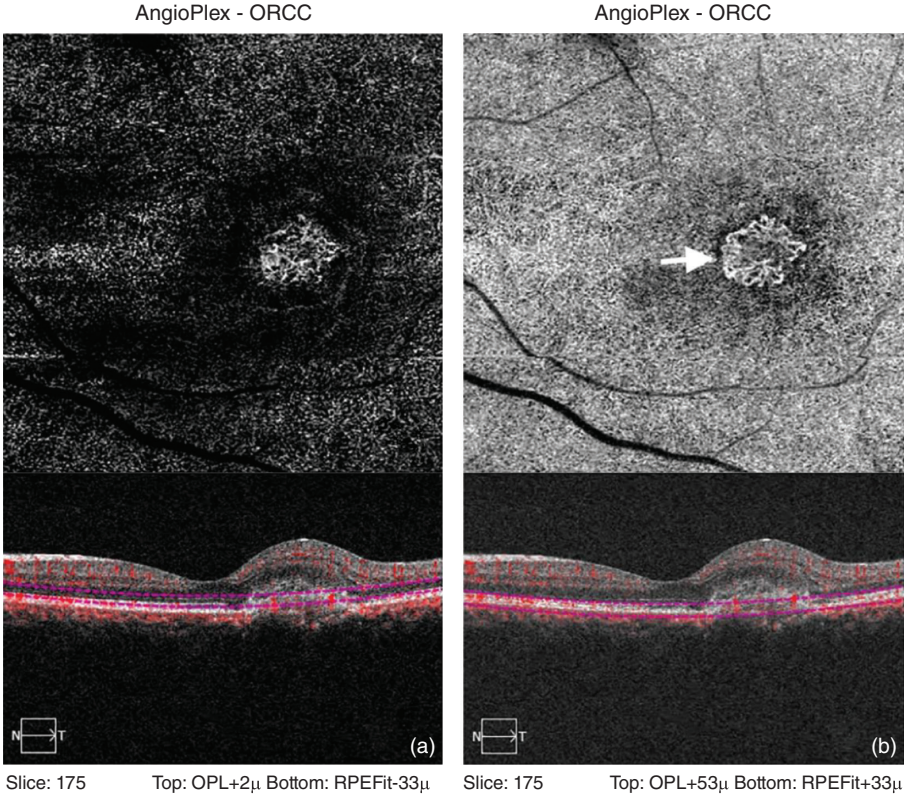

An inactive CNVM was recorded when it had long and large mature linear vessels and a dead tree appearance at the vessel termini without peripheral anastomosis, loops, or arcades (Figure 2).

Figure 2. (a) OCTA and structural OCT from an eye with inactive CNVM, with the use of automated segmentation, with poorly defined network. (b) OCTA and structural OCT from an eye with inactive CNVM, with the use of manual segmentation where the characteristic dead-tree appearance of network, which is the hallmark of end-stage disease, is well-appreciated

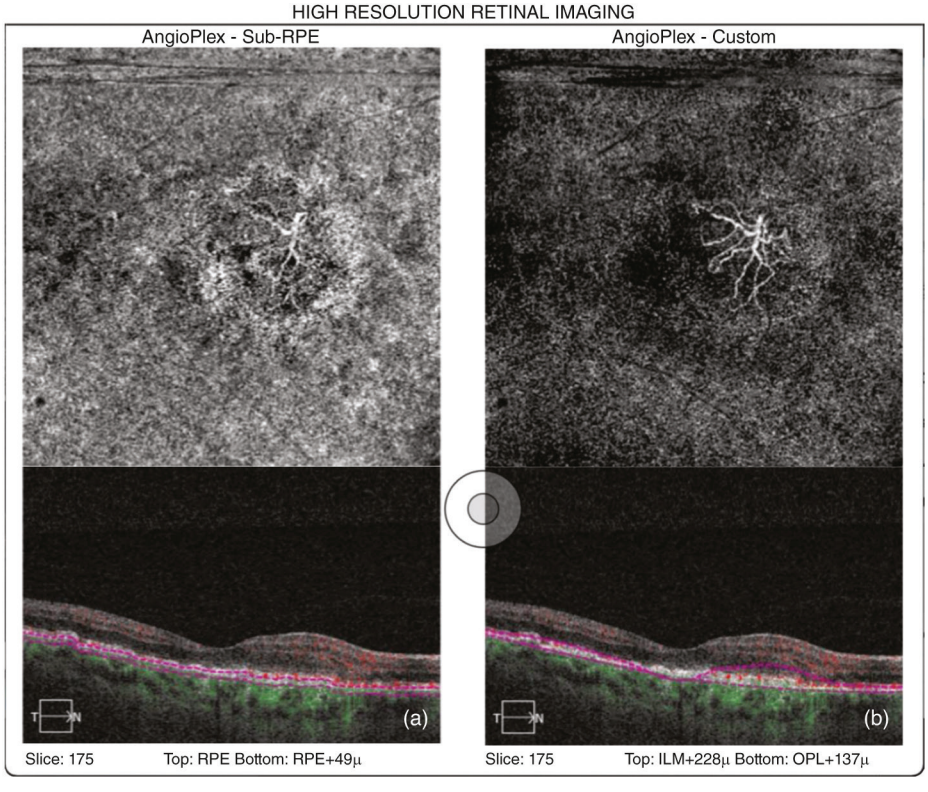

10.2.2. STATISTICAL ANALYSIS

All continuous variables were described as means with standard deviation and categorical variables were described as proportions (n, %). Differences between groups were analyzed using chi-square statistics and independent T-tests. The kappa statistic with 95% confidence interval (CI) was used to assess the concordance in disease activity between OCTA and OCT. All statistical analyses were done with SPSS statistical software (version 25, IBM Corp, Armonk, NY, USA). A p-value of <0.05 was considered significant.

10.3. RESULTS

We included 81 eyes of 81 patients with CNVM who satisfied inclusion criteria. Automated segmentation was reliable in 35 eyes (43%) while manual segmentation was required in the remaining 46 (57%). Table 1 shows a comparison between characteristics of eyes that had manual vs. automated image analysis. Eyes that were amenable to automated analysis had the CNVM predominantly in the ORCC whereas those that needed manual segmentation had a deeper location of the CNVM, with equal numbers in the sub-RPE and intra-PED regions (Table 1). Significantly more eyes in the automated OCTA group showed presence of SRF on structural OCT, but there was no difference in number of eyes with active disease based on OCTA characteristics. Automated segmentation did not depend upon type of CNVM either (Table 1).

Table 1. Descriptive for automated and manual segmentation.

Variable	Description	Segmentation		
		Automated	**Manual**	**p**
Number of eyes		35	46	
Type of CNVM	Type 1 CNVM	6 (17%)	12 (26%)	0.34
	Type 2 CNVM	29 (83%)	34 (74%)	
Location	Avascular	1 (3%)	3 (7%)	<0.001
	Choriocapillaris	2 (6%)	5 (11%)	
	Choroidal CNVM	0	2 (4%)	
	Deep vascular plexus	1 (3%)	3 (7%)	
	Deep plexus and Choriocapillaris	0	1 (2%)	
	Intra-PED	0	10 (22%)	
	ORCC	26 (74%)	8 (17%)	
	RPE-RPE Fit	0	4 (8%)	
	SUB-RPE	5 (14%)	10 (22%)	
SRF	Yes	13 (37%)	7 (15%)	0.023
Activity	Yes	20 (57%)	19 (41%)	0.16
Halo around CNVM	Yes	5 (14%)	7 (15%)	0.74
Peripheral arcades	Yes	14 (40%)	9 (20%)	0.073
Terminal Anastomosis	Yes	12 (34%)	11 (24%)	0.46

Out of the 81 eyes recruited, 18 (22%) had type 1 CNVM and the remaining 63 (78%) had type 2 CNVM. A comparison between eyes with type 1 and type 2 CNVM showed that significantly more eyes in the type 1 group (n=10, 56%) had presence of SRF on structural OCT compared to type 2 eyes (n=10, 16%) (P<0.001). Eyes with type 1 disease had marginally higher proportion of eyes detected as active on OCTA (n=12, 67%) compared to type 2 disease (n=27, 43%) (p=0.075).

Of the total of 81 eyes, 20 eyes (25%) were found to have active CNVM on the structural OCT on account of SRF whereas 39 eyes (47%) were found to harbor active CNVM on OCTA. On cross tabulating disease activity detected on OCT and OCTA (Table 2), we found that almost all eyes with activity on OCT showed active CNVM on OCTA. However, there was only modest concordance between disease activity detected using OCT and OCTA (Kappa=0.47, 95% CI=0.30 to 0.64) with half the eyes showing active CNVM on OCTA demonstrating no signs of disease activity on structural OCT. On OCTA, the hyporeflective halo around the CNVM was the least common finding in active lesions, both in the automated (25%) and manual (32%) segmentation groups.

Table 2. Activity on OCTA vs. activity on structural OCT.

		Activity on OCTA		Total
		Yes	No	
Activity on structural OCT	**Yes**	19 (49%)	1 (2%)	20 (25%)
	No	20 (51%)	41 (98%)	61 (75%)
Total		39 (100%)	42 (100%)	81 (100%)

10.4. DISCUSSION

We found that a majority of eyes with CNVM that could be successfully analyzed using automated segmentation had the CNVM complex in the ORCC whereas more than half the eyes that required manual segmentation had a deeper CNVM complex, i.e. either sub-RPE or intra-PED or in the choriocapillaris. Additionally, we noted that only half the eyes deemed to have active CNVM on OCTA demonstrated signs of disease activity on structural OCT. Branching pattern with peripheral loops, anastomosis and arcades were the main findings that lead us to label a CNVM as active while halo around the CNVM was the least helpful finding seen in only a third of the eyes. A significantly greater number of eyes with type 1 CNVM had SRF compared to type 2 eyes.

Ever since the advent of OCTA for evaluation of retinal and choroidal vascular diseases nearly a decade ago, it has been applied to study the characteristics of CNVM.[2,17,18] Coscas et al. described the qualitative features of CNVM in terms of the branching pattern to determine disease activity.[11] We used the same features to determine activity in our study. However, most studies have used the automated segmentation available with the OCTA machines to create the vascular slabs, though this may not always be feasible due to segmentation artifacts that make OCTA interpretation difficult and inaccurate.[14,15] We found that automated segmentation provided by the machine was reliable in less than half the cases in our series. In an excellent study published recently, Siggel et al. studied 102 eyes to determine the sensitivity and specificity of automated versus manually segmented OCTA images to detect presence of CNVM.[16] They showed that automated slabs at the ORCC had the highest ability to detect CNVM compared to the gold standard FFA, while slabs at the choriocapillaris level had the lowest. However, sensitivity of detection could be increased substantially using manual segmentation to produce custom slabs. They also found a significantly higher concordance between FFA and OCTA in detecting CNVM when manual segmentation was used as opposed to only moderate concordance when automated segmentation was used. Unfortunately, they did not comment on CNVM activity. Yet, our data coupled with theirs clearly shows that deeper CNVM complexes below the RPE require manual segmentation much more often than complexes in the ORCC.

Manual segmentation requires a lot of effort and time, has a steep learning curve and hence may be difficult to perform in high volume retina clinics where time is at a premium. Lauermann et al. have shown that segmentation artifacts occur most often in CNVM eyes.[15] However, when structural OCT shows a sub-RPE CNVM complex, interpreting the OCTA images from automated segmentation should be done with caution and should be relied upon only when the entire CNVM complex is visualized without any segmentation or motion artifacts. Retina specialists should be aware that manual segmentation would be needed on nearly half the occasions and hence additional time should be budgeted for this. Since OCTA utilizes differences in the phase and intensity information contained within sequential B-scans performed at the same position, it is possible that the RPE, especially in diseased states, interferes with signal phase and intensity transmission, making automated segmentation unreliable.

We were surprised to find that only half the eyes that were labeled as active CNVM on OCTA actually showed signs of disease activity on the structural OCT. A recent post-hoc analysis from the HARBOR study showed that the concordance between FFA and OCT in detecting disease activity was 99% in treatment naïve eyes with CNVM while this dropped to 36% at 2 years following treatment with anti-VEGF agents.[4] Considering our dataset, where there were many eyes with inactive disease, possibly due to varying levels of anti-VEGF exposure, we believe that structural OCT was unable to pick up disease activity whereas OCTA demonstrated this better. If this were indeed true, then eyes where treatment was withheld due to no activity on OCT but activity on OCTA, would develop signs of activity on OCT subsequently and require retreatment. This is what is seen in real-world clinical practice, where lack of a reliable structural indicator of CNVM activity on OCT has led us to adopt the treat and extent treatment regimen. With OCTA giving us a potentially better indication of disease activity, it may be prudent to adopt it for determining treatment protocols for individual patients, though our study is not adequately powered to make robust recommendations. On similar lines, a recently published by Corvi et al. found that OCTA appears to be superior to other imaging modalities (FFA, ICGA and OCTA) for identification of CNVM in eyes with macular atrophy.[19] However, OCTA is still evolving and more data is required before we use it ahead of structural OCT to determine disease activity.

This study has a couple of limitations, namely the lack of accurate history of anti-VEGF treatment and lack of FFA to compare disease activity. Additionally, the smaller number of eyes with type 1 disease, which is seen more often in clinical practice, makes it difficult to make generalized recommendations, although we feel that the trends may be applicable to most cases. On the other hand, the advantages of this study are the masking of the grader to outputs from other modalities at the time of grading, use of standardized and well-established definitions of CNVM activity on OCTA and use of an experienced grader capable of performing manual segmentation accurately when indicated.

In conclusion, OCTA requires manual segmentation to generate custom slabs and visualize the vasculature of interest whenever artifacts arise from automated segmentation. Need for manual segmentation progressively increases from CNVM in the ORCC to below the RPE and choriocapillaris. There is only a moderate concordance between OCTA and structural OCT in determining CNVM activity at present.

REFERENCES

1. Friedman DS, O'Colmain BJ, Muñoz B, et al. Prevalence of age-related macular degeneration in the United States. *Arch Ophthalmol.* 2004;122(4):564–572.
2. Mitchell P, Liew G, Gopinath B, Wong TY. Age-related macular degeneration. *Lancet.* 2018;392(10153):1147–1159.
3. Schmidt-Erfurth U, Waldstein SM. A paradigm shift in imaging biomarkers in neovascular age-related macular degeneration. *Prog Retin Eye Res.* 2016;50:1v24.
4. Khurana RN, Hill L, Ghanekar A, Gune S. Agreement of spectral-domain OCT with fluorescein leakage in neovascular age-related macular degeneration: post hoc analysis of the HARBOR study. *Ophthalmol Retina.* 2020;4(11):1054–1058.
5. Gao SS, Jia Y, Zhang M, et al. Optical coherence tomography angiography. *Invest Ophthalmol Vis Sci.* 2016;57(9):27–36.
6. Kashani AH, Chen CL, Gahm JK, et al. Optical coherence tomography angiography: a comprehensive review of current methods and clinical applications. *Prog Retin Eye Res.* 2017;60:66–100.
7. Told R, Sacu S, Hecht A, et al. Comparison of SD-optical coherence tomography angiography and indocyanine green angiography in type 1 and 2 neovascular age-related macular degeneration. *Invest Ophthalmol Vis Sci.* 2018;59(6):2393–2400.
8. Corvi F, Cozzi M, Barbolini E, et al. Comparison between several optical coherence tomography angiography devices and indocyanine green angiography of choroidal neovascularization. *Retina*. 2020;40(5):873–880.
9. Jia Y, Bailey ST, Wilson DJ, et al. Quantitative optical coherence tomography angiography of choroidal neovascularization in age-related macular degeneration. *Ophthalmology.* 2014;121(7):1435–1444.
10. Au A, Hou K, Dávila JP, et al. Volumetric analysis of vascularized serous pigment epithelial detachment progression in neovascular age-related macular degeneration using optical coherence tomography angiography. *Invest Ophthalmol Vis Sci.* 2019;60(10):3310–3319.
11. Coscas F, Lupidi M, Boulet JF, et al. Optical coherence tomography angiography in exudative age-related macular degeneration: a predictive model for treatment decisions. *Br J Ophthalmol.* 2019;103(9):1342–1346.

12. Yang J, Zhang Q, Motulsky EH, et al. Two-year risk of exudation in eyes with nonexudative age-related macular degeneration and subclinical neovascularization detected with swept source optical coherence tomography angiography. *Am J Ophthalmol.* 2019;208:1–11.

13. Rosenfeld PJ, Durbin MK, Roisman L, et al. ZEISS angioplex™ spectral domain optical coherence tomography angiography: technical aspects. *Dev Ophthalmol*. 2016;56: 18–29.

14. Spaide RF, Fujimoto JG, Waheed NK. Image artifacts in optical coherence tomography angiography. *Retina.* 2015;35(11):2163–2180.

15. Lauermann JL, Woetzel AK, Treder M, et al. Prevalences of segmentation errors and motion artifacts in OCT-angiography differ among retinal diseases. *Graefes Arch Clin Exp Ophthalmol.* 2018;256(10):1807–1816.

16. Siggel R, Spital C, Lentzsch A, Liakopoulos S. Comparison of automated versus manually modified OCT angiography en face slabs for detection of choroidal neovascularization. *Ophthalmol Retina*. 2020;4(5):471–480.

17. Al-Sheikh M, Iafe NA, Phasukkijwatana N, Sadda SR, Sarraf D. Biomarkers of neovascular activity in age-related macular degeneration using optical coherence tomography angiography. *Retina.* 2018;38(2):220–230.

18. Sambhav K, Grover S, Chalam KV. The application of optical coherence tomography angiography in retinal diseases. *Surv Ophthalmol.* 2017;62(6):838–866.

19. Corvi F, Cozzi M, Invernizzi A, Pace L, Sadda SR, Staurenghi G. Optical coherence tomography angiography for detection of macular neovascularization associated with atrophy in age-related macular degeneration. *Graefes Arch Clin Exp Ophthalmol.* 2021;259(2):291–299.

CHAPTER 11

ISOLATED RACEMOSE ANGIOMA

Sashwanthi Mohan, Supriya Dabir, Mohan Rajan

OPHTHALMOLOGY 2020; 127:1370

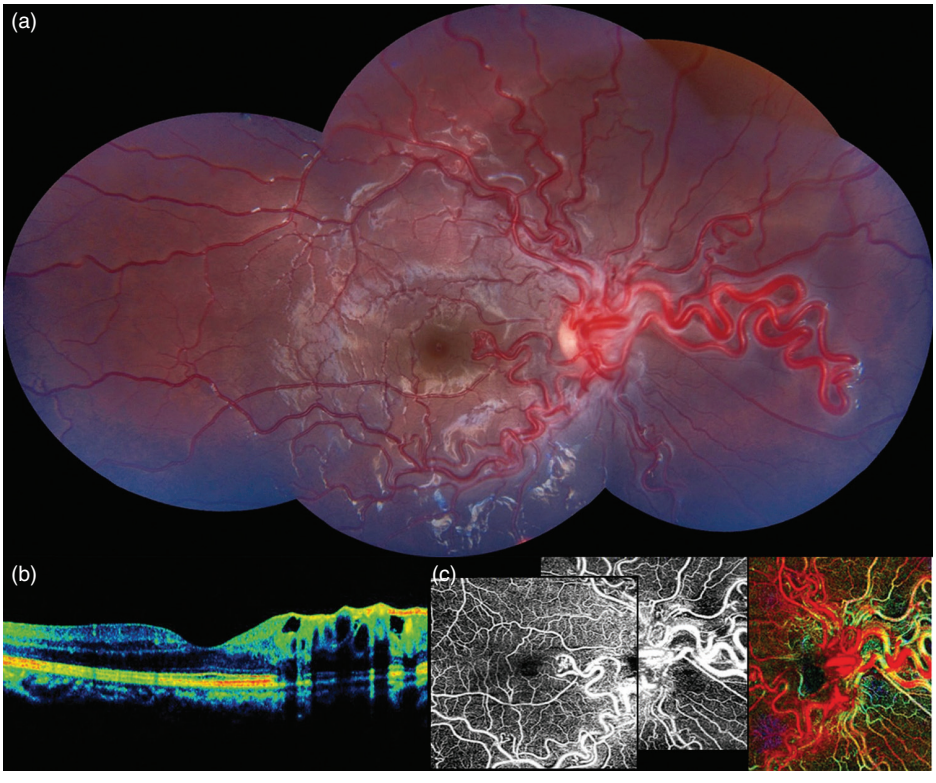

On dilated fundus examination, a 14-year-old girl's right eye revealed markedly dilated and tortuous vessels arising from the disc suggestive of racemose angioma (Figure a). Best corrected visual acuity was 6/6 in both eyes. OCT showed hyporeflective intraretinal vascular lumens with shadow effect nasal to the fovea (Figure b). OCT angiography showed dilated and tortuous vessels visible in the superficial retinal layers with increased intrinsic intraretinal vascular overlay (Figure c). Magnetic resonance imaging of the brain did not reveal any other arteriovenous malformation, ruling out Wyburn Mason Syndrome. Patient remained asymptomatic with benign and stable ocular findings at follow-up.

CHAPTER 12

GENERAL DISCUSSION

Retinal conditions can cause serious vision loss. Early detection and treatment may prevent vision loss or improve the treatment effect. This has been proved in glaucoma[1–3] and diabetic retinopathy.[4,5] Also in exudative age related macular degeneration (AMD) when one eye is treated, the occurrence of exudative AMD in the fellow eye can be discovered at an early stage and treatment outcomes may be better.[6]

Diagnosis with retinal imaging can only be made when structural changes have occurred, most often when vision loss has already occurred. Fundus photography and fluorescein angiography have traditionally been used for imaging but can hardly ever detect subtle structural changes to improve treatment outcome. Current imaging techniques like optical coherence tomography (OCT) have already led to the identification of subtle abnormalities as compared to fundus photography or fluorescein angiography and have shown a trend towards higher resolution in the past years.

However, current retinal imaging techniques are still limited in their ability to detect abnormalities of the retinal photoreceptors cells, capillaries and nerve fiber bundles. Newer imaging modalities that are able to detect retinal microstructures similar to in vivo histology, monitor changes and evaluate treatment outcome represent the basis for designing new management protocols for various preclinical stages of pathology. The emergent need for such sensitive, accurate, diagnostic and monitoring tools is due to newer treatments available like gene therapy, stem cell therapy, nano-targeted drug delivery devices and micro-pulsed lasers.[7]

Microstructures cannot be imaged with traditional fundus cameras even though they have high resolution, due to the inherent limitations of the human eye to lateral resolution. These limitations consist of diffraction caused by small pupils and the internal aberrations of the eye. These ocular aberrations can be divided into two groups, lower-order aberrations and higher-order aberrations. The lower-order aberrations are the normal refraction defects such as myopia, hyperopia, and astigmatism, which can be corrected. If there are irregularities in the refractive components of the eye, such as the tear film, the cornea, the lens or vitreous humor, these can cause higher-order aberrations. Higher-order aberrations are dominated by 3rd-order coma-like aberrations (vertical coma, horizontal coma, oblique trefoil, horizontal trefoil).[7,8]

In order to bring the lateral resolution of ophthalmoscopes to the microscopic scale, it is necessary to compensate for both lower- and higher-order aberrations.[7]

Adaptive optics in retinal imaging can be used with flood illumination or combined with both, the SLO and the OCT, to produce high-quality images whose lateral resolution permits cone discrimination and also allows the study of blood vessels and cells.[9,10] We used the rtx1, a flood illuminated AO camera.

By compensating for the aberrations caused by irregularities of the optics of the eye, lateral (transverse) resolution to the order of 2 microns can be achieved, thereby allowing for the visualization of individual cone photoreceptors.[11]

This thesis discusses the principles of AO, normative database of cone count and spacing in emmetropes and myopes of Indian origin, understanding of the structure and function correlation in the cone mosaic, and its variations in pathology.

We discussed the principles and different applications of AO.[12] It includes a review of the work done by different groups to assess the cone mosaic in normal and disease. It also describes the cone spacing in the myopes varying with respect to the axial length. Photoreceptor reflectivity in AO represents an optical biomarker of photoreceptor integrity. Variations in photoreceptor reflectivity have been observed in different disease states. AO imaging done in different retinal dystrophies has revealed varying degrees of retained cone structure. Studying the structure and function of retained cones can set a baseline to assess those patients who may benefit from treatment like gene therapy or stem therapy and to anticipate the degree of functional improvement that can be expected based on the patient's baseline cone count.[13] Hence, it can help prioritize those patients who can undergo trial of therapy (i.e. those with certain number of retained cones) over patients who may not benefit from therapy (those with absent cones).

It also describes the need for development of normative databases for different populations as a reference for disease states. There has been no literature published thus far describing the Indian population and our work is a step towards the development of normative database of individual variations in emmetropic subjects. With this in mind, we describe the parafoveal cone arrangement, their variations with eccentricity and interocular symmetry in emmetropic Indian eyes.[14] The rtx1 retinal camera was used for imaging the retina and the software, AO detect, was used for cone counting. AO detect is developed by Imagine Eyes and allows the user to obtain both local and mean density within a user defined region of interest (ROI). The positions of

photoreceptors are computed by automatically detecting the central coordinates of small circular spots where the brightness is higher than the surrounding background level. First, the averaged image, without contrast adjustment, is altered so that the local maxima of the resulting image is detected. The spatial distributions of these points are analyzed using Voronoi diagrams where the detected points serve as generators. The local density is obtained by computing the inverse of the Voronoi cell area surrounding each cone. This gives the minimum and maximum density within the ROI. The mean density is easily obtained by dividing the number of detected cones by the area of the ROI.

In our study, we found the average cone-packing densities at 1, 2, and 3 degrees from the fovea. At 1 degree, the counts were erroneous owing to the dense packing of the cones and hence the software was unable to count the cones that were < 2 micron, or the spacing was < 2 micron, leading to a gross under sampling of the cone density. Hence, they were not utilized for statistical analysis. The counts at 2 degrees, 25,350/mm^2 (stdev 5,300/mm^2, range 8,400–34,800/mm^2) differed significantly from those at 3 degrees, 20,750/mm^2 (standard deviation 6,018/mm^2, range 9,000–33,670/mm^2).

The numerical variations between the published western literature and our study could be because of various factors such as eyes with different axial lengths, the location of the foveal reference point, the difference in the sampling window size and the non-standardized approach used to calculate cone distribution among the various studies.

At 1.0 mm eccentricity, there were significant differences in the cone-packing density between the orthogonal meridians ($P<0.001$; nasal, temporal, superior, inferior). We found the highest density to be in the temporal meridian followed by superior, nasal, and inferior at both the eccentricities of 2 and 3 degrees. Our pattern describes the horizontal packing of cones to be denser than the vertical meridian, as noted by the various histological studies.

As cone density decreased with increasing distance from fovea, the spacing tended to accordingly increase. We found the average spacing to increase from a mean of 7.08 mm at 2 degrees to 7.86 mm at 3 degrees. Axial length played a significant role in the count. As the axial length increased, the cone count significantly decreased in emmetropes.

This leads us to understand the relation of axial length and refractive error with respect to the cone spacing.[15] It is well-established that the cones do not get distributed evenly as the expansion occurs non-uniformly. The retinal vasculature is said to restrict the

cone migration along the entire surface. In our current study, we found cone density was significantly less in myopes and also showed a similar difference in the count as the eccentricity increased from 2 degree off the fovea to 3 degree (18,560 ± 5,455 –16,404 ± 4,494/mm^2 respectively). When we used refractive error as the variable, the relation with cone density was less strong as compared to axial length as a variable. We grouped the myopes as low-, moderate- and high-based on their spherical equivalent (mild being 1D–3D, moderate = 3D–6D and high >6D) and evaluated the cone density at different eccentricities from the fovea to understand local anisotropia in correlation to increase in axial length. The cone count and spacing between the mild and moderate group was not found to be significantly different but statistically significant variation was found between the mild and the moderate group with the high myopes. This adds to the theory that the expansion is non-uniform.

Studying the cone mosaic shows different reflectance patterns with wide temporal and spatial variations. Multiple AO systems have described this variation in the cone reflectivity to be secondary to differences in the phase of phototransduction, length of the outer segment, disc shedding, wavelength of the light, and so forth. By just studying the cone mosaic, we are unable to assess the functional aspect of a visible cone and correlate whether a visible cone is a functional cone.

We further assessed the functional aspects of the cone mosaic and correlated the cone-packing with the retinal sensitivity utilizing microperimetry (MAIA) in emmetropes at different eccentricities.[16] It was interesting to understand whether areas with dense cone-packing are associated with higher-retinal sensitivities. Establishing the variations in normal structure-function relations in emmetropes is essential before we understand pathology. This will be useful in establishing the functional correlates of photoreceptor mosaic structure in patients with macular disease who develop central scotomas due to various diseases like age-related macular degeneration. They can then be coached to utilize a certain peripheral part of retina to fixate with, depending on the cone density and retinal sensitivity at that area. Children, after squint surgeries, may be trained to develop fixation by utilizing the structure function knowledge of the retinal areas.

There has been a lot of literature on the use of microperimetry alone to find the preferential retinal locus in patients with central macular disease and they have found it to be differing with respect to the task assigned to the patient. Hence it may be possible to rehabilitate these patients once we understand the areas in which relative

structural photoreceptor loss has led to relative functional loss. Our study shows that when the mean cone-packing density decreased with increasing eccentricity, the corresponding retinal sensitivity also decreased ($P < 0.05$).

After understanding the normative data, we started utilizing the role of AO in pathology. We then studied a case of melanoma-associated retinopathy.[17,18] After a thorough evaluation and routine tools diagnosed the patient, adaptive optics was then done to assess the cone mosaic. The cone count decreased when compared with age-matched normative data. AO may be useful in confirming the diagnosis of this rare disease, monitoring disease progression and evaluating response to therapy. This may help in monitoring the patient's response to immunotherapy by quantifying the cone density and hence revolutionize the way these patients are managed in the future.

Every imaging modality is designed to record a specific type of signal, and failing to understand the implications of this can lead to erroneous interpretations. A careless or unprincipled interpretation of an AO image can lead to erroneous conclusions. Such conclusions will not only compromise our collective understanding of a disease, but they will diminish the perceived value of AO technology.[19] A proper analysis and interpretation begins with a strong understanding of the imaging system and how it interacts with the retina. A deep understanding of the imaging modality can lead to innovative adaptations of it.

The results presented in this thesis aims to show the promise of AO for clinical applications. By all indications, AO has become increasingly important in ophthalmology. AO aids in evaluating new treatments to cure, prevent, or slow the progression of eye disease. AO offers two advantages: Firstly, the microscopic imaging can be done non-invasively in humans. Secondly, imaging the same cells in the same human eye longitudinally reduces noise caused by differences in treatment response between individual patients, possibly making clinical trials more efficient and conclusive. Moreover, the massive growth in our understanding of the genetics of eye disease suggests that it is just a matter of time before cohorts of subjects with well-known risk factors for eye disease will be studied and followed with AO imaging prior to developing any clinical symptoms. In addition, natural history studies of disease progression that include AO images will demonstrate the sensitivity and validity of this imaging technology. Finally, as newer treatments emerge, the importance of early diagnosis will increase.

Optical coherence tomography (OCT) angiography (OCTA) can produce images of blood flow that have unprecedented resolution of all the vascular layers of the retina in a rapid, non-invasive fashion. Fluorescein angiography (FA), an alternate method of imaging flow, has been used in clinical practice for over 50 years. Unfortunately, FA cannot image several important layers of blood vessels in the eye; essentially only the superficial vascular plexus can be seen. Still, FA was used to create the field of medical retina. OCT angiography (OCTA) offers the possibility of also imaging the radial peripapillary capillary network and the intermediate and deep capillary plexuses. This capability opens a wealth of possibilities for disease description and quantification, research into pathogenesis of disease, and development and evaluation of new treatments. OCTA comes at the heels of development of higher speed structural OCT imaging, which itself is under rapid development. Curiously, much of the recent drive to develop instrumentation platforms is to improve OCTA. Concurrently, the scanning strategies and software being developed for OCTA are improving quickly. While the rate of change is breath-taking and exciting, the challenge lies in trying to understand what OCTA is and what it can accomplish. Understanding OCTA requires a comprehensive knowledge of many facets of imaging, starting with how the imaging works, what the potential deficiencies as well as strengths are.[19]

In my thesis, we studied the use of OCTA in different clinical scenarios. We studied vascular changes in central retinal arterial occlusion documented on fundus fluorescein angiography to see if it was comparable with OCTA. We reported a patient in whom OCTA was done before and after anterior chamber paracentesis. It showed a prompt re-perfusion in the superficial layers despite the 7-day-old event. The repeatability constraints of invasive fundus fluorescein angiography can be overcome by the non-invasive OCTA.

Next, we wanted to understand whether cataract surgery has a truly pro-inflammatory influence on retinal circulation. Hence, we studied changes in the superficial retinal capillary microvasculature before and after cataract surgery using the OCTA in an Indian population. We found that there was a significant increment in retinal capillary perfusion and vascular density in the superficial capillary plexus. This relation persisted even after adjusting for the proportionally increased signal strength due to cataract removal. The clinical application may be to perform OCTA before cataract surgery, especially in eyes with diabetic retinopathy and other diseases prone to developing macular edema postoperatively. These are patients who need topical steroids and anti-inflammatory drops for a longer postoperative period.

Diabetic macular oedema (DME) is the most common vision threatening complication of DR and is estimated to be affecting ~9% of all patients with any form of DR in India.[20] In recent years, the use of intravitreal anti-VEGF injections has become the standard of care in managing diabetic macular oedema, preventing vascular leaks, and improving visual acuity. While fluorescein angiography is the established gold standard for assessing retinal vasculature, it is limited by its invasiveness, use of contrast, and limited ability to obtain quantifiable measurements of avascular area and vessel density.[21] To understand the recovery in retinal microvasculature and treatment responses to anti-VEGF agents, we performed serial OCTA measurements before and after monthly intravitreal anti-VEGF injections (Ranibizumab-Lucentis®). Changes in OCTA were reflective of functional recovery of DME with the use of multiple intravitreal anti-VEGF injections at the end of 3 months. Resolution of microvascular damage correlates with functional recovery and reduction in CMT was the most reliable predictor of response. Based on the study results we propose that OCTA (SCP) markers in a routine clinical scenario could play a good role in measuring early response to anti-VEGF therapy. This could help individualize the standard of care in individuals with retinopathy and macular oedema.

Ever since the advent of OCTA for evaluation of retinal and choroidal vascular diseases nearly a decade ago, it has been applied to study the characteristics of choroidal neovascular membrane (CNVM), especially secondary to neovascular age-related macular degeneration (nAMD). We found that a majority of eyes with nAMD that could be successfully analyzed using automated segmentation had the CNVM complex in the outer retina-choriocapillaris (ORCC) whereas more than half the eyes that required manual segmentation had a deeper CNVM complex, i.e. either sub-retinal pigment epithelium or intra-pigment epithelium detachment or in the choriocapillaris. Additionally, we noted that only half the eyes deemed to have active CNVM on OCTA demonstrated signs of disease activity on structural OCT. Branching patterns with peripheral loops, anastomosis and arcades were the main findings that lead us to label a CNVM as active while halo around the CNVM was the least helpful finding seen in only a third of the eyes.

This is what is seen in real-world clinical practice, where lack of a reliable structural indicator of CNVM activity on OCT has led us to adopt the treat and extent treatment regimen. With OCTA giving us a better indication of disease activity, it may be prudent to adopt it for determining treatment protocols for individual patients.

We described the superficial capillary plexus of an isolated racemose angioma in an asymptomatic young girl without any systemic associations. It was an interesting, incidental finding and has not been described using OCTA in literature till date.

The last two decades have witnessed major advancements in retinal imaging technologies thanks, in no small part, to improved light sources, detectors and high-speed computers. New research grade systems are continuously improving and some have obtained a degree of user friendliness and robustness that have facilitated their transition to clinical use. This thesis has added normative data for these imaging modalities, making clinical utilization possible.

Adaptive optics and optical coherence tomography angiography systems are becoming commonplace in modern ophthalmic clinics where they often provide unprecedented image quality with resolving powers down to the level of single retinal cells and capillaries in the living eye. Such richness in detail provides challenges and possible paradigm shifts. As enormous impact on improved diagnostics has been realized, we continue to work towards the ultimate goal of achieving healthy vision throughout life.[22]

Given the novelty of ultrahigh resolution retinal imaging technologies, the future looks promising for much improved diagnostic imaging as the limits of the methods are removed and their clinical usage continues to grow.

REFERENCES

1. Resnikoff S, Pascolini D, Etya'ale D, et al. Global data on visual impairment in the year 2002. *Bull World Health Organ.* 2004;82(11):844–851.
2. Quigley HA, Broman AT. The number of people with glaucoma worldwide in 2010 and 2020. *Br J Ophthalmol.* 2006;90(3):262–267.
3. McKean-Cowdin R, Varma R, Wu J, Hays RD, Azen SP. Severity of visual field loss and health-related quality of life. *Am J Ophthalmol.* 2007;143(6):1013–1023.
4. Early Treatment Diabetic Retinopathy Study design and baseline patient characteristics. ETDRS report number 7. *Ophthalmology.* 1991;98(5 suppl):741–756.
5. Nathan DM, Genuth S, Lachin J, et al. The effect of intensive treatment of diabetes on the development and progression of long-term complications in insulin-dependent diabetes mellitus. *N Engl J Med.* 1993;329(14):977–986.
6. Pieramici DJ, Bressler SB. Age-related macular degeneration and risk factors for the development of choroidal neovascularization in the fellow eye. *Curr Opin Ophthalmol.* 1998;9(3):38–46.
7. Lombardo M, Lombardo G, Ducoli P, Serrao S. Adaptive optics photoreceptor imaging. *Ophthalmology.* 2012;119(7):1498–1498. e1492.
8. Lombardo M, Lombardo G. Wave aberration of human eyes and new descriptors of image optical quality and visual performance. *J Cataract Refract Surg.* 2010;36(2):313–331.
9. Rosander F. Detection of pathological lesions in high resolution retinal images. 2013.
10. Ödlund E. *Dynamic characterization, modelling, and control of a deformable mirror for adaptive optics ophthalmic applications*. Canterbury, Kent: University of Kent; 2010.
11. Godara P, Dubis AM, Roorda A, Duncan JL, Carroll J. Adaptive optics retinal imaging: emerging clinical applications. *Optom Vis Sci.* 2010;87(12):930.
12. Battu R, Dabir S, Khanna A, Kumar A, Roy A. Adaptive optics imaging of the retina. *Indian J Ophthalmol.* 2014;62(1):60–65.
13. Carroll J, Kay DB, Scoles D, Dubra A, Lombardo M. Adaptive optics retinal imaging–clinical opportunities and challenges. *Curr Eye Res.* 2013;38(7):709–721.
14. Dabir S, Mangalesh S, Kumar K, Kummelil M, Roy AS, Shetty R. Variations in the cone-packing density with eccentricity in emmetropes. *Eye.* 2014;28(12):1488–1493.

15. Supriya D, Shwetha M, Kiran Anupama K, et al. Structural and function correlation of cone-packing utilizing adaptive optics and microperimetry. *Biomed Res Int*. 2015;2015:968672.

16. Supriya D, Shwetha M, Kiran Anupama K, et al. Structural and function correlation of cone-packing utilizing adaptive optics and microperimetry. *Biomed Res Int*. 2015;2015:968672.

17. Dabir S, Mangalesh S, Govindraj I, Mallipatna A, Battu R, Shetty R. Melanoma associated retinopathy: a new dimension using adaptive optics. *Oman J Ophthalmol*. 2015;8(2):125–127.

18. Roorda A, Duncan JL. Adaptive optics ophthalmoscopy. *Annu Rev Vis Sci*. 2015;1:19–50.

19. Spaide RF, Fujimoto JG, Waheed NK, Sadda SR, Staurenghi G. Optical coherence tomography angiography. *Prog Retin Eye Res*. 2018;64:1–55.

20. Rajalakshmi R, Behera U, Bhattacharjee H, et al. Spectrum of eye disorders in diabetes (SPEED) in India. Report # 2. Diabetic retinopathy and risk factors for sight threatening diabetic retinopathy in people with type 2 diabetes in India. *Indian J Ophthalmol*. 2020;68(13):21–26.

21. Virgili G, Parravano M, Evans JR, Gordon I, Lucenteforte E. Anti-vascular endothelial growth factor for diabetic macular oedema: a network meta-analysis. *Cochrane Database Syst Rev*. 2018;10(10):CD007419.

22. Choi SS, Elsner AE, Zawadzki RJ, Vohnsen B. Clinical applications of high resolution in-vivo retinal imaging. *J Ophthalmol*. 2013;2013:312974

CHAPTER 13

SUMMARY

The ability to look inside the living human eye is central to our understanding of how the normal eye works and the diseased eye fails. This thesis focuses on technological advances in the spatial resolution of retinal imaging during the last decade. These advances have transformed retinal imaging from a macroscopic to a microscopic modality in which individual cells can now be resolved. To better visualize the cellular microstructure and understand the processes in the living retina, high-resolution imaging is the key. In order to study dynamic processes, non-invasive imaging provides an exciting alternative to histology. We discuss two modalities in this thesis, namely adaptive optics to study the neural network of the retina and optical coherence tomography angiography to analyse the vascular plexus of the retina.

As adaptive optics imaging finds more clinical applications, normative databases need to be developed for different populations as a reference for disease states. It may help us understand the pathogenesis of diseases at a subclinical stage, thus paving way for the exciting possibility of early treatment for these diseases.

Imaging and analysis of the retinal vasculature can be a surrogate marker for systemic vascular health. Correlations between vascular abnormalities in the retina and elsewhere in the body have been demonstrated in a diverse array of conditions including diabetes, hypertension and stroke. The earliest change in disease begins at the level of the microvasculature, however, imaging retinal capillaries is difficult because of their small size, low contrast, and arrangement in multiple planes of varying retinal depth. Optical coherence tomography angiography (OCTA) is an exciting and new imaging modality that has revolutionized our understanding of the retinal and choroidal vasculature in a non-invasive manner in normal as well as diseased states.

Chapter 1 is an introduction to the thesis and discusses the anatomy of the eye, histology of the retina and principles of the two high-resolution imaging systems, adaptive optics and optical coherence tomography angiography.

Chapter 2 involves a review of literature on AO. Here, we described the basic principle of AO and some clinical applications of AO in photoreceptor analysis in retinal degenerations and dystrophies and in retinal vascular analysis. AO is an innovative new tool in the extensive armamentarium of ophthalmologists to explore the cellular details of the retina. It is possible that as more detailing of cellular structures becomes possible, we may need to develop better analytical tools.

Chapter 3 describes normative data in cone density in emmetropes. We described the distribution of density, spacing and the hexagonal packing arrangement of the cone photoreceptors at different retinal eccentricities across the parafovea in emmetropic young adults in the Indian population. A statistically significant drop in the cone-packing density was observed from 2° from the fovea to 3°. The spacing correspondingly increased with increase in distance from the fovea. As the axial length increases, the cone density significantly decreases. Interocular variations were noted. It is essential to establish normative data in order to detect early onset of pathology at a cellular level and intervene early.

Chapter 4 looks at the variations in the cone mosaic in a population of young myopic adults in relation to the axial length and extent of the refractive error. In myopic patients with good visual acuity, cone density around the fovea depends on the quadrant, distance from the fovea as well as the AL. The strength of the relation of AL with cone density depends on the quadrant and distance. The mean cone density was significantly lower as the eccentricity increased from 2° to 3° from the fovea. There was also a statistically significant difference between the four quadrants. The correlation of cone density and spacing with AL showed that there was a significant inverse relation of AL with the cone density.

Chapter 5 describes the structure-function correlation by correlating the cone-packing with the retinal sensitivity utilizing microperimetry (MAIA) in emmetropes at different eccentricities. A drop in retinal sensitivity was observed as the eccentricity increased. It was also found that as cone-packing density decreased retinal sensitivity also decreased in all quadrants. This may be useful in establishing the functional correlates of photoreceptor mosaic structure in patients with macular disease who develop central scotomas due to various macular diseases like age-related macular degeneration.

Chapter 6 discusses the case of a patient with history of cutaneous melanoma in the foot, who developed MAR. Combined imaging and functional tools aided in

assessment of early pathological retinal alterations. This chapter describes the role of AO in detection and assessment of the extent of pathology in MAR.

Chapter 7 is a case report describing improvement in perfusion of the superficial capillary plexus immediately after anterior chamber paracentesis in acute central retinal artery occlusion. This shows the immediate recovery in vascular perfusion that occurs with intraocular pressure reduction. OCTA, being a non-invasive vascular imaging modality, helped document it before and after procedure.

Chapter 8 discusses the role of OCTA in detecting increase in macular perfusion and vascularity indices immediately after cataract surgery independent of improvement in signal strength. These increments were slightly lower but still statistically significant in the parafoveal and perifoveal regions. It may be prudent to perform OCTA before cataract surgery, especially in eyes with diabetic retinopathy and other diseases prone to developing macular edema postoperatively.

Chapter 9 demonstrated that the changes in OCTA measurements were reflective of use of 3 consecutive intravitreal anti-VEGF injections (Ranibizumab-Lucentis®) for the functional recovery of DME at the end of 3 months. It suggests that the resolution of microvascular damage noted on OCTA – FAZ, VD, and PD reliably correlates with the functional recovery (improved BCVA), and that reduction in CMT was the most reliable predictor of response.

Chapter 10 showed that manual segmentation of OCTA is required in more than 50% eyes with CNVM and this progressively increases from CNVM in ORCC to below the RPE. There is moderate concordance between OCTA and structural OCT in determining CNVM activity, with OCTA perhaps, being better at detecting disease activity.

Chapter 11 shows the superficial capillary plexus of an isolated racemose angioma in an asymptomatic young girl without any systemic associations.

Chapter 12 is the discussion of important findings, issues, and implications for future studies based on the above chapters.

CHAPTER 14

IMPACT

This is a golden age in ophthalmic imaging since ophthalmology is among the most technology-driven medical specialities with major advances in imaging techniques, both in hardware and software. They have led to reduction in discomfort of invasive tests and more detailed ocular examination with high-quality images. This results in better understanding of the eye in health and pathology, prognosis and response to therapy. Furthermore, the eye being mostly optically transparent, acts as a window to the cardiovascular and nervous systems.

Right through my internship I felt drawn towards the field of ophthalmology and decided to major in it. During my residency, I met many patients with end stage diabetic retinopathy, advanced age-related macular degeneration and inherited retinal disorders. That is when I decided to work on understanding the pathophysiology of these diseases and finding ways for early diagnosis and timely interventions to prevent irreversible blindness.

While pursuing my fellowship, I was exposed to various imaging technologies, one of them being time domain optical coherence tomography (TD-OCT), which at that time, revolutionised the management of retinal diseases. The beauty of being able to see the individual layers of the in vivo retina was riveting. It changed the way we managed active choroidal neovascular membranes and diabetic macular oedema. Further, it coincided with the initiation of anti-vascular endothelial growth factor therapy. Advances in the technology of OCT led to the era of spectral domain SD-OCT and swept source OCT which resulted in new terminology for different layers being formulated.

It was 2012 when I attended the ARVO meeting at Fort Lauderdale, and, I first saw the adaptive optics (AO) technology and the work being done with it. By compensating for the aberrations caused by irregularities of the optics of the eye, resolution to the order of 2 μm could be achieved, thereby allowing, for the visualization of individual cone photoreceptors. Intrigued by this, we visited the Imagine eye office at Paris, France, and some of their users in Rome, Italy. We soon acquired the machine and started working with it. As we understood the clinical application and the possibilities of the machine, we wrote a review on it (Chapter 1). We then established a normative baseline for emmetropes (Chapter 2) and myopes (Chapter 3) in our clinic. As a clinician, our interest is always on the functional outcomes. Whether they are patients with maculopathy or retinal detachment, our aim is always to improve their vision through intervention. Hence establishing a structure-function correlation becomes vital. This was the basis of

our study (Chapter 4). We had an interesting patient with minimal clinical features, but adaptive optics and electrophysiology clinched the diagnosis of melanoma associated retinopathy and helped in assessing the extent of pathology (Chapter 5). This leads to the use of adaptive optics in many different diseases, like hydroxychloroquine toxicity, serpiginous choroiditis and inherited retinal disorders. A baseline image of the patient would be established and then subsequent scans done to show progression, if any, to either stop the toxic medicines or in cases of inherited retinal disorders, the patients were explained the progressive nature of the disease, the rate of progression and its possible implication with regard to lifestyles and rehabilitation.

We went on many international podiums like Asia ARVO, 2013, World Ophthalmic Congress, 2014, to organise special interest groups and presented at multiple national podiums. Since Narayana Nethralaya, Bangalore, was the first hospital in India to work with a commercially available adaptive optics machine, it became our responsibility to discuss results with all our Indian colleagues. There had been no literature published thus far from the Indian population and our work helped in the development of a normative database in emmetropic subjects. This now allows us to understand early pathology at the cellular level and intervene. Newer therapeutic modalities that are targeted at the cellular level like micro-pulse laser, stem cells, gene therapy etc. are also better monitored in terms of safety and efficacy. These therapies are designed to cause early and subtle changes in the photoreceptors as a response rather than showing any gross changes in the SD-OCT.

Optical coherence tomography angiography (OCTA) is a new non-invasive imaging technique that employs motion contrast imaging to high-resolution volumetric blood flow information generating ocular angiographic images in a matter of seconds. It helps understand the vascular pattern of the different layers in the eye. OCTA was used to study the architecture of the vascular tree in an isolated racemose angioma (Chapter 6). In the retina clinic, most patients with macular edema are either with diabetic retinopathy (Chapter 7) or post cataract surgery (Chapter 9). We started doing OCTA to understand the pathogenesis of why some patients develop it and some do not.

We analysed the vascular parameters and the foveal avascular zone in diabetics and realised the circularity gets affected initially. These may be the patients who later go on to develop macular edema. These subtle changes can be diagnosed early in the course of diabetes, followed-up closely, allowing early intervention. The response to antivascular endothelial growth factor treatment is variable in diabetic macular edema. Understanding the vascular biomarkers is critical to individualize the standard of care and predict the response to treatment.

OCTA scans have now become a standard baseline investigation for all patients with choroidal neovascular membranes. But we realized that automated segmentation was missing many of the membrane complexes unless it was manually corrected (Chapter 8). I am now a part of a group that collects and analyses data for machine learning with the help of AI, the machine itself decides when manual or automated segmentation is preferable.

This made me realise that the serious limitations of the current OCTA machines is in the analysis software. It is time consuming and varies with every OCTA machine. Hence, I am now working with my colleagues on analysis tools with quantitative indices that help in establishing a baseline in pathology.

The remarkable advances in ophthalmic imaging have transformed simple photographic documentation into powerful investigative methods enabling clinicians to make objective measurements and assessments of retinal structures in detail. The future would be to have a unified software platform with integrated investigations such that for every patient at a given retinal location, the cellular details (AO), tomography (SD OCT) and vascular details (OCTA) along with the functional tests of the retina (MAIA, electrophysiology) can be documented. This will give a holistic view of the retina and help in early detection and treatment of pathology.

CHAPTER 15

ACKNOWLEDGEMENTS

This thesis has been the culmination of an incredible journey for me. My friend and colleague, Dr Debashish Das was instrumental in planting the idea that, I could aspire to be a PhD scholar.

Subsequently, Dr Rohit Shetty, Vice Chairman, Narayana Nethralaya connected with Maastricht University and he kindly encouraged me to take on the PhD course. For a clinician, at the time, it seemed a leap of faith given my unfamiliarity with the world of research and scientific writing. I am very thankful to him for his constant encouragement and learning opportunities throughout my tenure at the hospital.

I would like to express my sincere gratitude to my advisor, Dr Tos Berendschot, for the continuous support of my PhD study and related research, for his patience, motivation & immense knowledge. His guidance, despite the restrictions and uncertainty during COVID times, has helped me navigate the quantitative interpretation of the data and in the writing of this thesis. I could not have imagined having a better advisor and mentor for my PhD study.

I would like to thank Dr Jan Schouten, who would patiently read through all my initial few manuscripts and make excellent suggestions. My sincere thanks to Prof Webers whose positive words of encouragement and support made this thesis possible.

To my colleagues, Dr Shwetha Mangalesh and Dr Anupama Kiran Kumar – Thank you for helping me with the data collection and analysis of the cone counts. They were always there as either a shoulder to cry on when the going got tough or for a party after every publication.

Dr Rajani Battu who has always made me believe everything was possible and rerouted me in the right direction when lost and Dr Abhishek Appaji for guiding me through the entire process of compiling the thesis. Dr. Shyam Vasudeva Rao for being a constant source of encouragement.

My sincere thanks and appreciation go to my colleagues, Dr Naresh Yadav, Dr Mathew, Dr Priya Srinivasan, Dr Padmamalini, Dr Subhash, Dr Santosh Gopi Krishna and Dr Devanshi for their help at every stage of my thesis.

My imaging colleagues, Mukunda, Siva, Leo, Alex, Sandhya and Dikshit, deserve a lot of credit for their painstaking and time-consuming tasks of always getting the

best images possible. Many thanks also to my paramedical team—Jagannath, Asha, Lakshmi and Bhagya for being my cheerleaders.

My thesis would have been incomplete without the unstinting support from Dr Mohan Rajan and Dr Sujatha Mohan, who have always encouraged me.

To my friends and long-time colleagues, Dr Preetam Samant, Dr Deepak Bhatt and Dr Ashwin Mallipatna for patiently listening to me vent and for helping me cross every hurdle encountered.

Finally, on a personal note, to my parents, Mr & Mrs Suresh Dabir for instilling in me, the confidence that I can accomplish anything that I set my mind to. Their support has been invaluable & they have been my backbone every step of the way. My sister, Sandhya, who has always guided me to give my best. My cousin, Dr Srivatsa Shastry for helping me with edits in my study design and manuscripts.

My parents in law, Mr & Mrs N.Venkataramani who have supported me at every step and never let me give up. My son, Advaith, who at his age, has been so understanding when I have spent hours at work, when he would rather have me play with him.

And last but not the least, my husband and best friend, Gautam, who has been my strength through the entire journey. You have never let me quit, made me believe it was possible and been my biggest cheerleader as well as critic. This would not have been possible without you.

CHAPTER 16

CURRICULUM VITAE AND PUBLICATIONS

Dr. Supriya Dabir Gautam is the head of vitreoretinal services at Rajan Eye Care Hospital, Chennai. She has spearheaded the establishment of the retina department at Voluntary Health Services, Chennai, and volunteers her expertise for the less privileged patients. She has set up the rotary project for retinopathy of prematurity (Rotaropp) and is actively involved in the clinical management of the affected babies. She has experience working at both government hospitals, such as J. J. Group of Hospitals, Mumbai, and private institutes, such as Narayana Nethralaya, Bangalore.

Dr. Supriya completed her medical graduation at MGM Medical College, Mumbai, in 2003, her master's in ophthalmology from St. John's Medical College, Bangalore, in 2006, and then her vitreoretinal fellowship from Aditya Jyot Eye Hospital, Mumbai, in 2008. Having completed the prestigious GK Saraf fellowship at Sankara Nethralaya, Chennai, in 2008, she went on to finish her Diplomate of National Board in 2009 and the ICO examinations in 2010.

A keen academician, she has presented at multiple international and national podiums as an invited speaker, and also conducted multiple workshops for skill transfer at multiple state and national conferences. She has won multiple accolades, such as the Best Paper Award at the annual conference held by the Bombay Ophthalmologists' Association, 2008, the YKC Pandit Award at the annual meet by the Maharashtra Ophthalmic Society, 2008, the second prize at the International Conference on Nanomedicine and Recent Advances in Ophthalmic Research, 2008, and Dr. Basheer Mekhri Award at the annual meet of Karnataka Ophthalmic Society, 2011.

As a co-editor of the book "Textbook of Vitreoretinal Diseases and Surgery" (Jaypee Publishers), Dr. Supriya has also published multiple papers in indexed journals, and written chapters in Indian textbooks for postgraduates. She has been a co-investigator of multiple international phase III clinical trials, such as VIEW2 ScyFIX. She has also been the principal investigator of in-house clinical trials, such as VEGF analysis in retinal vascular disorders. Among the first few to work on imaging modalities, such as adaptive optics, retina oximetry, and optical coherence tomography angiography in India, many postgraduates have been guided by her towards the completion of their DNB thesis.

She is highly passionate about her work and bringing the best possible care to all her patients.

PUBLICATIONS

1. Assessment of microvascular changes using optical coherence tomography angiography after phacoemulsification surgery in an Indian population.
   Supriya Dabir, Mohan Rajan, Sujatha Mohan, Vaidehi Bhatt, M.Ravishankar, Sowmya Sunil, Deepak Bhatt, Preetam Samant, Berendschot TTJM, Webers CAB
   J Clin Exp Ophthalmol, Vol.12 Iss.S8 No:1000002

2. Early functional and morphological responses to anti-vascular endothelial growth factor therapy in diabetic macular oedema using optical coherence tomography angiography.
   Supriya Dabir, Mohan Rajan, Liji Parasseril, Vaidehi Bhatt, Preetam Samant, C A B Webers, T T J M Berendschot
   Clin Ophthalmol. 2021; 15: 331–339. Published online 2021 Jan 28.

3. Need for manual segmentation in optical coherence tomography angiography of neovascular age-related macular degeneration
   Supriya Dabir, Vaidehi Bhatt, Deepak Bhatt, Mohan Rajan, Preetam Samant, Sivakumar Munusamy, C. A. B. Webers, T. T. J. M. Berendschot
   PLoS One. 2020; 15(12): e0244828. Published online 2020 Dec 31.

4. Isolated racial angioma
   Mohan S, **Dabir S**, Rajan M.
   Ophthalmology. 2020 Oct;127(10):1370.

5. Perivascular and quadrant nerve fiber layer thickness and its relationship with oxygen saturation.
   Mohan A, **Dabir S**, Kurian M, Shetty R, Chidambara L, Kumar RS.
   Curr Eye Res. 2016 Sep;41(9):1223-8.

6. Spectral domain optical coherence tomography angiography features in a patient of central retinal arterial occlusion before and after paracentesis.
   Bhanushali DR, Yadav NK, **Dabir S**, Chidambara L, Srinivasan P, Shetty R.
   Retina. 2016 May;36(5):e36-8.

7. The use of handheld spectral domain optical coherence tomography in paediatric ophthalmology practice: Our experience of 975 infants and children.
   Mallipatna A, Vinekar A, Jayadev C, **Dabir S**, Sivakumar M, Krishnan N, Mehta P, Berendschot T, Yadav NK.
   Indian J Ophthalmol. 2015 Jul;63(7):586-93.

8. Structural and function correlation of cone packing utilizing adaptive optics and microperimetry.
Supriya D, Shwetha M, Kiran Anupama K, Kummelil Mathew K, Berendschot TT, Schouten JS, Bharamshetter R, Naresh YK, Rohit S, Hegde B.
Biomed Res Int2015; 2015; 968672. Published online 2015 Jun 8.

9. Melanoma associated retinopathy: A new dimension using adaptive optics.
Dabir S, Mangalesh S, Govindraj I, Mallipatna A, Battu R, Shetty R.
Oman J Ophthalmol. 2015 May-Aug;8(2):125-7.

10. Microscope-integrated optical coherence tomography: A new surgical tool in vitreoretinal surgery.
Jayadev C, **Dabir S**, Vinekar A, Shah U, Vaid T, Yadav NK.
Indian J Ophthalmol. 2015 May;63(5):399-403.

11. Axial length and cone density as assessed with adaptive optics in myopia.
Dabir S, Mangalesh S, Schouten JS, Berendschot TT, Kurian MK, Kumar AK, Yadav NK, Shetty R.
Indian J Ophthalmol. 2015 May;63(5):423-6.

12. Normative database of retinal oximetry in Asian Indian eyes.
Mohan A, **Dabir S**, Yadav NK, Kummelil M, Kumar RS, Shetty R.
PLoS One. 2015 Apr 29;10(4): e 0126179.

13. Subthreshold micropulse yellow laser (577 nm) in chronic central serous chorioretinopathy: safety profile and treatment outcome
N K Yadav, C Jayadev, A Mohan, P Vijayan, R Battu, **S Dabir**, B Shetty, R Shetty
Eye (Lond) 2015 Feb; 29(2): 258–265. Published online 2015 Jan 23.

14. Variations in the cone packing density with eccentricity in emmetropes.
Dabir S, Mangalesh S, Kumar KA, Kummelil MK, Sinha Roy A, Shetty R.
Eye (Lond) 2014 Dec; 28(12): 1488–1493.

15. Adaptive optics imaging of the retina.
Battu R, **Dabir S**, Khanna A, Kumar AK, Sinha Roy A.
Indian J Ophthalmol. 2014 Jan;62(1):60-5.

16. Differential systemic gene expression profile in patients with diabetic macular edema: Responders versus non responders to standard treatment.
Supriya S Dabir, Debashish Das, Jeyabalan Nallathambi, Shwetha Mangalesh, Naresh Kumar Yadav, Jan S A G Schouten
Indian J Ophthalmol. 2014 Jan; 62(1): 66–73.

17. Spectral domain-optical coherence tomography study of retinas with a normal foveal contour and thickness after retinal detachment surgery.
Sheth S, **Dabir S**, Natarajan S, Mhatre A, Labauri N.
Retina. 2010 May;30(5):724-32.

18. Aspergillus iris granuloma: a case report with review of literature.
Jain V, **Dabir S**, Shome D, Dadu T, Natarajan S .
Surv Ophthalmol 2009;54: 286–291.

19. Factors affecting visual overcome in herpes zoster: a prospective study
Nithyanandam S, **Dabir S**, Stephen J, Joseph M.
Clin Exp Ophthalmol 2010 Dec;38(9):845-50.

20. Eruption severity and characteristics in herpes zoster ophthalmicus: correlation with visual outcome, ocular complications, and postherpetic neuralgia.
Nithyanandam S, **Dabir S**, Stephen J, Joseph M.
Int J Dermatol. 2009 May;48(5):484-7.